DETERMINING THE FUNCTION OF THE INTERLEUKIN-1 RECEPTOR ASSOCIATED KINASE PATHWAY IN PRIMARY EFFUSION LYMPHOMA

Jedediah David Seltzer

A dissertation submitted to the faculty of the University of North Carolina at Chapel Hill in partial fulfillment of the requirements for the degree of Doctor of Philosophy in the Department of Microbiology and Immunology.

Chapel Hill
2020

Approved by:

Dirk Dittmer

Blossom Damania

Nat Moorman

Cary Moody

Jason Whitmire

ABSTRACT

Jedediah Seltzer: Determining the function of the interleukin-1 receptor associated kinase pathway in primary effusion lymphoma
(Under the direction of Dirk Dittmer)

Kaposi's sarcoma-associated herpesvirus (KSHV) is necessary but not sufficient for the development of Primary effusion lymphoma (PEL). Alterations in cellular signaling pathways are also a characteristic of PEL development. Other B cell lymphomas have acquired an oncogenic mutation in the myeloid differentiation primary response-88 (MYD88) gene. The MYD88 L265P mutant results in the activation of the Interleukin-1 Receptor Associated Kinase (IRAK) pathway and a pro-inflammatory environment. To probe IRAK/MYD88 signaling in PEL, we employed CRISPR/Cas9 technology to generate stable deletion clones in BCBL-1Cas9 cells. To look for off-target effects, we determined the complete exome of the BCBL-1Cas9 cell line.

Deletion of either MYD88, IRAK4, or IRAK1 abolished IL-1β signaling; however, we could grow stable sub-clones from each population. RNA-seq analysis of IRAK4 knockouts showed that the IRAK pathway induced cellular signals constitutively, independent of IL-1β stimulation, which was abrogated by deletion of IRAK4. Transient complementation with IRAK1 increased NF-kB activity in MYD88KO, IRAK1KO, and IRAK4KO cells even in the absence of IL-1β. We also saw that IL-10, a hallmark of PEL, is engaged with the IRAK pathway as IRAK4 knockouts reduce IL-10 levels. We surmise that, unlike B-cell receptor (BCR) signaling, MYD88/IRAK signaling is constitutively active in

PEL, but that under cell culture conditions, PEL rapidly becomes independent of this pathway.

For my family who have supported me:
My wife Tischan and my son Jonah.

My parents Jay and Terry Seltzer.

My siblings: Jeremiah, Rebekah, Susanna, Liz and Abigail as well as my bonus siblings Scott and Meredith.

Dedicated with a grateful heart.

ACKNOWLEDGEMENTS

First, I would like to acknowledge my family and my friends for the support I have received. A PhD is a long road to travel and the support of friends and family helped me stay sane and on track. To my wife Tischan who has encouraged me and has had to personally sacrifice her time while I completed this experience. To my brother, Jeremiah, who set me on this track by a random conversation when I was in the 11th grade. My parents, Jay and Terry, for supporting and encouraging me. To my other siblings, Rebekah, Susanna, Liz, and Abigail as well as my bonus siblings Scott and Meredith, for putting up with my science talk and not asking "when are you graduating" every time I saw them.

I would also like to acknowledge my friends who have been an amazing community while I went through this process. The fellowship and encouragement I received made this road more enjoyable to travel. Through the laughter, smiles, tears and grimaces you all stood by me, and in many cases hiked by me across this state and I appreciate each one of you.

I would like to acknowledge my principal investigator Dirk Dittmer for providing the resources to conduct experiments in his lab at UNC. I want to thank all of the members, past and current, of the Dittmer lab who helped me on my way, whether it was providing scientific insight or just eating lunch together, I appreciate you all. I am grateful for my thesis committee for challenging me and asking good questions, as well as providing feedback. Thank you all for helping me grow as a scientist and as a person. Nat Moorman, Cary Moody, Jason Whitmire and Blossom Damania, you all were a great committee and I enjoyed our committee meetings, after the fact. Additionally, I would like to thank Dixie

Flanner who was an amazing student service manager and to Michelle Hightower who took up Dixie's mantle. I never would have had all the paperwork done without the reminders!

Finally, I want to thank my funding sources, the virology training grant as well as the NIH grants that supported this work. Since all of my funding comes from taxed income, it is really the hard-working taxed American workers to whom I owe my acknowledgements here. May some of the knowledge gained by this funding compensate the people who funded it and make a difference at large.

TABLE OF CONTENTS

LIST OF TABLES

LIST OF FIGURES

LIST OF ABBREVIATIONS

AIDS	Acquired immunodeficiency syndrome
BCR	B-cell receptor
BL	Burkitt’s lymphoma
BTK	Bruton's Tyrosine Kinase
CHOP	Cyclophosphamide, doxorubicin, vincristine and prednisolone
CRISPR	Clustered regularly interspaced short palindromic repeats
CTG	CellTiter-Glo® Assay
DLBCL	Diffuse large B-cell lymphoma
DMEM	Dulbecco modified Eagle medium
DMSO	Dimethyl sulfoxide
DNA	Deoxyribonucleic acid
EBV	Epstein–Barr virus
FADD	Fas-associated protein with death domain
FBS	Fetal bovine serum
FLICE	FADD-like IL-1β-converting enzyme
HAART	Highly active anti-retroviral therapy
HEK 293	Human embryonic kidney cells 293
HHV-8	Human herpesvirus 8
HIV	Human immunodeficiency virus
HL	Hodgkin's lymphoma
Hpi	Hours post infection
HSV1	Herpes simplex virus 1

IFN	Interferon
IL	Interleukin
IL-1β	Interleukin-1 beta
IL1R	Interleukin-1 receptor
IL-6R	Interleukin-6 receptor
IKK	IκB kinase
IRAK	Interleukin-1 receptor-associated kinase
JAK	Janus kinase
KICS	KSHV-associated inflammatory cytokine syndrome
KS	Kaposi's sarcoma
KSHV	Kaposi's sarcoma-associated herpesvirus
KSHV-MCD	KSHV-associated multicentric Castleman's disease
LANA	Latency-associated nuclear antigen
MCD	Multicentric Castleman's disease
MOI	Multiplicity of infection
MYD88	Myeloid differentiation primary response 88
NFκB	Nuclear factor kappa-light-chain-enhancer of activated B cells
ORF	Open reading frame
PAMP	Pathogen associated molecular patterns
PBMC	Peripheral blood mononuclear cell
PBS	Phosphate-buffered saline
PEL	Primary effusion lymphoma

Pen-Strep	Penicillin and streptomycin
RNA	Ribonucleic acid
RTA	Replication and transcription activator
RT-PCR	Real-time PCR
STAT	Signal transducer and activator of transcription
TANK	TRAF family member-associated NF-kappa-B activator
TRAF6:	TNF receptor associated factor
TBK	TANK-binding kinase
TLR	Toll Like Receptor
TNF	Tumor necrosis factor
UV	Ultraviolet
vFLIP	Viral FLICE inhibitory protein
vIL	Viral interleukin
WN	Waldenstrom macroglobulinemia

LIST OF SYMBOLS

α	Alpha
β	Beta
γ	Gamma
κ	Kappa

CHAPTER 1: INTRODUCTION

Introduction

In completion of my graduate studies in the laboratory of Dr. Dirk Dittmer, the following Dissertation will examine the relevance of the interleukin-1 receptor-associated kinase (IRAK) pathway in primary effusion lymphoma (PEL). The thesis will be broken into four parts starting with a broad introduction to cancer, PEL, IRAK and KSHV (chapter 1), followed by a chapter on experimental results from testing the function of the IRAK pathway in PEL. Chapter three will conclude and summarize the findings as well as provided a road map for moving this project forward. The final section will be an appendix that contains supporting information for chapter two.

Cancer and Viruses

Cancer is a global affliction that affects most living organisms (1-3). The rate of cancer in humans is high, as one in three individuals are diagnosed with a type of cancer during their lifetime, according to the American Cancer Society (4). There are over 130 types of human cancers, which have many different causes (NCI) such as exposure to harmful chemicals known as carcinogens, smoking, genetics, and environmental influences (5). Infectious agents, such as viruses, account for nearly 20% of all human cancer cases globally, and the scientific community's understanding of virus-induced human cancers continues to improve with advancements in sequencing technologies (6-10).

An important reason for this differentiation between virus-induced and non-viral cancers is that viruses introduce foreign genes into human cells and rely on disrupting host

pathways for survival of the infected cells. The viral genes can function as oncogenes, driving a normal cell into malignancy (7, 11, 12). Another distinction with virus-induced cancers is that viruses can be targeted with antivirals or vaccines, which changes the approach for treatment and preventive actions of non-viral cancers (6-8, 13). The interplay between the virus and the host is extremely important for cancer progression as only a fraction of individuals infected with viruses develop cancer, and only a small subset of viruses are known to cause cancer.

Cancers are caused by the dysregulating of cellular pathways. Typically, a single mutation will not cause cancer, instead it takes an accumulation of mutations over time (10, 14, 15). There are multiple steps of cellular dysregulation that occur throughout the course of a lifetime. An example would be a mutation in a tumor suppressor protein that is present in an individual who smokes, which induces new mutations that compound the effects of the inherited mutation, resulting in the development of lung cancer in the individual (16-18). This is only one example, however, and there are many known cellular pathways in humans that can function in cancer development, predisposing an individual to develop cancer. One such pathway that has been reported to predispose individuals to cancer is the IRAK pathway, which I will discuss later in this introduction (19-24). To understand the importance of the IRAK pathway in the context of this thesis, we must first understand KSHV, PEL and the concept of tumor plasticity.

Tumor Plasticity

Tumor heterogeneity is the genetic variation between malignant cells within a single patient (25). The heterozygote nature of tumors leads to resistance to treatment and cancer metastasis (26). Traditionally there were two main ideas for how this tumor heterogeneity

developed. One hypothesis was that of clonal evolution, or unique epigenetic/stochastic changes, which results in the development of tumor heterogeneity from individual cancer stem cells (25). The second hypothesis proposed was the cancer stem-like cell model, where a subset of the tumor cells have the ability to differentiate into various subtypes of cancer cells, causing variation within a tumor (27).

A recently developed model, known as the cell plasticity model, combines aspects of both the cancer stem-like cell and the clonal models (25). This new model predicts that, due to changes in the tumor environment, cancer stem-like cells can undergo clonal expansion and epigenetic differentiation while maintaining a subset in the cancer stem-like cell state. The result of this ability is that, in response to stressors in the environment, such as inflammation or injury, the various subtypes of the cancer cells can survive and lead to resistance to therapy. One of the largest drivers of the plasticity seen in tumor cells is the ability of self-renewing and dysregulation (28). Just a few examples of dysregulation that can lead to plasticity in a tumor are loss of tumor suppressor proteins (such as p53, RB1 and PTEN), increased inflammatory compounds that induce differentiation towards stem-like cells, and the ability of these stem-like cells to remodel the microenvironment by influencing the differentiation of non-tumor cells into cells that support tumor growth (25, 29).

A major problem with tumor cell plasticity is that it leads to resistance to targeted therapies. For example, targeted treatment of small-cell lung cancer leads to resistance, however, after a gap in treatment, the cells were re-sensitized to the drug (30), which demonstrates that the changes that lead to resistance are not always genetic. One of the best-documented cases of the plasticity model and cancer resistance to targeted therapies is in epithelial-mesenchymal transition, which results in phenotypical changes between cell types

and resistance to therapies (18, 31). The ability of tumor cells to undergo lineage plasticity results in drug ineffectiveness and allows the tumor to proliferate beyond control. Prostate cancer, small-cell lung cancer, breast cancer, and basal cell carcinoma are only a few examples where targeted therapies have been challenged by tumor plasticity (18).

The mechanism of drug resistance through plasticity is thought to occur when cells have inherent mutations that circumvent the target of the therapeutics, or when slow-growing cells bypass the pathway entirely through activation of alternate pathways (18, 32). Due to the complications of tumor plasticity, researchers must now seek to address these issues when developing targeted therapeutics. Concepts such as alternate dosing or combination therapies are currently leading the way to overcome tumor plasticity. Furthermore, the idea of tumor plasticity is important for this thesis as we examine the ability of tumor cells to circumvent inhibition of a host pathway in the context of a virus-induced lymphoma.

Kaposi's Sarcoma-associated Herpesvirus

Kaposi's sarcoma-associated herpesvirus (KSHV), also known as human herpesvirus 8 (HHV8), is one of two members of the gamma herpesvirus family known to infect humans, the other being the Epstein Bar virus (EBV) (6, 33, 34). KSHV is the causative agent of Kaposi's sarcoma (KS), primary effusion lymphoma (PEL), KSHV inflammatory cytokine syndrome (KICS), as well as cases of Multicentric Castleman disease (MCD) (35-38). The various aspects of the virus life cycle are crucial for understanding how these different diseases develop. The focus of this thesis will be on PEL, which will be discussed in the next section.

KSHV is an enveloped DNA virus with a large genome of approximately 165-kilo bases (39-41). KSHV encodes for approximately 85 proteins and microRNAs (36, 42-44).

Upon infection, the default programming of KSHV is to go into latency, where the viral genome is maintained as an episome tethered to the host genome by the latency associated nuclear antigen (LANA), making it difficult for the immune system to detect the virus (40, 45-47). KSHV must evade the cellular innate immune response to infect cells efficiently (48-50). During latency, only a subset of genes is expressed, LANA being one of those genes and having multiple functions including maintaining latency (11, 51-53). Another latency-associated protein is the vFLIP that engages the nuclear factor kappa-light-chain-enhancer of activated B cells (NFκB) protein and activates the downstream signaling pathway to promote a positive environment for latency (54-57).

The vFLIP activates the NFκB pathway by modulating the NF-κB-inducing kinase (NIK) as well as both the IKK2-independent and dependent processes to activate p100 NFκB thus providing pro-inflammatory signaling, a hallmark of KSHV diseases (55). This activation of the NFκB pathway has long been believed to be critical for PEL survival (54, 58-61). Additionally, vFLIP activation of NFκB is thought to inhibit the KSHV lytic cycle through activation of the AP-1 pathway, which down-regulates the KSHV ORF50 protein, the major lytic activator of KSHV (62). vFLIP also appears to inhibit cell death by competing with caspase 8 for binding death receptors (63). It has been shown that vFLIP is important to PEL survival, and studies conducted with the NFκB pathway inhibitor BAY11-7082 have supported this idea (54, 58, 61). However, additional research has determined that BAY11-7082 has off-target effects that can result in cell death independent of NFκB inhibition (64, 65). Upstream of NFκB is the IRAK pathway and toll like receptors (TLR) pathway, which are also known to exert effects on the KSHV life cycle in the context of PEL.

TLRs are innate immune sensors that recognize specific ligands and function in immunity by recognizing pathogens. TLRs, with the exception of TLR3, typically signal through the IRAK pathway to activate NFκB and stimulate innate immunity (66-72). TLRs, in the context of KSHV, signal through the downstream TRIF/TLR3 or MYD88/IRAK pathways (73). Within KSHV infection, TLRs have a function in reactivation from latency. The virus must overcome the TLR signaling cascade to establish infection (35, 74). The situation is complex, with KSHV activating some components of the pathway while shutting down others. Since most TLRs signal through IRAK1, KSHV encodes miR-K9, which down regulates IRAK1 during infection to dampen inflammation and establish latency (75). In primary infection of monocytes, KSHV infection results in activation of TLR3, which recognizes viral single stranded and double stranded RNA. The KSHV protein, ORF50, can degrade downstream effectors of TLR3 activation (35). The KSHV proteins, vIRF1 and vGPCR, inhibit TLR4 signaling during the advent of new infections, but during latency in KS spindle cells TLR4 activation is induced by the virus (76). If TLR7/8 are activated in cells that are latently infected with KSHV, it results in the reactivation of the virus (74). Therefore, we see that the interplay between the TLRs and KSHV is complex, with the degree of inhibition and activation depending on the life stage of the virus. We will next delve more into the PEL disease indication.

Primary Effusion Lymphoma

PEL is a non-Hodgkin's B cell lymphoma (NHL) characterized by effusions in the peritoneal, pleural, and pericardial cavities (77, 78). Phenotypically, PEL cells are larger than healthy lymphocytes, which aids in identification (39). PEL is primarily seen in HIV positive males with low CD4 counts, although cases of PEL in HIV negative individuals and females

have been reported (36, 78, 79). The medium life expectancy following a PEL diagnosis is 6 months (17, 80). PEL is currently treated with CHOP (cyclophosphamide, hydroxydaunorubicin, oncovin, and prednisone) therapy in most cases, which has limited success, as is evident by the short life expectancy (80). KSHV infected B-cells are responsible for PEL development, and it is thought that these cells are clonal and develop post germinal center (81). KSHV-EBV coinfections are common in PEL (34, 40).

PEL cells have distinct features, including expression of CD138/Syndecan-1 as well as no expression of the B cell receptor (BCR) or CD79 co-receptor (80), despite exhibiting plasmacytoid features. It is thought that viral proteins such as vGPCR, K1, and K15 provide for constitutive activation of PI3K and PLC-K resulting in cell proliferation and survival (35, 36, 56, 80, 82, 83). PEL expresses elevated levels of IL-10 and varying amounts of IL-6 in a cell line dependent manner (81, 84). Additional cytokines with high levels of expression in PEL are oncostatin and IL-6 soluble receptor (84, 85).

PEL can appear concurrently with Kaposi sarcoma (KS) or independently, suggesting that KSHV infection profoundly reprograms B-cell signaling in an alternate mechanism to Kaposi sarcoma, a disease primarily in endothelial cells (36, 39, 40, 86). It is important to note that *de novo* KSHV infection results in latency not lytic replication, which in turn results in the expression of latently expressed viral oncogenes (64). In addition to the latency genes, PEL depends on different host pathways that KSHV modulates to carry out the viral life cycle (73, 87-89).

One cellular pathway, studied extensively, is the mTOR pathway, which is required for PEL survival (87, 90-92).Viral proteins play a role in overriding the normal functions of host pathways for the benefit of the virus. LANA is known to be critical for PEL survival as well

as dysregulation of the immune response, such as blocking of p53 functions and upregulating ß-catenin (36, 40, 93). Another cellular pathway that is important for PEL survival and of interest to this thesis is the IRAK/NFκB pathway. The vFLIP is known to interact with the IRAK pathway by activating NFκB. The vFLIP is thought to aid in B-cell tumorigenesis, as was shown in mice (56, 94). Research has shown that HSP90 inhibition blocks vFLIP activation of NFκB and leads to cell death in PEL lines (95). Other work has shown that IKKγ mimetic peptides can lead to apoptosis in PEL (96). IKKγ is an upstream regulator of NFκB activation. To summarize, we see that PEL is an aggressive disease that causes dysregulation of cellular pathways and that KSHV infection is necessary but not sufficient for PEL development.

The IRAK-MYD88 Signaling Pathway

The IRAK pathway has important roles in innate immunity. When pathogens invade our bodies, cells can recognize various pathogen-associated molecular patterns (PAMP) (70, 73, 97). These PAMPs include bacteria lipids, virus RNA, and virus DNA to name a few. PAMPs are recognized by TLRs. Additionally, cells can produce cytokines when stimulated by PAMPS, which alerts the immune system and other cells in the environment of the infection. One such cytokine is interleukin-1 Beta (IL-1β), recognized by the interleukin-1 receptor (ILR1) (19, 98). There are 13 TLRs and 38 ILRs in humans (66, 99). Of these TLRs and ILRs, many signal through the IRAK pathway.

Table 1. 1 List of TLRs that can signal through the IRAK pathway.

TLR/ILR	TLR1	TLR2	TLR3	TLR4	TLR5	TLR6	TLR7	TLR8	TLR9	TLR10	IL1R
Signals through the IRAK pathway	Yes	Yes	No	Yes	Yes	Yes	Yes	Yes	Yes	Yes	Yes

When the IRAK pathway is activated by either TLR or ILR activity, a signaling cascade is initiated that results in the transcription factor NFκB being released to change cellular transcription and create a pro-inflammatory environment (19, 22, 100). For fighting infection in an acute response, activation of NFκB is good for the human body (20, 22, 70, 71, 97, 101). However, chronic inflammation due to NFκB can induce conditions such as arthritis and cancer (21, 22, 61, 97, 100, 102, 103).

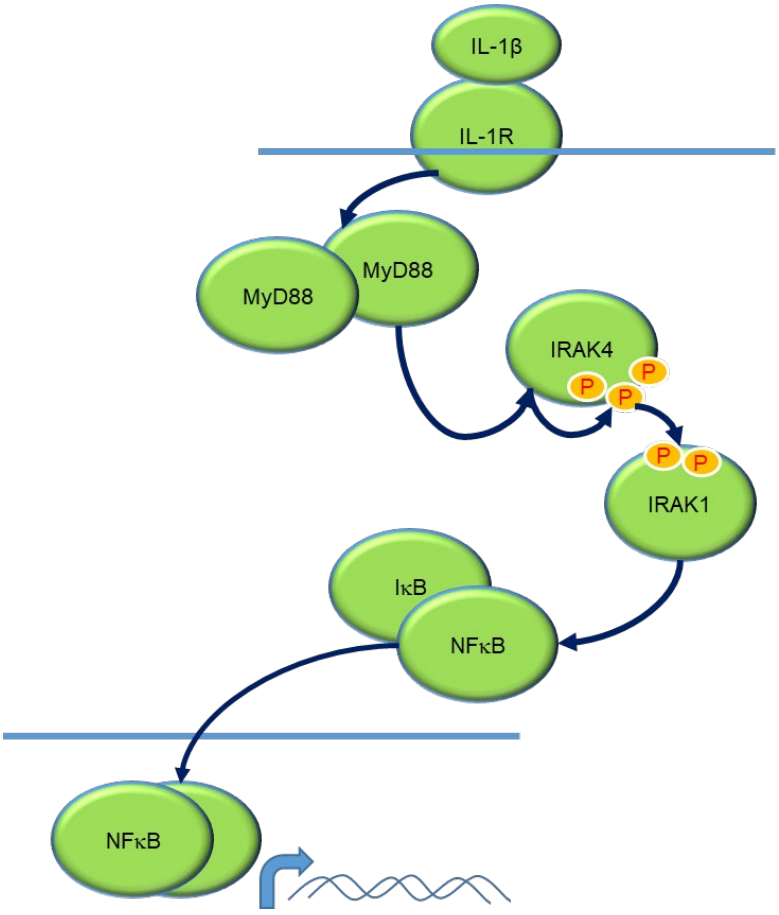

Figure I. 1: The IRAK pathway functions to activate NFκB.

Since inflammation is tightly controlled by various cellular pathways, it is important to understand how the IRAK pathway functions properly in healthy cells. Initially, a TLR or ILR is activated by a ligand. The receptors then dimerize, and this change in confirmation recruits the adapter protein myeloid differentiation primary response protein (MYD88) (69,

104). MYD88 recruits interleukin associated protein 4 (IRAK4) to the complex, which is phosphorylated upon recruitment (19). Phosphorylation of IRAK4 allows for interleukin associated protein 1 (IRAK1) to be recruited into the complex (105, 106). This MYD88-IRAK4-IRAK1 complex is known as the Myddosome, and its crystal structures has been solved (107). Following Phosphorylation of the IRAK1 activation site by IRAK4, IRAK1 undergoes hyper auto-phosphorylation, which causes its release from the complex and association with TRAF6 and TAK1 (19, 108-110). These two proteins are activated and remove the suppression of the IKK complex, allowing the release of NFκB (108, 111).

There are many variables within the IRAK pathway. The kinase activity of IRAK1 is not required for IL-1β signal propagation in some cell types (112). IRAK1 can activate STAT3, directly resulting in IL-10 transcription, which is dependent on kinase activity (113). IRAK-M is a negative regulator of the signaling pathway, preventing the phosphorylation of IRAK1 and IRAK4, but IRAK-M is primarily seen in monocytes and macrophages and is not expressed in B-cells (19, 100, 114). IRAK1 and IRAK4 are the most commonly expressed of the IRAK proteins in cancer cells (100). In T-cell acute lymphoblastic leukemia, inhibition of IRAK1-4 kinase activity resulted in cell arrest but not death (100). IRAK1 or IRAKM knockout mice had functional NFκB activity when stimulated with IL-1β. It is believed that IRAK2 compensates for the loss of IRAK1 in these situations; however, this is not the case in PEL (115, 116). IRAK2 is also linked to late-phase TLR response, whereas IRAK1 is present in early-phase TLR signaling (117). IRAK2 has expression levels near the detection limit in PEL whereas IRAK1 is highly expressed in PEL according to our RNA-seq data. Loss of both IRAK1 and IRAK2 results in the same inhibition of NFκB activation in response to IL-1β as an IRAK4 knockout (117). IRAK1 has also been shown in mouse

models to regulate type I Interferon production induced by TLR7 and TLR9 in distinct cell types (66). IRAK1 is known to bind and phosphorylate IRF7 in a TLR7 and TLR9 dependent manner, and the IRAK1 kinase activity is indispensable for phosphorylation of IRF7 (118). The IRAK pathway is complex and of its many players, each appear to have non-canonical functions. When the pathway is dysregulated, there can be extremely negative effects, which will be discussed in the next section.

IRAK-MYD88 and Lymphoma

In a subset of diffuse large B cell lymphomas, MYD88 L265P is an activating mutation that results in constitutive activation of the NFκB pathway and development of a more aggressive lymphoma (119-122). The L265P mutation is referred to as a driver mutation and 30% activated B-cell like (ABC), 60% central nervous system, 77% testicular DLBL, and upwards of 90% Waldenstrom's macroglobulinemia (WM) have this mutation (120, 123-125). The mutated MYD88 results in an increase in IRAK1 phosphorylation and NFκB activation (126). It should be noted that these numbers are contested by some research groups, who suggest that the percentage of MYD88 L265P cases are lower (127). Cells with the MYD88 L265P mutation also display increased levels of JAK/STAT signaling and activation of the Bruton's Tyrosine Kinase (BTK) pathway (119, 124).

Treating these L265P-mutant cells with an IRAK4 inhibitor was effective at reducing cellular proliferation, demonstrating that targeting the IRAK pathway could potentially serve as a drug target for certain lymphomas such as ABC-DLBCL (128). However, the members of the IRAK pathway have unique functions that depend on specific cell types and stimulations, which could also vary in different lymphomas depending on what stage of B-cell development the lymphoma is characterized by (100). It was also seen that knockdown

of MYD88 in WM decreased the BTK signaling that was associated with the MYD88 L265P mutation (129). In this case, MYD88 was shown to act synergistically with CD79B mutations in the activation of NFκB, resulting in BTK inhibitor resistance (120).

The IRAK pathway is also activated in other systems such as acute myeloid leukemia (AML) in which IRAK1 is overexpressed and hyper-phosphorylated at the T209 activation site (22, 130). In head and neck cancer, IRAK1 promoted cell survival and the inhibition of IRAK1 resulted in cell death (131). An analysis from the cancer genome atlas, performed in 2017, demonstrated that IRAK1 has a role in cellular dysregulation and contributes to several other cancers such as melanoma, lung cancer, and breast cancer, by stimulating downstream proinflammatory pathways (132, 133). We have covered how two separate IRAK pathway members, MYD88 and IRAK1, have a role in cancer development and will next turn to the interplay between the IRAK pathway, KSHV, and PEL.

The Interaction between KSHV and the IRAK Pathway

This section will highlight the interplay between IL-1β and KSHV, as well as discuss the IRAK pathway as studied in PEL. IL-1β is a cytokine that relays its signal through the IRAK pathway, activating NFκB (19). KSHV is known to produce a pro-inflammatory environment by activating the NFκB pathway during latency (134). Activation of cells by IL-1β also activates the NFκB pathway.

The Dittmer group demonstrated that IRAK1 has a conserved SNV in 15 out of 16 sequenced PEL samples (135). This SNV, rs1059702 (F196S), is reported to increase basal levels of NFκB, produce a worse outcome of sepsis, and increase the risk of autoimmune diseases (136-140). The high prevalence of this SNV that results in enhanced NFκB signaling is very similar to what is seen with the MYD88 L265P mutation, which lead the Dittmer

group to explore this pathway, eventually culminating in this thesis work. Preliminary research involving inhibitors and shRNA suggested that IRAK1 was essential for PEL survival (135). However, with the advancement of CRISPR and a greater understanding of the field, our hypothesis has changed to conclude that the IRAK pathway is important for the development of PEL but can be circumvented once the virus is established and the disease has progressed.

In KSHV-associated multicentric Castleman disease (MCD), KSHV can induce clinical flair-ups of IL-1β production (141). Yet, KSHV encodes for microRNAs that target both IRAK1 and MYD88, helping the virus to control this inflammatory pathway and it was demonstrated that KSHV RTA was able to degrade the TRAF protein, blocking IL-1β signaling during reactivation of the virus (40, 76, 142-144). IL-1β has a protective effect on serum-starved AIDS-KS cells, protecting them from apoptosis (145). These apparent contradictions suggest that the interplay between KSHV and IL1 signaling is complex and not yet fully understood.

PEL primarily occurs in HIV infected individuals, and it has been shown that HIV infection raises the levels of IL-1β, which can enhance KSHV infection (146-148). Closer examination of KS demonstrated that IL-1β induced an autocrine growth factor loop leading to uncontrolled cellular growth (149). Increased IL-1β levels are also associated with KSHV/EBV co-infected PEL cases (86). It is likely that IL-1β serves an important function during the PEL disease progression, both paracrine acting on the tumor microenvironment and paracrine acting of PEL. Thus, clinically we can see the importance of IL-1β in many aspects of KSHV infection, as well as the importance of the IRAK pathway.

In the case of PEL, the scientific community has long held the view that NFκB was crucial for PEL survival and that vFLIP was largely responsible for activating NFκB. Inhibitor studies using the IKK inhibitor, BAY11-7082 , gave supporting evidence to this view as did shRNA studies on vFLIP (58, 61, 64). However, as inhibitors were further studied, the off-target effects of BAY11-7082 were seen to be mainly responsible for PEL cell death (150, 151). The traditional viewpoint that one protein, such as NFκB, could be a silver-bullet therapeutic target has been rebutted as a greater understanding of tumor plasticity developed (18, 25). In 2018 Manzano *et al.* group released a genome-wide CRISPR knockout screen conducted in BCBL-1 cells, a PEL tumor line, that demonstrated no individual member of the NFκB pathway was required for PEL survival (12). The result of this screen aligns with the plasticity model of cancer and is reshaping the view on the NFκB/IRAK pathway within the KSHV/PEL field. Multitarget therapeutics will most likely be more effective at treating PEL. Resistance to multitarget therapy would be less likely to develop, which would explain the effectiveness of BAY 11 off-target effects. Of the downstream genes turned on by NFκB activation, two of the most important for PEL are IL-10 and IL-6.

Interleukins in KSHV Infection and Disease

Two important human cytokines that influence KSHV infection and disease are IL-10 and IL-6 (84, 85). First, dysregulation of IL-10 is associated with the survival of cancers and lymphomas as it provides proliferation and anti-apoptotic signals (152). Second, IL-10 is linked to immune evasion for intracellular pathogens such as *Tuberculosis* and *Leishmania* through inhibition of MHC-II *(152, 153)*. Both IL-10 and IL-6 can activate the JAK-STAT pathway, which is associated with cell survival and proliferation (153, 154). IL-6 functions in

promoting lymphocyte migration and is expressed at high levels in human serum in various disease such as KS. Dysregulation of IL-10 and IL-6 occurs across all four KSHV-related diseases: KS, PEL, KICS, and MCD as discussed below.

KSHV is responsible for the increase of IL-10 and IL-6 expression in PEL (155-157). In one study, 19 PEL patients were compared with 20 HIV-associated DLBCL cases, and the PEL samples had elevated IL-10 and IL-6 levels when compared to the DLBCL (158). When comparing classic KS with AIDS-associated KS, higher levels of IL-10 were observed in AIDS-associated KS. Of the AIDS-associated KS, the highest levels of IL-10 were in individuals with the most aggressive disseminated KS lesions (159). In KS lesions, the TLR4 pathway is constitutively active and results in increased IL-6 levels and STAT3 activation (160). Both KICS and MCD are characterized by high levels of IL-6 and IL-10 (161). In one study conducted on KICS, IL-10 and IL-6 levels were evaluated for all ten individuals (males that were HIV positive). These patients had an increased risk of death, lower hemoglobin and albumin, and displayed increased C-reactive protein levels (162).

MCD can be divided into HIV negative and HIV positive cases, with better outcomes for those who are HIV negative (163). Approximately 50% of MCD patients have uncontrolled KSHV infections (164). KSHV viral load, vIL-6, IL-6, IL-10, TNF and IL-1β are used to evaluate KSHV+ MCD (141, 165-167). In KSHV+ MCD, gene expression is less regulated than is typically observed in KS. This lack of KSHV gene regulation in MCD leads to increased activation of vIL-6 (168, 169). vIL-6 or IL-6 can work together or independently to cause MCD flares (141). In KSHV+ MCD, a subset of patients developed hemophagocytic lymphohistiocytosis, a severe condition linked with IL-6 levels (165).

KSHV encodes a homolog of IL-6, vIL-6, which shares 25% homology with IL-6. vIL-6 binds directly to the gp130 receptor without the need of the IL-6R co-receptor that is required for IL-6 signal relay (170). KSHV vIL-6 can activate cells that do not respond to IL-6 (171). N-linked glycosylation is required for optimal vIL-6 function (172, 173). Two KSHV proteins, vIL-6 and vGPCR, are linked to upregulation of Angiopoietin-2, a secreted proangiogenic and lymphangiogenic (174). KSHV RTA binds to and activates the IL-10 promoter in collaboration with human specificity proteins 1 and 3 (175). KSHV vFLIP can block lytic replication by inhibiting RTA, yet RTA activation of vIL-6 is not inhibited (176). Epigenetic modifications are important for the function of vIL-6 because, during latency in PEL, the vIL-6 promotor is in an open chromatin formation but it differs in each viral episome (177, 178). KSHV encodes a viral endonuclease, SOX, which degrades cellular mRNA. Notably, IL-6 mRNA is protected from this degradation through a 3' untranslated region (179). Tumor associated macrophages have been seen to play an important role in PEL disease progression (180).

In PEL cells IL-10 has a role in HSV1 induced reactivation of KSHV (181). EBV has a homolog of IL-10 (vIL-10) (182, 183). Infection of endothelial cells with KSHV activates IL-10, IL-6 and IL-13, which results in the development of monocytes into tumor-associated macrophages (180). Binding of KSHV to dendritic cells (DC) resulted in increased levels of IL-10, IL-6, and IL-23, which activated STAT3 and blocked autophagy in the DC cells. This could allow for the establishment of KSHV and the development of KSHV associated diseases (184).

In addition to viral proteins, KSHV encodes viral microRNAs that interact with these pathways. KSHV miR-K12-3 can regulate IL-10 expression and suppress STAT3 and

STAT5 (185, 186). Using bioinformatics, KSHV miR-K12-3 and miR-K12-7 were shown to target the 3'UTR of the transcription factor C/EBPβ, which regulates IL-6 and IL-10. Follow-up experiments revealed that these two miRNAs reduce expression of the C/EBPβ protein (187). During development of tumorigenesis, the KSHV miR-K12-1 activates NFκB and thus indirectly STAT3 (188). KSHV miR-K-10b and miR-K-12-12* have elevated levels in patients with sepsis. These miRNAs were also elevated postoperative but returned to normal after 7 days. KSHV miR-K-10b and miR-K-12-12* acted against TLR8 and are thought to have a function in increased IL-10 and IL-6 levels (189). Exomes are known to carry host and KSHV miRNAs. When exosomes were harvested from PEL effusions and used to treat endothelial cells, an increase in IL-6 and cellular migration was observed (190).

When mice were generated with inducible vFLIP in endothelial cells, KICS symptoms developed including increased IL-6 and IL-10 levels (191). The mouse KSHV homolog, murine gamma-herpesvirus 68 (MHV68) M2 protein, was shown to activate IRF4 and, in turn, IL-10, resulting in enhanced proliferation and survival (192, 193). When mice where engineered to express vIL-6, MCD symptoms quickly appeared, however, when vIL-6 mice were made in a IL-6 KO background, no symptoms appeared, leading to the conclusion that both vIL-6 and IL-6 are required for development of MCD (194).

When measuring disease function in KS patients treated with Omega3 fatty acid (Fish oil), there was a slight reduction in IL-6 levels (195). Studies have combined inhibitors PEP005 (protein kinase C activator) with JQ1 (bromodomain and extra-terminal inhibitor) and this resulted in a reduction of IL-6 in PEL cells while reactivating the virus (196). Treatment of MCD has been advanced by targeting CD20 with rituximab combined with virus reactivation drugs, zidovudine and valganciclovir, and has increased the one year

survival rate to around 85% (197, 198). Tocilizumab, a monoclonal antibody against IL-6, has also been used to successfully treat MCD (199). Adding liposomal doxorubicin with rituximab causes a decrease in KSHV viral load, vIL-6, IL-6, C-reactive protein, and serum immunoglobulin (200). In 2014 the FDA approved siltuximab for the treatment of MCD (201). Even when KSHV MCD is successfully treated, the patients remain at risk of developing NHL (201).

CRISPR in PEL

Clustered Regularly Interspaced Short Palindromic Repeat (CRISPR) is a bacterial defense system that degrades invading phage DNA (202). The mechanism of CRISPR relies on RNA "PAM and guides" that recognize the invading phage genome coupled with a CRISPR-associated endonuclease (Cas) protein that cuts the target DNA, thus neutralizing the phage threat. This technique has been modified for use in mammalian cells by making guide RNAs (gRNA) that can target specific DNA sequences and when used with expression of a Cas9 protein, produce cuts in the DNA (202). The CRISPR technique is now extensively utilized and has been applied to create knockouts as well as gene knock in cell lines and model organisms.

One CRISPR technique is to generate stable Cas9 expressing cells through lentivirus transduction and selection, followed by a second lentivirus transduction with a gRNA under the control of a different selection marker. This technique was the system used in this thesis. A second CRISPR method uses lentivirus to deliver a construct that has the Cas9 and the guide together, however, this system was not as adaptable for PEL in this study (34). A third mechanism to employ CRISPR is to transfect the plasmids into cells and sort/select for cells that have the plasmid using flow cytometry and a fluorescent tag. Primarily, when working

with CRISPR, clonal populations are generated. For short-term effects and whole genome CRISPR screens, this third technique can be useful. The PEL cell lines that we studied in this thesis are derived from B-cells, and as such, we determined that the two-step system described in the first technique would provide the best results since B-cells can be challenging to work with.

One of the first CRISPR experiments applied to KSHV was conducted by knocking out cellular genes encoding for the ALX/FPR proteins in U2OS cells and infecting these lines with KSHV to observe whether these proteins functioned in infection (203). This method, however, was not conducted in PEL cells, and U2OS cells are easily transduced and transfected unlike PEL, which can be difficult to manipulate. Previous research in the Dittmer lab transfected CRISPR plasmids that targeted the Epstein-Barr virus (EBV) genome into KSHV/EBV co-infected PEL cell lines (34). Using this method, *Bigi et al* demonstrated that, in KSHV/EBV co-infected PEL cells, the loss of the EBV genome resulted in decreased viability of PEL cells (34).

In 2018, as mentioned prior, Manzano *et al.* published results from a genome- wide CRISPR screen in BCBL-1 cells (12). The initial results of this study examined pooled cells, not clones, as we do in this thesis. The authors later used clonal populations to verify that members of the NFκB pathway were individually dispensable. Manzano *et al.*, as in this thesis, also opted to use the two-part CRISPR system with the initial establishment of Cas9 positive cell lines. Since the 2018 screen, several more papers have been published by Manzano *et al.*, confirming the results of the CRIPSR screen and demonstrating the usefulness CRISPR in PEL studies (12, 204, 205).

At the time of writing of this thesis, the most recent application of CRISPR in PEL was using a one-part system with the Cas9 and two guides that target the KSHV protein, ORF57, transduced into BCBL-1 cells (206). Similar to what *Bigi et al.* showed when targeting EBV, after ORF57 was eliminated from BCBL-1 cells, the KSHV episome was destabilized (34, 206). Therefore, we see that although CRISPR is being used to study PEL, the techniques and methods are different, varying in the delivery system, host versus virus targets, and clonal versus pooled read outs following the CRISPR. The research in this thesis advances the study of PEL using CRISPR. In conclusion, CRISPR is a powerful tool to examine cellular pathways, and we adapted it to study the IRAK pathway in the context of PEL in this thesis.

In summary, this chapter has introduced how cancer can be induced by viral infections, KSHV being one such virus. We have discussed PEL and the severity of the disease, as well as the aberrant host pathways of PEL cells, particularly the IRAK pathway. This chapter also summarized what is known about dysregulation of the IRAK pathway in other systems, and it concluded with the importance of IL-1β in the KSHV life cycle during infection, detailing the relationships between the IRAK and NFκB pathways and KSHV.

CHAPTER 2: IRAK SIGNALING IN KSHV INDUCED PEL[1]

Importance

100% of Primary effusion lymphoma (PEL) cases are associated with Kaposi Sarcoma-associated herpesvirus (KSHV). PEL cell lines, such as BCBL-1, are the workhorse for understanding this human oncovirus and the host pathways that KSHV dysregulates. Understanding their function is important for developing new therapies as well as identifying high-risk patient groups. The MYD88/IRAK pathway, which has pro-growth functions in other B cell lymphomas, has not been fully explored in PEL. By performing CRISPR/Cas9 KO studies targeting the IRAK pathway in PEL, we were able to determine that established PEL cell lines can circumvent the loss of IRAK1, IRAK4, and MYD88; however, the deletion clones are deficient in IL-10 production. Since IL-10 suppresses T cell function, this suggests that the IRAK pathway may serve a function *in vivo* and during early-stage development of PEL.

Introduction

Primary Effusion Lymphoma (PEL) is a currently incurable B cell lymphoma. The medium survival time is estimated at 6 months following diagnosis. Kaposi's Sarcoma-associated herpesvirus (KSHV) is the etiological agent of PEL. Unlike the Epstein-Barr virus (EBV), KSHV infection of primary human cells in culture does not cause transformation.

[1] Jedediah Seltzer, Razia Moorad, Jason Schifano, Justin Landis, and Dirk P. Dittmer. 2020. Interleukin-1 Receptor Associated Kinase (IRAK) signaling in Kaposi Sarcoma-associated herpesvirus (KSHV) induced Primary Effusion Lymphoma. J Virol. 2020 Mar 11. pii: JVI.02123-19. doi: 10.1128/JVI.02123-19.

This suggests that host cell mutations are required to explain the PEL phenotype, in addition to virus infection (207). As with all other cancers, these host mutations can be inborn, existing prior to KSHV infection, or they can develop under selection during tumor evolution. Tumor suppressor genes, such as p53 and Rb, exemplify the former and the latter are demonstrated by BCL6 and c-Myc, which become activated during germinal center passage of B cells and contribute to Burkitt lymphoma (10).

PEL is observed primarily in end-stage AIDS patients, although isolated cases of PEL have also been reported in HIV-negative patients (reviewed in (36)). Most PEL cases arise in males. PEL manifests as effusions in body cavities such as the peritoneum. Several PEL effusions gave rise to culture-adopted cell lines, such as BC-1 (208) and BCBL-1 (209). During initial outgrowth, these cell lines depended heavily on autologous human serum but later adapted to growth in solely fetal bovine serum. PEL persists in a highly inflammatory environment, often with concurrent microbial infections. Markers of inflammation, such as IL-10, precede lymphoma development in AIDS patients, and IL1-β is one of the cytokines that is elevated in KS lesions as well as in KSHV-associated multicentric Castleman's disease (MCD) (141, 210-213). It remains unknown how this inflammatory microenvironment shapes PEL tumor initiation and growth. This represents a gap in our knowledge of KSHV biology. Understanding the impact of predisposing genome variants in inflammatory signaling pathways may uncover novel targets of intervention and/or prevention for PEL.

The Interleukin 1 Receptor Associated Kinase 1 (IRAK1) functions in the MYD88/IRAK pathway, an immune signaling pathway that relays signals from Toll-like receptors (TLRs) and Interleukin receptors (ILRs) (19, 71, 214). When one of these receptors

recognizes a ligand, the receptors dimerize, resulting in the recruitment of the adapter protein MYD88. MYD88 then recruits Interleukin 1 Receptor Associated Kinase 4 (IRAK4), which undergoes auto-phosphorylation and activation. IRAK4 recruits IRAK1 to form a large complex composed of multimerized MYD88, IRAK4 and IRAK1 proteins, termed the "Myddosome" (215). There are two additional Interleukin 1 Receptor Associated Kinases: IRAK2 and IRAKM. IRAK2 has recently been shown to have limited kinase activity and IRAKM is an inhibitory protein, which is not expressed in PEL (103, 117, 135). IRAK4 phosphorylates IRAK1, which induces IRAK1 auto-phosphorylation at T209 and release from the "Myddosome" (19, 216). Phosphorylated IRAK1 activates TRAF6/TAK1, translocating p65/RELA into the nucleus and activating multiple NFκB responsive genes. IRAK1 is then either degraded or marked for nuclear transport through K48 or K63 ubiquitination respectively (19, 115, 217). IRAK1 is necessary and sufficient for IL-1β signaling in most cells, including B cells (71, 130). There are, however, cell lineages that deviate from this rule, where IRAK2 can substitute for IRAK1 (100), or where the presence of the IRAK1 protein is required but not its kinase activity (19). Additionally, MYD88 can signal through other downstream adaptors in addition to IRAK1/4, depending on the nature of the trigger (216, 218, 219).

MYD88 sometimes harbors a mutation, L265P, pertinent to B cell lymphoma. L265P results in constitutive activation of the IRAK pathway in a fraction – 44-75% subtype specific – of diffuse large B cell lymphoma cases, and over 85% of Waldenstrom's macroglobulinemia cases (WM) (123, 220-224). WM is of post-germinal center lineages, like PEL, and has features of both plasma cells and lymphoid cells. Treating WM cells with an IRAK4 inhibitor or a MYD88 inhibitor was effective at reducing cellular proliferation,

demonstrating that the IRAK pathway could potentially serve as a drug target for WM (128, 225-227). In this study, we set out to understand the IRAK pathway in PEL, and to test the hypothesis that this pathway could, as in WM, be exploited as a therapeutic target.

Methods

Cell Culture: Suspension cell lines were cultured in RPMI 1640 (Gibco), and adherent cells were cultured in DMEM (Gibco). Both mediums were supplemented with 100 U/mL penicillin-streptomycin (Gibco), 2 mM L-glutamine (Gibco), and 10% "Fetalgro" Bovine Serum (VWR). Stable Cas9-transduced BCBL-1 cells were maintained in 10 μg/mL Blasticidin. Cells were maintained at 37°C in 5% CO_2 and passaged for no more than 3 months at a time. All cell lines were obtained from the ATCC. For STR typing, cell pellets were submitted to Genetica DNA Laboratories, Burlington, NC using the PowerPlex®16HS assay (Promega) to provide results for 16 genetic test sites. Results were compared to reference data from ATCC. All cells underwent periodical mycoplasma testing (Lonza, LT07-701).

Lentivirus production: Lentivirus particles were produced in 293T cells using ViraPower (Thermo-Fisher, #K497500) or purchased from Millipore Sigma Sanger clone library. All plasmids used in the lab are assigned a unique identification number known as a pDD number. CRISPR plasmids were obtained from Millipore Sigma: pDD2160-61 (IRAK1, #HS5000019451-2), pDD2162-63 (MYD88, #HS5000001249-50), or from Addgene: pDD2125 (Cas9, #52962), pDD2126 (EV, #52963), pDD2127-29 (IRAK4 guides #75664-6). Packaging mix and transfer plasmid were co-transfected into 293T cells using ViraPower,

according to the manufacturer protocol. Virus particles were harvested 48-72 hours post-transfection, filtered, aliquoted, and stored at -80°C until use.

Stable Cas9 cell line generation: A Cas9 expression plasmid was obtained from Addgene (#52962). This Cas9 is under constitutive expression in mammalian systems. 293T cells were transfected with the Cas9 plasmid and ViraPower mix as described in previous section. Cas9 lentivirus were harvested and BCBL-1, BC-1 and BJAB cells were inoculated with the Cas9 lentivirus. Following spinfection positive Cas9 stable cells were selected using 10 μg/mL Blasticidin selection. Stable Blasticidin resistant cells were probed by western blot for Cas9 expression and used in all CRISPR experiments.

Spinfection procedure: For purchased particles, 50,000 cells were plated in 24-well plates with 100 μL of serum free media. 200 μL of particles, MOI of 5 (Particle titers determined by manufacturer using a p24 assay) were added with 10 μg/mL polybrene. The plates were centrifuged for 90 minutes at 1,500 RPM (1000 x g). Media was changed 18 hours following centrifugation. Selection media, containing 2.5 μg/ml of puromycin, was added 24 hours post centrifugation. Half of the cells were plated into three 1 mL colony formation assays for single cell clone selection; see colony formation assay methods. Trypan Blue (Millipore Sigma, #T8154) cell counting was used for all growth proliferation assays and live/dead cell counting.

CRISPR Knockout: For CRISPR KO, we used the same spinfection protocol as mentioned previously and performed a second spinfection with a second guide on the same target cell population. Following the second spinfection, 5,000 cells were plated in a 1% methylcellulose medium with 2 μg/mL puromycin to select for single cell clones. After three weeks of growth, clonal colonies were selected and grown in 5 μg/ml puromycin media.

Flanking PCR and gel analysis on a Perkin Elmer LabChip GX Touch HT instrument validated CRISPR cutting. PCR primer sequences for CRISPR validation are as follows, IRAK1-F: 5'-CCTCTGGCCTCACCTGGA, IRAK1-R: 5'-CAGAACGCTGACCTGGAGTG, IRAK1-FB: 5'-TGGTGTGCGGTCTGAAGC, IRAK1-RB: 5'-CTTCGCTTCGAGAGCCTCA, MYD88-F: 5'-GCTGAACTAAGTTGCCACAGGA, MYD88-R: 5'-GAGCTTACCTGGAGAGAGGC, IRAK4-F: 5'-ACTGGAAAAAGTCCCACTTCTGA, IRAK4R: 5'-ACTTTCTTACAGCCTAAGCCAGA, IRAK4-FB: 5'-ACTGGCTGAAAAGAGAAGTATTTGC, and IRAK4-RB: 5'-GGCAACCCAGTTGTTGACAT.

Western blotting: One million cells were harvested; lysed with 100 µL "RIPA" buffer (150 mM NaCl, 1% Triton X, 0.1% SDS, 1% Na-Deoxycholate, 50 mM Tris pH 7.4, H2O); supplemented with protease inhibitor cocktail (Millipore Sigma, P8340), 30 mM beta glycerol phosphate, 50 mM NaF, 1 mM Sodium Orthovanadate, and Benzonase Nuclease (Millipore Sigma, 712053); and incubated for 30 minutes on ice, with 15 seconds of vortexing every ten minutes. Depending on the assay, 10-15 µL of cell lysate, normalized by cell counts or Bradford Assays, was loaded onto 10% SDS-polyacrylamide gel, separated by electrophoresis, and transferred to a PVDF membrane (Millipore Sigma, GE10600023). Membranes were blocked using 10% milk or OneBlock (Genesee 20-313). Anti-Actin rabbit and mouse (#4970 & #3700), MYC-Tag (#2272), IRAK1 (#4504), MYD88 (#4283), NFκB p65 (#8242), and NFκB Pp65 (#3022) were purchased from Cell Signaling. Anti-IRAK4 (#AF3919) was purchased from R&D systems. HRP-conjugated rabbit and mouse secondary antibodies (Vector Labs, #PI-1000 & #PI-2000) were used to detect western signals and

developed using Pierce ECL western blotting substrate (Thermo-Fisher, #32106) on film (Genesee, #30-810L) or with Clarity ECL (Bio-Rad, #1705061) on a ChemiDoc (Bio-Rad) or iBright (Thermo-Fisher) imaging device. For the p-NFκB (p65) western blots, samples were harvested 10 minutes after stimulation with 1 ng/mL of TNF-α or IL-1β.

Colony Formation Assay (CFA): Cells were plated in 6-well dishes in triplicate using 10% FBS, complete RPMI media, 1% methylcellulose, and 2 μg/mL of puromycin to select for stable knockouts. Light images of wells were obtained 3 weeks after plating, using 10X magnification. The number of colonies was quantified using ImageJ software.

NFκB reporter assay: 3 μg of Pglo44 NFκB driven luciferase reporter plasmid (Promega), pDD3209, was nucleofected into 1 million cells using 100 μL Ingenio electroporation solution (Mirus, #MIR50117) and the Lonza 4D nucleofector. Cells were stimulated with 1 ng/mL TNF-α, IL-1β, or PBS 24 hours post-transfection. The luciferase values were measured after 6 hours. ONE-Glo (Promega, #E6120) firefly reagent was used, and activity was measured using a FLUOstar Optima plate reader (BMG Labtech). We used the same set-up as above to test the effects of inhibitors on luciferase production. 15 minutes before stimulation with IL-1β, IRAK inhibitors were added to the plate at 100, 50, and 25 μM. The NFκB reporter assay was performed at 6 hours post IL-1β stimulation.

IRAK1 complementation: We obtained three IRAK1 expression plasmids from Origene: pDD1951 (#RC221544, PEL phenotype full length IRAK1), pDD1952 (#RC224107, IRAK1 isoform B), pDD1953 (#RC204869, IRAK1 isoform C), and the empty vector control pDD1957 (EV, pCMV6-entry). Blue Heron Biotech synthesized three additional IRAK expression plasmids based on the same pCMV6 vector: pDD2147 (kinase dead non-PEL IRAK1), pDD2148 (IRAK1 non-PEL), and pDD2149 (PEL IRAK1 kinase dead). 3 μg/μL

plasmid was nucleofected into 1 million cells using 100 µL Ingenio solution (Mirrus) and the Lonza 4D nucleofector. Western blots were performed 48 hours post transfection. For the complementation experiment to test NFκB signaling, we co-transfected the expression plasmid pDD3209 with Pglo44 NFκB plasmid (Promega), stimulated 24 hours after nucleofection, and viewed as described in the reporter method above. WT, ΔIRAK1, ΔIRAK4, and ΔMYD88 cell lines were all tested in this manner. All plasmids were sequence verified by complete plasmid sequencing on the Ion Torrent S5 platform at the UNC Lineberger Vironomics Core (https://www.med.unc.edu/vironomics/).

Inhibitor EC50 assays: For generating IRAK, NFκB, BTK, and MYD88 inhibitor EC50 values, serial dilutions of the inhibitors were added to 96 well plates containing 5,000 cells per well and incubated for 48 hours. After 48 hours, cell viability assays were carried out using CellTiter-Glo® 2.0 Luminescent Cell Viability Assay (Promega, #G9242) per manufacturer instructions. Luminescence was measured at 560 nm using the FLUOstar Optima (BMG Lab Tech). EC50 values were calculated using the R package DRC (version 3.5.3). Inhibitors used in this study were as follows: inh1 (CAS No: 1042224-63-4), inh2 (CAS No: 928333-30-6), inh3 (CAS No: 1012343-93-9), inh4 (CAS No: 1012104-68-5), inh6 (CAS No: 1042672-97-8), inh1-4 (CAS No: 509093-47-4), BAY11-7082 (CAS No: 19542-67-7), STAT2825 (CAS No: 894787-30-5), Acalabrutinib (CAS No: 1420477-60-6), AVL-292 (CAS No: 1202757-89-8), and Ibrutinib (CAS No: 936563-96-1).

Inhibitor KINOMEscan: We obtained KINOMEscan profiles from DiscoverX-Eurofins for each of the six IRAK inhibitors used in this study, which screened each inhibitor at 50 and 250 nM concentrations against 480 human kinases. From this profiling, we were able to generate specific kinase profiles for each inhibitor.

RNA-sequencing analysis: 1 million cells were harvested, flash frozen in TRIzol (Invitrogen, 15596026), and shipped on dry ice to Novogene for Illumina-based RNA-sequencing. Raw sequence data fastq files were imported into CLC genomics workbench (Qiagen, version 12). Read alignment was performed using default parameters, where reads were annotated by their genes as well as transcripts from annotations on the Homo sapiens (hg38) sequence mRNA. The resultant gene expression (GE) tracks were used as input for further analysis and to generate figures in R (version 3.5.3 (2019-03-11)) and Bioconductor v3.10 using DESeq2(228). Heat maps illustrating the gene expression for the WT and clones treated with IL-1β and IL-1β + inhibitors were generated on CLC genomics, using the GE tracks as input. The Hierarchical clustering was performed by measuring the Euclidean distance between clusters, which were defined by their average linkage. Filtering was performed based on a fixed number of features, with a minimum of 10 and a maximum of 100 genes. All reads were submitted to SRA under PRJNA590509 https://www.ncbi.nlm.nih.gov/sra/PRJNA590509.

Exome sequencing and mutation calling analysis: DNA was extracted from 1 million cells using a MagNA Pure Compact nucleic acid isolation I large-volume kit (Roche 3730972001) and quantitated by Qubit 3.0 double-stranded DNA (dsDNA) high-sensitivity (HS) assay (Life Technologies). Barcoded exome sequencing libraries were prepared from 100 ng DNA following Life Technologies protocol MAN00009808 Rev: A.0. with an Ion AmpliSeq Exome RDY library preparation kit (Life Technologies A38262) (92). Samples were sequenced on the Ion S5 system using methods as previously reported (92). The SRA accession number is PRJNA596731 https://www.ncbi.nlm.nih.gov/sra/PRJNA596731.

Statistics: Colony formation count data was transformed to the square root of the total number of colonies. The square root transformation is a variance-stabilizing transformation for Poisson distributed random samples. A Tukey-post Test was run on count data to obtain significance and confidence intervals for the data and to adjust for multiple comparisons. All calculations were performed using R version 3.5.3 (2019-03-11). Data and code is available under (https://bitbucket.org/ddittmer/r_irak2019/src/master/)

Data availability

RNA-seq data for WT and IRAK4 knockout cells are available here on the SRA database https://www.ncbi.nlm.nih.gov/sra/PRJNA590509. Twenty samples were sequenced, Accessions numbers are as SRX7194576-SRX7194595. The Exome-seq data of the IRAK pathway knockout cells were submitted to the SRA and the accession number is PRJNA596731 https://www.ncbi.nlm.nih.gov/sra/PRJNA596731. Individual accession numbers are SRX7417321- SRX7417326 with detailed description on each sample. For volcano plots and RNA-seq analysis R was used to perform the analysis. All code used in this study is deposited here (https://bitbucket.org/ddittmer/r_irak2019/src/master/).

Results

MYD88 is functional, but dispensable for PEL growth. PEL has a unique B cell signaling pathway network consistent with its presumed cell of origin (81, 229, 230). Unlike other B cell lymphomas, PEL does not express an active B cell receptor, CD79 or CD20 (Figure II. 1A). Furthermore, PEL does not express Burton's tyrosine kinase (BTK). Rather, PEL expresses high levels of MYD88, TLR1, 3, 4, 6-10, CCR5, and IL-10. TLR 7/8 signaling is functional in PEL and results in KSHV reactivation (74). The initiating protein

for the MYD88/IRAK4/IRAK1 Myddosome, the MYD88 coding regions for the BCBL-1, BC-1, BC3, BCP1, JSC1, and VG1 PEL lines as well as seven primary PEL patient samples were sequenced to test whether PEL contains activating mutations in MYD88 (Figure II. 1B). The MYD88 gene sequence was WT, and no L265P activating mutation was observed (Figure II. 1C &D).

To test the hypothesis that MYD88 is essential for PEL survival, we utilized the two-part CRISPR system. First, we generated stable Cas9-expressing cells, BCBL-1-Cas9. Following selection for stable, constitutively expressing Cas9-positive cells, we infected these cells with lentiviral vectors encoding MYD88-targeting gRNAs. We generated two MYD88-deficient cell lines (ΔMYD88.1 and ΔMYD88.2) following two rounds of single cell cloning (Figure II. 2). Western blot analysis showed that MYD88 protein was no longer expressed (Figure II. 2A). The growth rates of the ΔMYD88 were the same as empty-vector infected sub clones that had undergone the same procedure, or as wild-type BCBL-1Cas9 cells (Figure II. 2B). There was no difference in the ability of the ΔMYD88 cells to form colonies in soft agar, a rigorous measure of single cell viability (Figure II. 2C&D). Flanking PCR was used to verify for genomic DNA editing. The PCR product was run on a LabChip GX Touch HT (Perkin Elmer) instrument and showed that the MYD88 gene was edited in the ΔMYD88.1 and ΔMYD88.2 cells compared to non-edited WT cells (Figure II. 2E). In summary, MYD88 was not mutated and is dispensable for growth of BCBL-1Cas9 cells.

IRAK signaling is functional in PEL but can be readily dispensed upon selection. We had previously shown that 95% of PEL cases have a non-synonymous SNV (rs1059702) in the coding region of IRAK1 (135). Since the same SNV was present in primary PEL biopsies, it is unlikely that this represents an adaptation to growth in culture. IRAK1 has

multiple isoforms (19, 231). We determined that the three canonical splice variants of IRAK1 were transcribed in PEL. Additionally, we observed a previously unreported fourth IRAK1 isoform (Schifano, unpublished observation). A protein in size consistent with the full-length isoform was observed by western blot, but no smaller species (Figure II. 3A).

To test the hypothesis that IRAK1 was essential for PEL survival, we again used CRISPR to generate IRAK1 knockout BCBL-1-Cas9 cell lines, ΔIRAK1.1 and ΔIRAK1.2 (Fig. 3). Western blot verified the absence of IRAK1 protein (Figure II. 3A). Proliferation rates for knockouts were not significantly different from WT (Figure II. 3B), and neither was colony formation in semisolid medium. PCR verified deletion of IRAK1 (Figure II. 3E). The complete exomes of the parent and deletion clones were determined by NGS to explore possible off-target effects of CRISPR/Cas-9 mutagenesis. As expected, both private and common SNV were observed, but none in regions of known clinical or biological significance, SRA PRJNA596731. We were able to obtain stable deletion clones of BCBL-1Cas9 cells, ΔIRAK4.1 and ΔIRAK4.2, that had no discernable growth disadvantage (Figure II. 4). Western blot showed an effective KO (Figure II. 4A), and cellular growth was observed to be the same as WT (Figure II. 4B). There was no difference for growth in semi-solid medium for ΔIRAK4 cells compared to WT cells (Figure II. 4C&D). Deletion of IRAK1 was verified by PCR (Figure II. 4E). In conclusion, PEL can survive in culture in the absence of IRAK or MYD88 signaling. We conducted CRISPR experiments in a second PEL cell line, BC-1, to confirm the results we obtained in BCBL-1 were not cell line specific (Figure II. 5). We see by western blot that we have knockdown of MYD88, IRAK1, and IRAK4 (Figure II. 5A-C). One interesting result is instead of a clean knockout for BC-1 ΔIRAK4 we see a shift in western band size implying we generated a fusion protein. We only

see a band shift like this for BC-1 IRAK4 westerns. We determined knocking out these three proteins in BC-1 didn't hinder growth (Figure II. 5D-F), or the ability of BC-1 cells to form colonies in the CFA assay (Figure II. 5. G-I).

To test the hypothesis that BCBL-1Cas9 cells were capable of MYD88/IRAK signaling in the first place, control and deletion clones were exposed to IL-1β. The phosphorylation status of NFκB (p65) was probed using phospho-NFκB specific antibodies. No NFκB phosphorylation was observed in any of the deletion clones, whereas WT BCBL-1Cas9 had a strong p-NFκB signal in response to IL-1β stimulation within 10 minutes of exposure to 1 ng/mL IL-1β (Figure II. 6-8A). Additionally MYD88/IRAK activation was evaluated by NFκB reporter assay. Wild-type BCBL-1Cas9 responded robustly to IL-1β (Figure II. 6-8 B&C). By contrast, IRAK1, IRAK4 and MYD88 deleted clones did not respond. Levels of TNF-α induced activation were similar across all cell lines, demonstrating that the luciferase plasmids were present and functional in these experiments, as TNF-α induced activation of NFκB is independent of the MYD88/IRAK pathway (Figure II. 6-8) (116). These experiments demonstrate that each of the three components of the IL-1β pathway, MYD88, IRAK1 and IRAK4, are functional in PEL and are independently required to transmit IL-1β-initiated signals.

To verify that only the intended gene in the pathway was deleted and that downstream responses remained fully functional in the deletion clones, we performed complementation experiments in all knockout cell lines with four different IRAK1 expression plasmids (Figure II. 9). Each plasmid expressed full length IRAK1. pDD1951 encodes the PEL genotype, pDD2149 encodes the D340N site mutation that was previously shown to abolish kinase activity (232) , pDD2148 is the non-PEL genotype, and pDD2147 encodes the D340N

mutation in the non-PEL background. Empty vector plasmid pDD1957 was used as control. The kinase-dead IRAK1 isoforms were expressed at higher protein levels, presumably since auto-phosphorylation primes IRAK1 for ubiquitin-mediated degradation (Figure II. 9A) (112). Upon nucleofection of any of the four IRAK isoforms into IRAK1 KO cells, NFκB signaling was restored and active independent of IL-1β (Figure II. 9B). As expected, posthoc comparison shows a statistically significant (adjusted $p \leq 0.0001$) difference between wild-type BCBL-1 and IRAK1 KO cells. WT BCBL-1 cells responded to IL-1β stimulation, whereas IRAK1 KO cells did not. Introduction of any one of the IRAK1 expression plasmids is able to complement the IRAK1 deficiency, whereas the vector plasmid is not (adjusted $p \leq 0.0001$ for each pairwise comparison) (Figure II. 9B).The same phenotype was detected in IRAK4 and MYD88 KO cells (Figure II. 9C). These experiments demonstrate that the downstream targets of IRAK1 were intact in IRAK1, IRAK4 and MYD88 KO cells. Furthermore, it was demonstrated that IRAK1 is downstream of MYD88 and IRAK4 in the signaling pathway, as expected, and that IRAK1 functions in one of the pathways that induce NFκB in PEL. Our IRAK1 results substantiates earlier observations that IRAK1 can induce NFκB independently of its kinase activity under circumstances of ectopic expression (66, 214, 232-234).

Many small molecule tool-compounds that target MYD88 and IRAK1/4 exhibit substantial off-target effects. MYD88, IRAK1 and IRAK4 have been the subject of intensive drug discovery efforts (103, 126, 235, 236). Several tool compounds have been developed, and AMGEN has advanced an IRAK1/4 inhibitor into phase I clinical trials for non-cancer indications (237). To explore the phenotypes of inhibiting the MYD88/IRAK4 pathway pharmacologically, we tested the effectiveness of six IRAK, one MYD88, and three BTK

inhibitors in PEL (Figure II. 10). *In vitro* kinase assays for 480 human kinases (KINOMEscans) were evaluated on the six presumed IRAK inhibitors to validate the target specificity of the six IRAK inhibitors. Most of these compounds showed extensive off-target activity. Three of the IRAK inhibitors were selected for detailed characterization in PEL (Figure II. 10C). (i) The AMGEN compound "IRAK inhibitor-1-4" had the greatest *in vitro* specificity. KINOMEscan identified that only four proteins were inhibited by greater than 80% at 250 nM concentration of inhibitor: IRAK1, CLK4, CLK1 and IRAK4. “IRAK inhibitor 1-4” was the least effective at killing BCBL-1 cells (Figure II. 10A). Despite having a high EC50 value of over 200 μM “IRAK Inhibitor 1-4” reduced IL-1β activation at levels far below the EC50 value when the cells would not be killed from the inhibitor treatment (Figure II. 10B). (ii) Compound “IRAK inhibitor-1" was less specific *in vitro*. In addition to IRAK4, 19 other kinases were inhibited by greater than 80% at 250 nM (Figure II. 10C): FLT3, JAK3, MKNK2, GAK, MEK5, BIKE, RIOK3, PHKG2, RIOK, AAK1, PIP5K2B, PDGFRB, RSK4, PHKG1, KIT, ROCK1, PFCDPK1, RSK1 and SIK2. (iii) Compound “IRAK inhibitor-4", had no strong hits on the KINOMEscan (Figure II. 10C). IRAK1 and IRAK4 were inhibited to ~20% at 250 nM. Both compounds reduced IL-1β induced luciferase activity; however, it was not possible to separate the specific IRAK4 inhibition from effects on other targets or cell death caused by the inhibitors, as the EC50 for IL-1β signaling inhibition was equal or above the EC50 for non-specific growth inhibition (Figure II. 10A&B).

Next, these compounds were evaluated in the IRAK and MYD88 KO cells. The MYD88 dimerization inhibitor, ST2825 (219, 225) was included as an additional control. ST2825 killed cells, but displayed no change in EC50 values in WT (8.42 ± 3.44 μM n=4)

compared to the ΔMYD88 (5.16 ± 2.79 μM n=4) ΔIRAK1 (8.0 ± 7.6 μM n=4) or ΔIRAK4 (14.07 ± 16.6 μM n=4) cell lines (Table 2. 1). Likewise, none of the IRAK inhibitors showed any significant change in EC50 comparing WT to ΔIRAK4 BCBL-1CAS9 as seen in (Table 2. 2) The EC50s for ΔIRAK4 BCBL-1 were Inh1 (15.08 ± 16.1 μM n=4), Inh4 (5.1 ± 3.5 μM n=4) and inh1-4 (231 ± 236 μM n=4). This suggests that any anti-proliferative activity for these compounds in PEL was independent of their inhibition of IRAK4 kinase activity.

Baseline IRAK signaling is elevated in PEL, which contributes to PEL-specific paracrine phenotypes and limits viral replication. To determine the consequences of MYD88/IRAK1/IRAK4 ablation genome-wide, RNA-seq analysis of ΔIRAK4 and WT BCBL-1Cas9 was conducted under several treatment conditions. Each RNA-seq experiment was conducted across multiple independent deletion clones. There was minimal change between harvesting biological replicates three weeks apart from the same clone (pairwise Spearman correlation across all mRNAs 0.9722, 0.9675, and 0.9671 for n=3 biological replicates). The combined results are summarized in a heat map representation (Figure II. 11D). First, we observed differences in baseline gene transcription between WT and ΔIRAK4 BCBL-1Cas9 cells. Two independently derived ΔIRAK4 cell lines were examined and common transcriptional changes were quantitated using false-discovery rate adjusted p-values for individual genes. Changes are visualized by Volcano plot (Figure II. 11A), which verifies the functional inactivation of IRAK4-dependent immune signaling. When treated with IL-1β, WT cells responded with upregulation of canonical IL-1β-responsive transcripts Figure II. 11B), and by contrast, ΔIRAK4 cells did not respond (Figure II. 11C).

The following genes were transcribed in BCBL-1Cas9 but not in ΔIRAK4 cells in the absence of exogenous IL-1β: ARHGAP30, B2M, BCL7A, ENG, EPB41L3, FTL,

HSP90AA1, RPS12, SELPLG, SLC16A3, SULT1A1, and YWHAQ (Figure II. 11A & D). IPA suggested that this gene pattern of upregulated cells is linked to aberrant cellular growth and cancer. The transcription of these genes was abrogated by deletion of IRAK4 as seen in two different clones (Figure II. 11D). Hence, we conclude (i) that IRAK signaling is constitutively active in PEL and (ii) that these transcripts mediate the constitutive phenotype of IRAK4 in PEL. Both clones also upregulated a number of transcripts that were not transcribed in WT cells to compensate for the loss of the IRAK phenotype (Figure II. 11D). These would be expected to compensate for loss of constitutive IRAK signaling; however, we did not observe any transcripts that were common among both KO clones. Rather, each ΔIRAK4 clone compensated for loss of IRAK4 activity with a unique set of transcriptional adaptations. The significance of these adaptive transcriptional changes is unclear.

IL-10 was one of the transcripts differentially regulated between WT and IRAK4 KO cells. IL-10 is expressed at high levels in BCBL-1 cells and many other PEL cell lines (90, 212), and is central to the biology of PEL and KSHV infection *in vivo*, e.g. in KICS (38). ELISA verified the transcriptional phenotype for secreted IL-10 protein across all IRAK KO cell lines (Figure II. 11F, G). IL-10 levels were lower in the IRAK1, IRAK4, and MYD88 cell lines as compared to wild-type BCBL-1Cas9 cells, demonstrating the robustness of the profiling results.

To put the individual changes in gene transcription into context, we conducted gene network analyses using Qiagen IPA software. IRAK4 KO cells exhibited a decrease in TNF-α, IL1α and IL-1β networks compared to WT. Knockout of IRAK4 translates into an overall down regulation of the pro inflammatory milieu, which is a classic hallmark of PEL (Figure II. 11E).

Discussion

All PEL cases require KSHV for survival. Dual-infected PEL cases require both KSHV and EBV, presumably because EBV stabilizes the KSHV episome (15, 34, 238). In addition, PEL also acquired multiple genetic changes in the host genome, analogous to EBV-transformed BL (239, 240). PEL's rarity has provided a challenge to developing definitive genomic analyses. Within these limitations, however, several SNVs in the protein coding regions of genes were identified, present across multiple PEL cases and cell lines at a higher frequency than in the general population (135). One of these SNVs occurred on the IRAK1 gene, which is located on the X chromosome and transcribed in PEL. IRAK1, IRAK4 and MYD88 constitute the Myddosome, which mediates IL-1β and TLR signaling. MYD88 is mutationally activated in a large proportion of diffuse large B-cell lymphomas, such as WM, resulting in constitutive activation of the MYD88/IRAK pathway and driving proliferation of these cancers (121, 223, 241). This phenomenon prompted us to explore the biological function of MYD88/IRAK signaling in PEL.

MYD88 was not mutated in any of the PEL cases analyzed and upon CRISPR/Cas-9 facilitated deletion of MYD88, the BCBL-1Cas9 PEL cell line rapidly acquired MYD88/IRAK independence (Fig. 1-4). The same phenotype, of IRAK independence was observed in BC-1 cells (Fig. 5). Furthermore, MYD88-deleted cells were deficient in IL-1β signaling (Fig. 6). The same held true for IRAK1 and IRAK4 deleted BCBL-1CAS9 cells (Fig. 7-8). Interestingly, IRAK4 deleted BCBL-1Cas9 cells lost the expression of several genes that were highly transcribed at steady-state, i.e. prior to IL-1β stimulation and in the presence of an IRAK1/4 kinase inhibitor. One of these target genes was IL-10. IL-10 secretion was downregulated in every MYD88, IRAK1 or IRAK4 deletion clone (Fig.

11F&G). This suggests that IRAK signaling was constitutively active in PEL, at least the part of the IRAK signaling cascade that is independent of kinase activities - as has been previously observed (19, 66, 233). Another result of these experiments demonstrated that current tool compounds that target IRAK1/4 or MYD88 derived their anti-proliferative efficacy in PEL largely from off-target effects (Fig. 10). This does not invalidate the utility of these inhibitors but suggests a different mechanism of action. Since, in PEL, IRAK1 induced both kinase independent as well as kinase dependent targets, it remains unclear what the direct benefit of targeting IRAK kinase activity in PEL would be.

Another important piece of information to consider when examining data is in the differences in experimental designs. Small molecule inhibitor, siRNA, and shRNA screens measure acute phenotypes, often within hours after addition. These agents act effectively on dividing as well as on non-dividing cells since they target mRNA and protein and do not depend on homologous recombination. CRISPR/Cas9 requires each cell to traverse multiple replication/division cycles. Our approach of evaluating single cell clones differed from bulk CRISPR/Cas9 studies that were designed to measure a relative enrichment within the total population. Consistent with our results, Manzano et al. (12) reported a CRISPR/Cas9 screen in which PEL cells survived after deletion of NFκB, which is a downstream target of IRAK1 as well as a multitude of other signaling pathways. NFκB is also a target of the KSHV vFLIP and based on pharmacological studies was believed to be a driver for PEL growth (55, 56, 60). Yet, within a few generations, PEL clones that were independent of NFκB emerged.

Whole exome sequencing data show that, like most transformed cell lines, PEL is mutable when exposed to drug selection or CRISPR/Cas9 selection SRA PRJNA596731 (92). This culture plasticity is even more evident at the mRNA level, e.g. in response to

rapamycin (92). In this study RNA-seq analysis of the ΔIRAK4 clones demonstrated that the cells adapted other means to support survival, which was the phenotype that the CRISPR/Cas9 experiments select for (Fig. 11), but they did not adapt a means to transmit the IL-1β signal, since IL-1β responses were not selected for during the CRISPR/Cas9 process (Fig. 4).

It is important to remember that BCBL-1, like all cancer cell lines, has been selected for continuous growth in culture. Therefore, vulnerabilities that exist in patients may not manifest themselves under ideal growth conditions. For example, one would expect PDX or direct xenograft models (242) to be more susceptible to agents that modulate autocrine and/or paracrine signaling pathways or that augment the host immune response. IL-1β is present at high levels in KS lesions (243), precedes NHL development in AIDS patients, and likely has its most important role in modulating the PEL microenvironment *in vivo* (45). One would expect PEL (or KSHV-infected precursors to PEL) to respond to some pro-inflammatory cytokines, such as IL-1β, by releasing IL-10, dampening T cell activity and counteracting viral clearance. If this is the case it may explain the prevalence of the IRAK1 SNV seen in PEL patients as this SNV results in higher levels of NFκB signaling (136, 244). This leads us to suspect a continued importance of the IRAK pathway in PEL, especially at the onset of infection.

Acknowledgements

This work was funded by public health service grants CA239583 and CA019014 to DPD. The authors would like to acknowledge Tischan Seltzer and Kaitlin Porter for proofreading the manuscript, Carolina Caro-Vegas and Tiphaine Calabre for expertise in ELISAs, all of

the members of the UNC Vironomics Core, Femi Villamor, (https://www.med.unc.edu/vironomics/) for sequencing and KSHV viral load assays, and all members of the Dittmer and Damania labs for comments and suggestions.

Tables

Table 2. 1: MYD88 inhibitor in IRAK pathway knockouts.

Results from treating IRAK pathway knockout cells with the MYD88 st2825 dimerization inhibitor are represented below in μM. Three biological replicates, each the average of 4 technical replicates are shown.

Cell line	Replicate 1 EC50 value (μM)	Replicate 2 EC50 value (μM)	Replicate 3 EC50 value (μM)	Average EC50 value (μM)	Standard Deviation
BCBL-1 WT	4.38	7.11	8.8	6.76	2.23
ΔIRAK4.1	9.37	3.35	4.9	5.87	3.13
ΔIRAK4.2	4.9	5.4	17.85	9.38	7.34
ΔIRAK1.1	28.9	2.27	5.15	12.11	14.61
ΔIRAK2.2	16	2.61	5.4	8.00	7.06
ΔMYD88.1	3.64	3.46	8.39	5.16	2.80
ΔMYD88.2	3.66	2.65	7.9	4.74	2.79

Table 2. 2: IRAK inhibitors in IRAK pathway knockouts.

IC50 values for three IRAK inhibitors conducted in WT and IRAK4 knockout BCBL-1 cell lines. Represented is the average and standard deviation of 4 biological replicates.

	IRAK inhibitor-1 EC50 value (μM)	IRAK inhibitor-4 EC50 value (μM)	IRAK inhibitor-1-4 EC50 value (μM)
BCBL-1 WT	14.93 ± 14.9	5.5 ± 0.5	275.4 ± 52
ΔIRAK4.1	21.98 + 38	6.7 + 1.7	334.58 ± 170
ΔIRAK4.2	15.08 ± 16.1	5.1 ± 3.5	231 ± 236

Figures

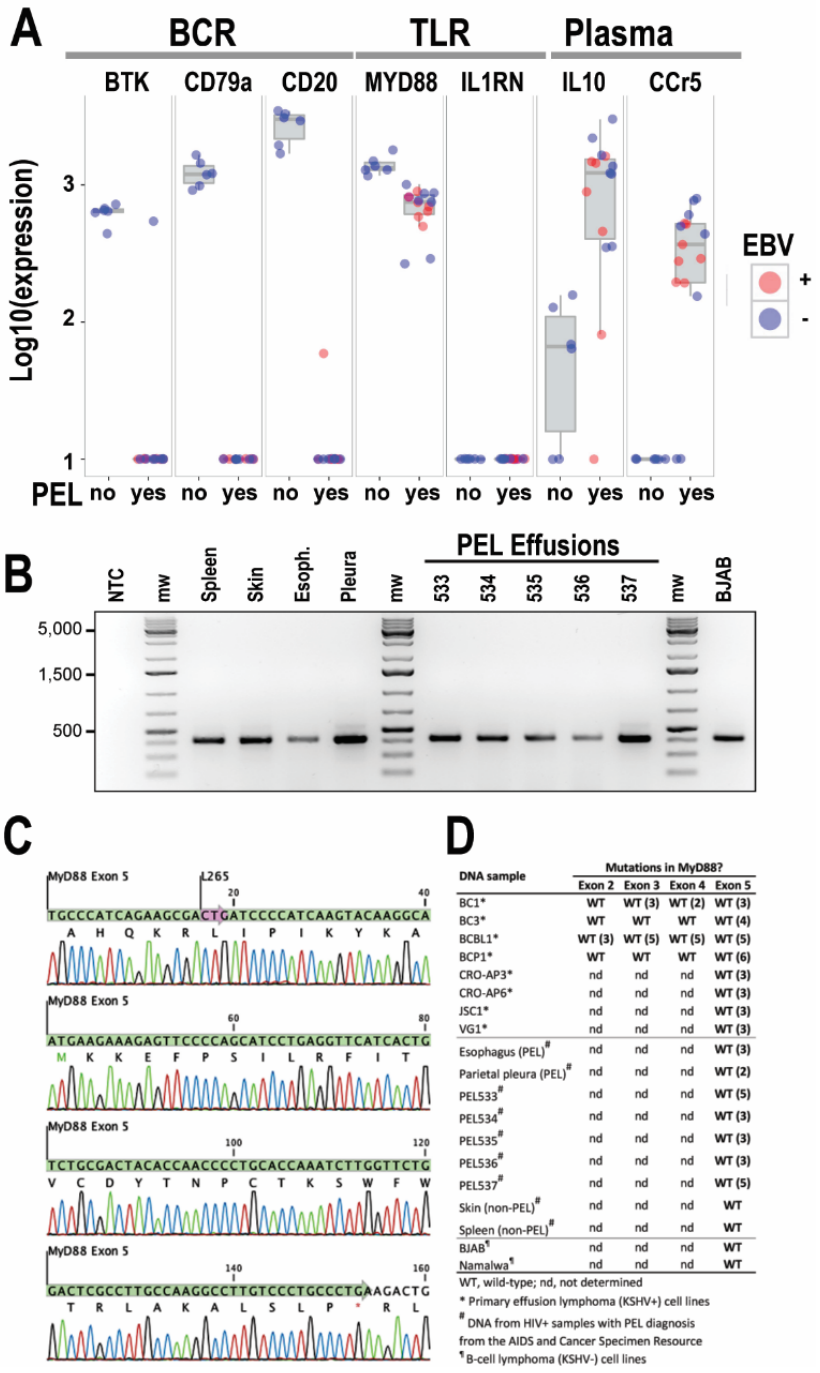

Figure II. 1: PEL cells do not contain the L265P mutation in MYD88. **A)** Gene Expression Omnibus (GEO) analysis of mRNA levels in PEL and lymphoma for BTK, BCR, TLRs and MYD88 (from PRJNA91407). Shown on the vertical axis is the relative expression on a log10 scale. Shown on the horizontal axis is classification as PEL or not. "Yes" means the cells are PEL and "No" represents non-PEL samples. Colors indicate the presence of EBV in the sample. **B)** Genomic DNA from several KSHV-positive PEL cell lines, KSHV-negative B-cell lymphoma cell lines, and HIV-positive patient samples (PEL & non-PEL) was PCR-amplified. The ~400-bp amplicon flanking MYD88 exon 5 PCR product was ran on agarose gel. **C)** The PCR products were

subjected to Sanger sequencing to screen for the Leu265Phe (L265P) mutation in exon 5 of MYD88. Trace file of MYD88 exon 5 in BC-1 cell line. Exon 5 is highlighted in green, and the codon for L265 is in pink. **D)** Table summarizing which MYD88 exons were examined from each cell line or patient sample. WT, wild-type; (#), number of clones sequenced; non-PEL, normal tissue; nd, not determined.

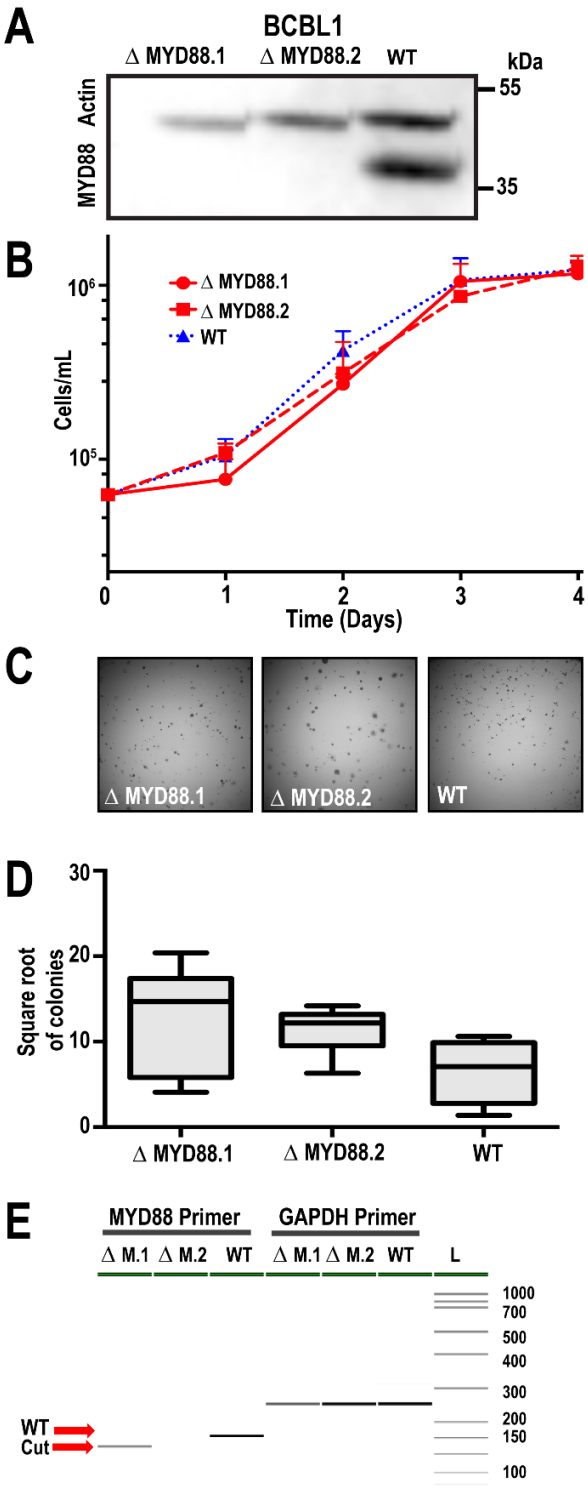

Figure II. 2: MYD88 is not required for PEL survival.

A) MYD88 western blot of BCBL-1Cas9 cell line (WT), and two independent sublines ΔMYD88.1 and ΔMYD88.2 deleted for MYD88 loading control is β-actin. **B)** Growth curves for parent and ΔMYD88 clones obtained via Trypan blue cell counting. Two ΔMYD88 clones and an empty vector control were used in this experiment. **C)** Representative images from colony formation assays of ΔMYD88 and wt BCBL-1Cas9 imaged at 10X magnification. Cells are plated in 1% methylcellulose medium and grown for three weeks. **D)** Quantification of colony formation. Colony counts were obtained using ImageJ and the square root of the number of colonies was plotted, N=15.**E)** PCR analysis using primers that flanking the CRISPR cut-site. Visualization using PerkinElmer LabChip GX-Touch.

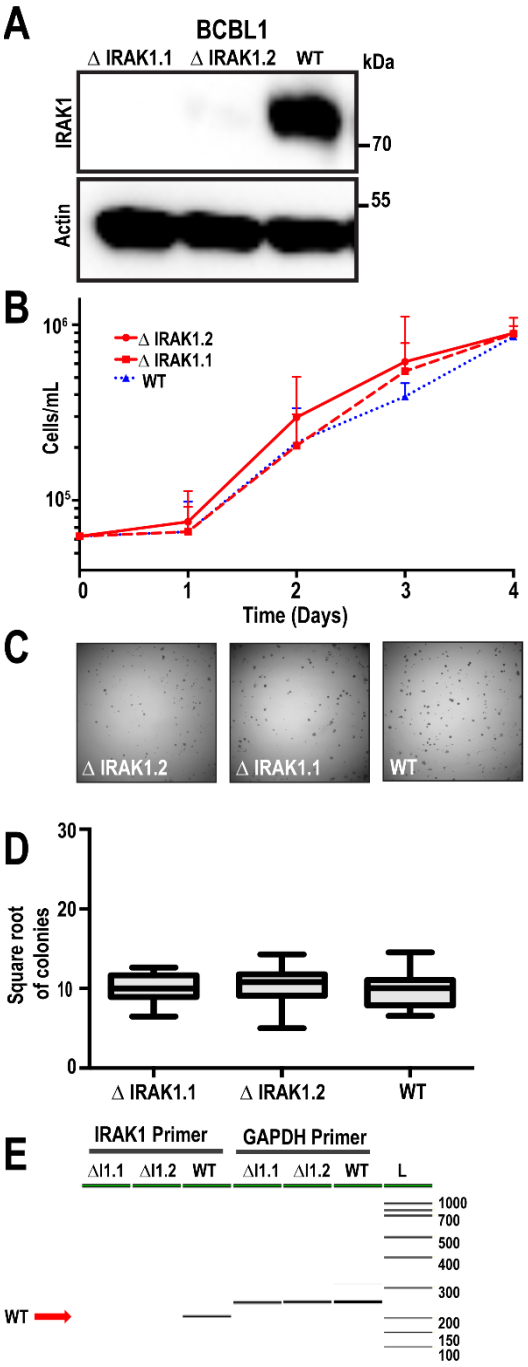

Figure II. 3: IRAK1 is not required for PEL survival.

A) IRAK1 western blot of BCBL-1Cas9 cell lines showing complete knockout, loading control is β-actin. **B)** Growth curves for BCBL-1Cas9 ΔIRAK1 clones obtained via Trypan blue cell counting. Two ΔIRAK1 clones and an empty vector control were used in this experiment. **C)** Representative images from colony formation assays of ΔIRAK1 BCBL-1Cas9 imaged at 10X magnification. Cells were plated at a low cell density in 1% methylcellulose medium and grown for three weeks. **D)** Quantification of colony formation in BCBL-1Cas9 ΔIRAK1 stable cell lines. Colony counts were obtained using ImageJ and the square root of the number of colonies was plotted, N=15. **E)** Flanking cut site PCR analysis using PerkinElmer LabChip GX-Touch. Primers were designed flanking the cut site. Image analysis revealed changes in band size of the KO vs WT cells.

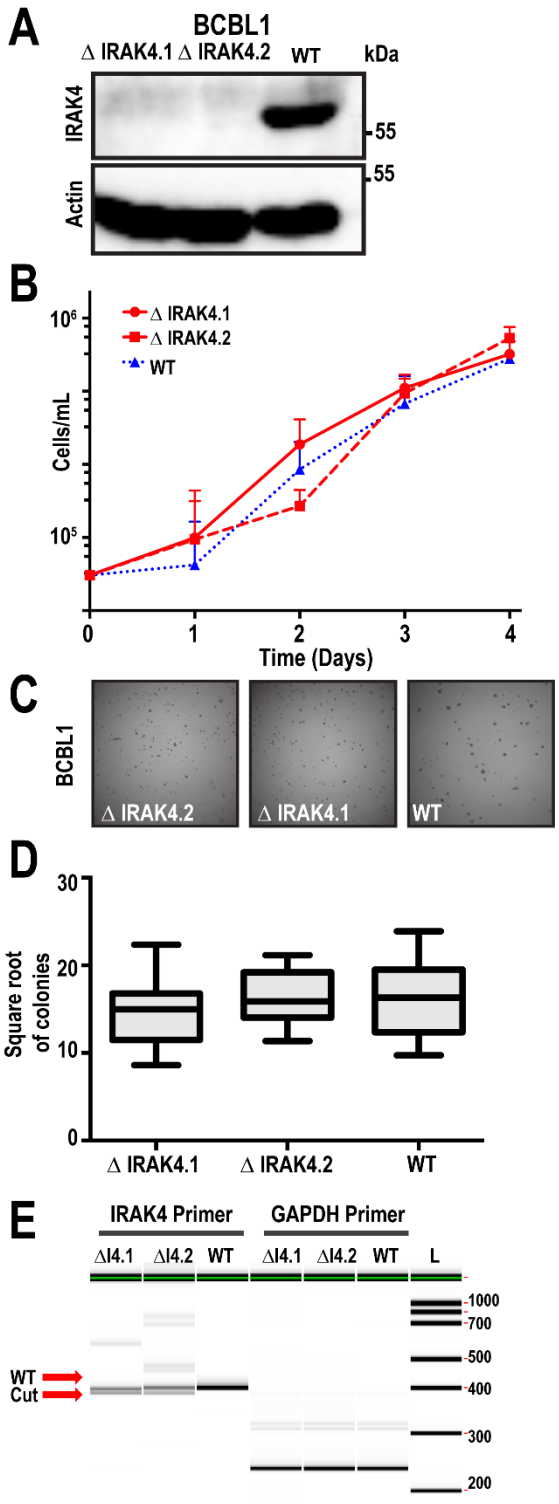

Figure II. 4: IRAK4 is not required for PEL survival.

A) IRAK4 western blot of BCBL-1Cas9 cell lines showing complete knockout, loading control is β-actin. **B)** Growth curves for BCBL-1Cas9 ΔIRAK4 clones obtained via Trypan blue cell counting. Two ΔIRAK4 clones and an empty vector control were used in this experiment. **C)** Representative images from colony formation assays of ΔIRAK4 BCBL-1Cas9 cells imaged at 10X magnification. Cells were plated at a low cell density in 1% methylcellulose medium and grown for three weeks. **D)** Quantification of colony formation in BCBL-1Cas9 ΔIRAK4 stable cell lines. Colony counts were obtained using ImageJ and the square root of the number of colonies was plotted, N=15. **E)** Flanking cut site PCR analysis using PerkinElmer LabChip GX-Touch. Primers were designed flanking the cut site. Image analysis revealed changes in band size of the knockout vs WT cells.

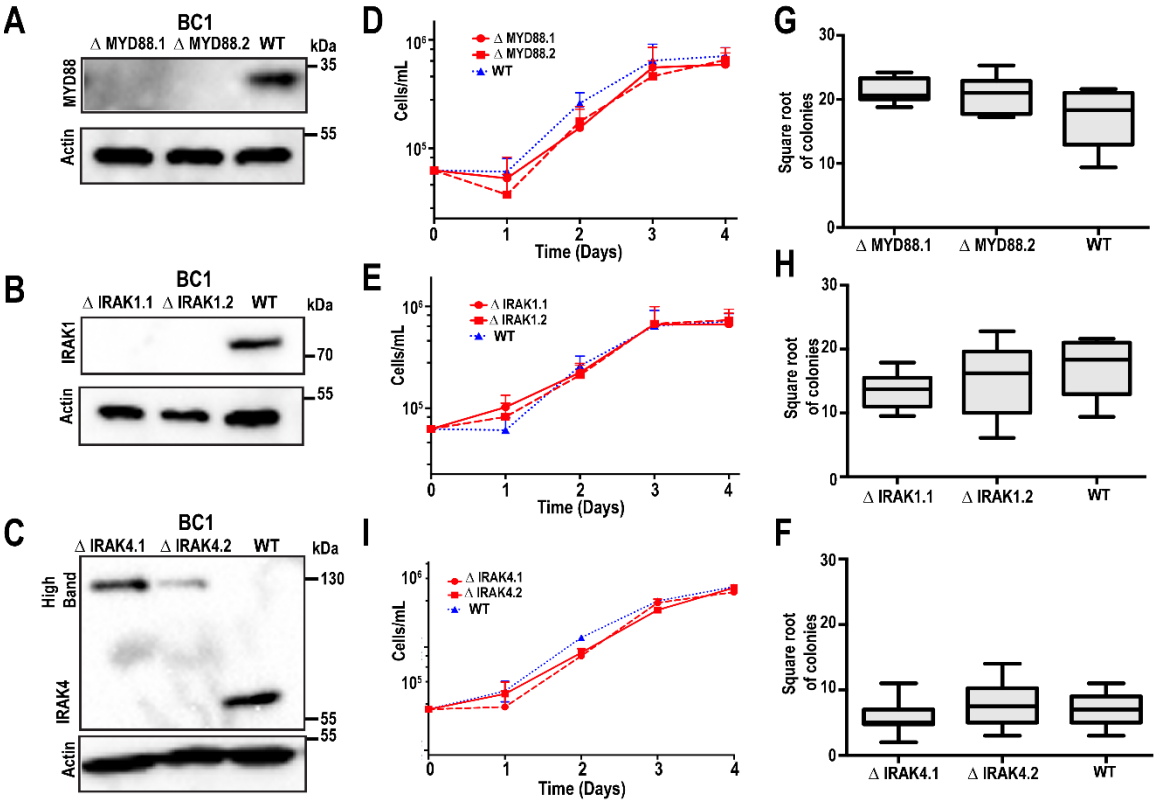

Figure II. 5: MYD88, IRAK1 and IRAK4 are dispensable in BC-1

A) MYD88 western blot of BC-1Cas9 cell lines showing complete knockout, loading control is β-actin. **B)** IRAK1 western blot. **C)** IRAK4 western blo.t **D)** Growth curves for BC-1Cas9 ΔMYD88 clones obtained via Trypan blue cell counting. Two Δ MYD88 clones and an empty vector, WT control were used in this experiment. **E)** Growth curves for BC-1Cas9 ΔIRAK1 clones. **F)** Growth curves for BC-1Cas9 ΔIRAK4 clones. **G)** Quantification of colony formation in BCBL-1Cas9 ΔMYD88 stable cell lines. Colony counts were obtained using ImageJ and the square root of the number of colonies was plotted, N=15. **H)** Quantification of colony formation in BCBL-1Cas9 ΔIRAK1 stable cell lines. **I)** Quantification of colony formation in BCBL-1Cas9 ΔIRAK4 stable cell lines.

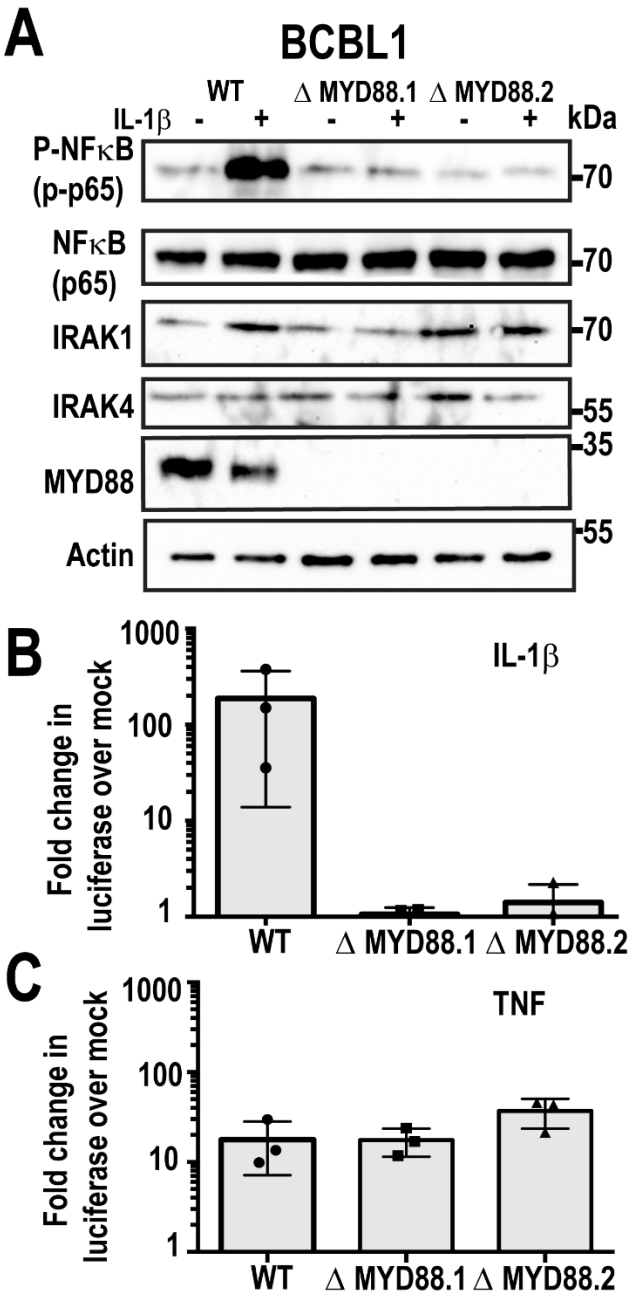

Figure II. 6: NFκB activation by IL-1β is not functional in ΔMYD88 clones. **A)** A western blot for phospho-NFκB and the IRAK pathway proteins IRAK1, IRAK4 and MYD88 in WT and ΔMYD88 BCBL-1Cas9 cells 15 minutes post IL-1β stimulation (1 ng/μL IL-1β). **B)** Quantification of luciferase production using an NFκB reporter assays system. Two ΔMYD88 clones and WT BCBL-1Cas9 cells were stimulated with 1 ng/μL IL-1β, or mock PBS for 24 hours following transfection, and luciferase values measured 6 hours post stimulation. Results are fold change over mock. **C)** Two ΔMYD88 clones and WT BCBL-1Cas9 cells were stimulated with TNF-α (1 ng/mL), and the response was compared to mock using the same procedure as in panel B.

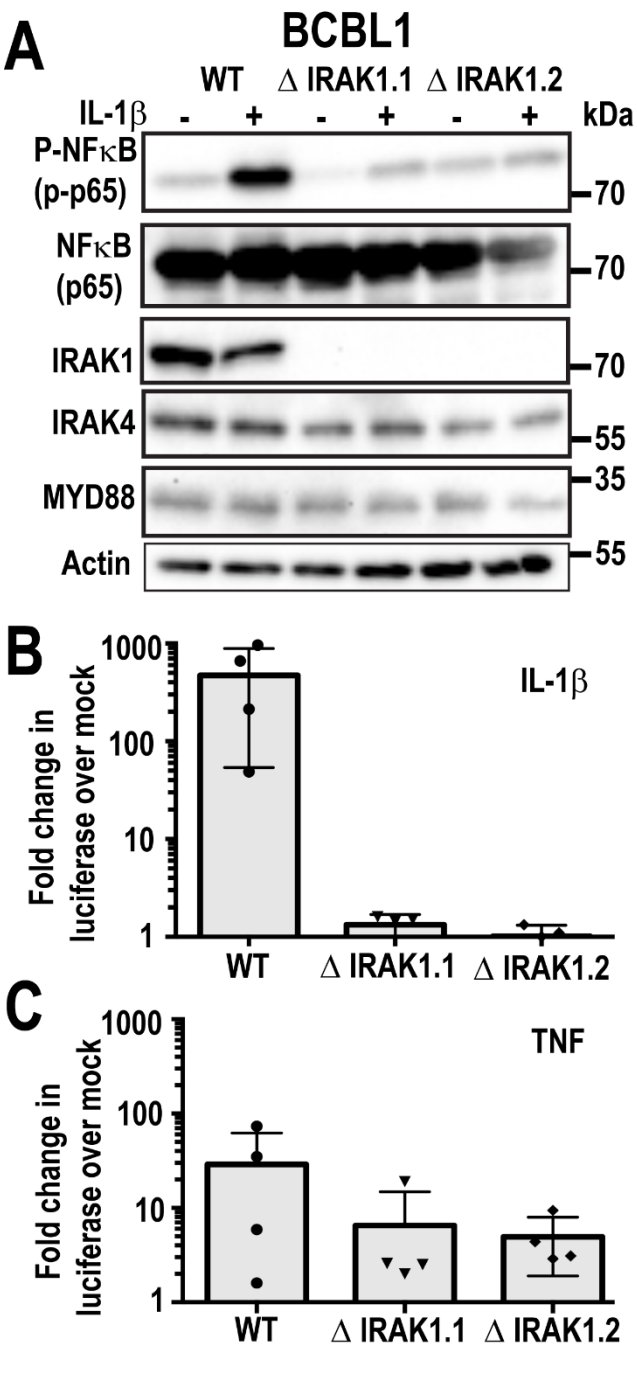

Figure II. 7: NFκB activation by IL-1β is not functional in ΔIRAK1 cells.

A) A western blot for p-NFκB and the IRAK pathway proteins in WT and ΔIRAK1 BCBL-1Cas9 cells 15 minutes post IL-1β stimulation, 1 ng/μL IL-1β. **B)** Quantification of luciferase production using an NFκB reporter assays system. Two ΔIRAK1 clones and WT BCBL-1Cas9 cells were stimulated with 1 ng/μL IL-1β, or mock PBS. Cells were stimulated 24 hours following transfection, and luciferase values measured 6 hours post stimulation. Results are fold change over mock. **C)** Two ΔIRAK1 clones and EWT BCBL-1Cas9 cells were stimulated with TNF-α, and the response was compared to mock using the same procedure as in panel B.

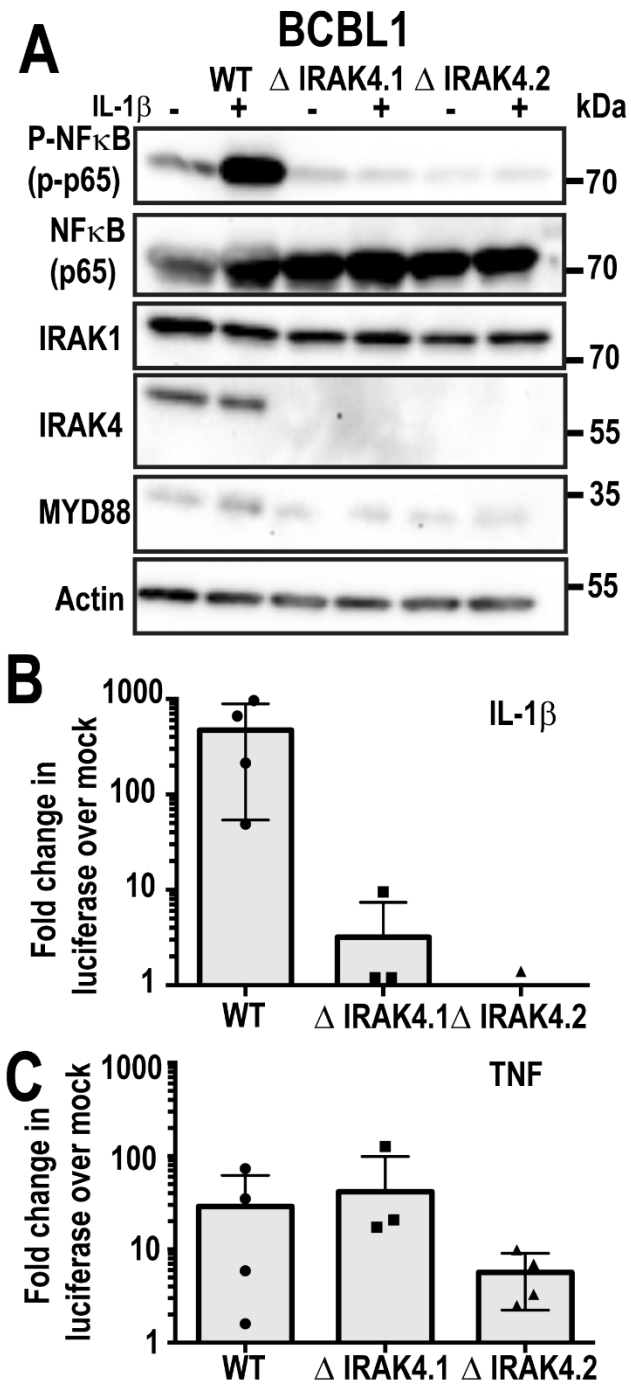

Figure II. 8: NFκB activation by IL-1β is not functional in ΔIRAK4 cells.

A) A western blot for p-NFκB and the IRAK pathway proteins in WT and ΔIRAK4 BCBL-1Cas9 cells 15 minutes post IL-1β stimulation, 1 ng/μL IL-1β. **B)** Quantification of luciferase production using an NFκB reporter assays system. Two ΔIRAK4 clones and WT BCBL-1Cas9 cells were stimulated with 1 ng/μL IL-1β, or mock PBS. Results are fold change over mock. Cells were stimulated 24 hours following transfection, and luciferase values measured 6 hours post stimulation. **C)** Two ΔIRAK4 clones and WT BCBL-1Cas9 cells were stimulated with TNF-α, and the response was compared to mock using the same procedure as in panel B.

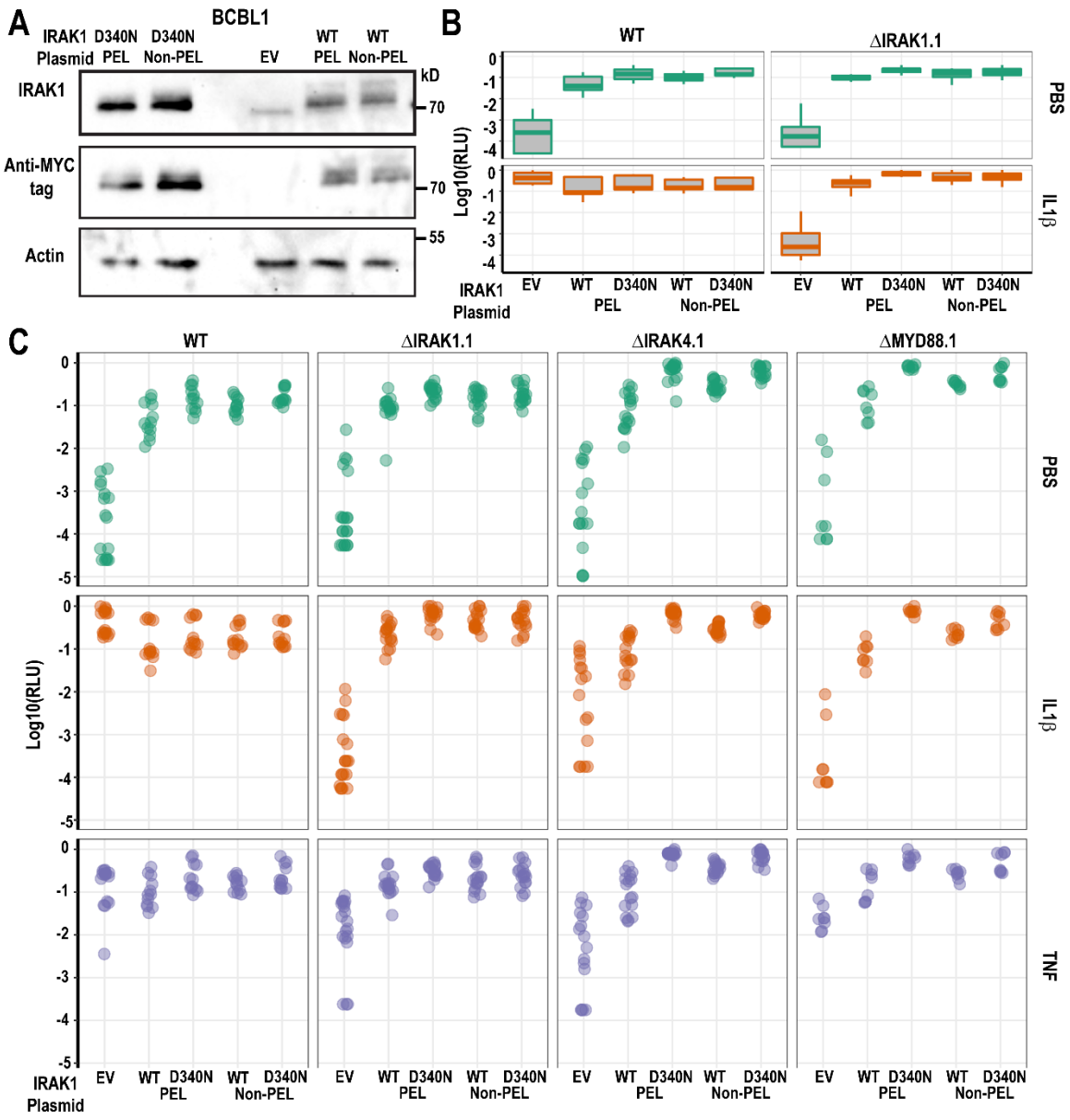

Figure II. 9: Complementation of IRAK1 restores signaling function in KO cells.

A) Western blot in WT BCBL-1Cas9 cells showing expression of Myc-tagged IRAK1 inBCBL-1Cas9 cells. **B)** IRAK expression plasmids were co-nucleofected with an NFκB reporter driven luciferase plasmid into WT or ΔIRAK1 BCBL-1Cas9 cells. Cells were stimulated with IL-1β or PBS (mock), and luciferase values measured 6 hours post stimulation. Shown are relative activity adjusted across multiple biological replicates and

scales as fraction of maximal response on a log10 scale. **C)** IRAK expression plasmids were co-nucleofected with an NFκB reporter driven luciferase plasmid into WT, ΔIRAK1, ΔIRAK4, or ΔMYD88 BCBL-1Cas9 cells. Cells were stimulated with IL-1β, TNF-α or PBS (mock), and luciferase values measured 6 hours post stimulation. Shown are relative activity adjusted across multiple biological replicates and scales as fraction of maximal response on a log10 scale.

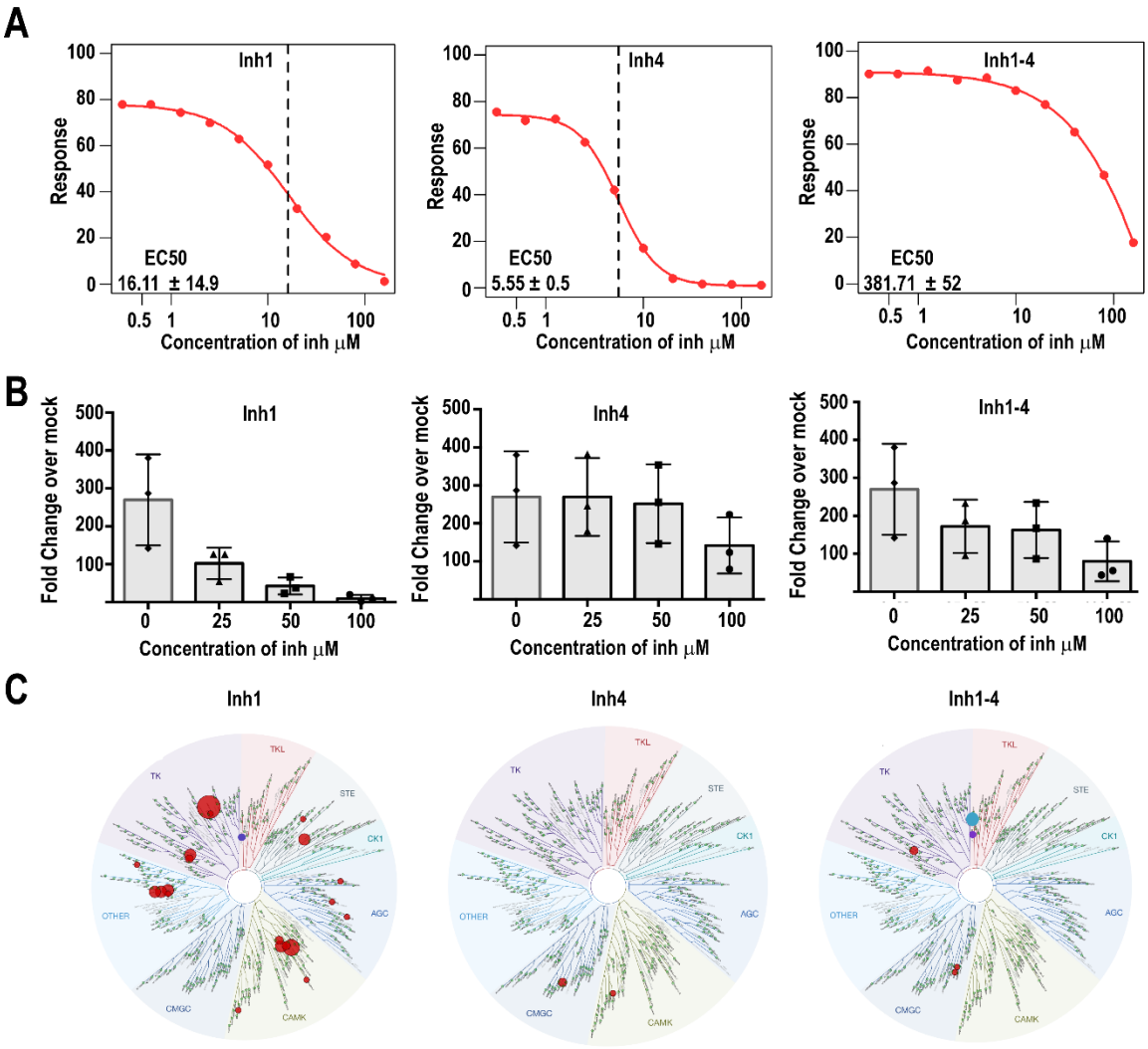

Figure II. 10: Comparison of in vitro and in culture IRAK inhibitor activity.

A) EC50 curves (growth) for three commercially available IRAK inhibitors. Fraction of response is shown on the vertical axis and concentration in μM on the horizontal axis. Inh1 (CAS No: 1042224-63-4), inh4 (CAS No: 1012104-68-5), and inh1-4 (CAS No: 509093-47-4). The EC50 value on each plot is the average of four experiments. **B)** Quantification of luciferase production in cells transfected with an NFκB-driven luciferase plasmid, incubated with inhibitor, stimulated with 1 ng/μL IL-1β. Luciferase values were measured 6 hours post stimulation. All values are fold change over mock PBS stimulation on the vertical axis and

inhibitor concentration in μM on the horizontal axis. **C)** A DiscoverX Kinome scan analysis for each IRAK inhibitor at 250 nM. Arrows point to either purple or blue dots and represent IRAK4 and IRAK1 kinase respectively. Size of the circle is proportional to percent activity inhibited by the inhibitors.

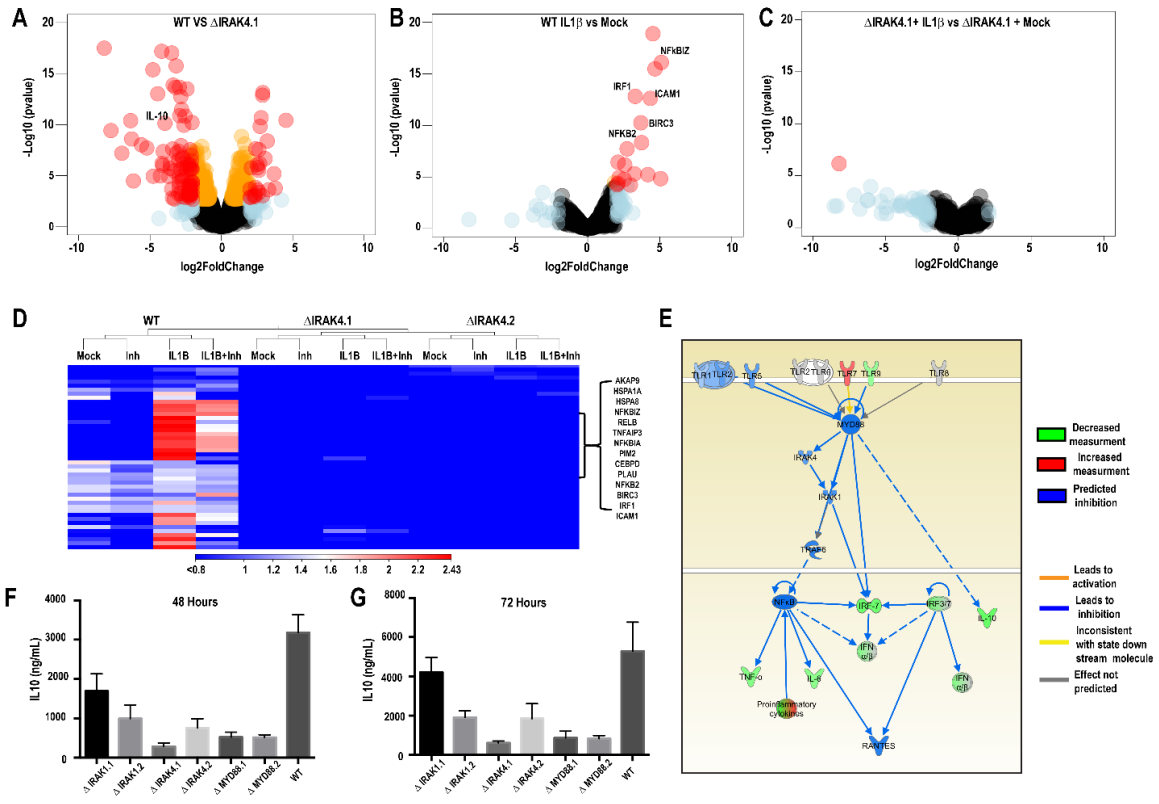

Figure II. 11: RNA-seq analysis of IRAK4 CRISPR KO.

A) Volcano plots showing the genes that are differentially expressed in WT vs ΔIRAK4. **B)** WT ± IL-1β. **C)** ΔIRAK4 ± IL-1β. The vertical axis shows negative log10 of the unadjusted p-value, the horizontal axis shows log 2 of the fold change for each RNA in a paired comparison. **D)** Heat map of the top 20 most altered transcripts as obtained by unsupervised clustering of mRNA levels of ΔIRAK4 compared to WT BCBL-1Cas9 cells under the different conditions indicated above. Blue indicates that the gene is down regulated and red is upregulated relative to the overall mean. IL-1β response genes are indicated on the right. **E)** An IPA network map for RNA-seq data comparing WT vs ΔIRAK4. Proteins shaded red are upregulated in ΔIRAK4 vs WT, Green shaded proteins are down regulated, blue means it is predicted to be downregulated, and orange is predicted up regulated. **F)** IL-10 ELISAs were

run on IRAK pathway knockouts with data points collected at 48 hours. **G)** IL-10 ELISAs from 72- hour time points, reflecting the same time points as the RNA-seq harvests.

CHAPTER 3: CONCLUSION AND FUTURE DIRECTIONS

Summary

In this thesis, we have explored the interaction between KSHV and the IRAK pathway in the context of PEL. KSHV is a γ-herpesvirus that causes four diseases including PEL. PEL is currently untreatable with a 6-month life expectancy (80). Since PEL is so deadly, the need for new therapies is pressing. We explored the function of the IRAK pathway in PEL as well as whether it could function as a potential therapeutic target for PEL. We were drawn to this pathway by previous work done in the Dittmer lab that identified the IRAK1 gene as having a single nucleotide variation (SNV) in 95% of PEL cases (135). Out of the genes with conserved SNVs in the genome, IRAK1 was of primary interest as the IRAK pathway is a critical innate immune signaling pathway responsible for reacting to pathogens and causing inflammation. The IRAK pathway has been linked to other lymphomas as well as arthritis and other inflammatory conditions (22, 23, 100, 118, 245). In various cases of WM and DLBCL, the adapter protein for the IRAK pathway, MYD88, is mutated resulting in a more aggressive cancer (119, 222, 241, 246, 247). The research reported in this thesis has probed how the IRAK pathway functions in PEL and whether this pathway has potential as a therapeutic target to treat the deadly disease that is PEL.

The IRAK Pathway Members are Dispensable for PEL Survival

Chapter two of this thesis highlights our research into the IRAK pathway in PEL. We discovered that the IRAK pathway can function in a canonical manner in PEL where IL-1β stimulation activates NFκB. We validated our reagents through various experiments shown in

Appendix A. We tested the effects of knocking down members of the IRAK pathway with shRNA or by knocking out the genes with CRISPR in PEL. We looked at three main pathway members, IRAK1, IRAK4, and MYD88. We observed in the shRNA experiments that knockdown of MYD88 and IRAK1 and 4 results in a minor decrease in cell survival that is quickly overcome, and we obtained stable CRISPR knockouts of these pathway members. This led us to conclude that, although the IRAK pathway is potentially important for PEL, if you inhibit one member of the pathway, PEL cells can quickly compensate for the loss and survive. This phenomenon is not unexpected as resistance often develops quickly with current single-target therapies in the cancer field (248). RNA-sequencing allowed us to look for compensatory changes in our knockout cell lines.

By performing RNA-seq, we saw that when IRAK4 was removed from the BCBL-1 cells, thus inhibiting the IRAK pathway, a subset of genes was no longer expressed in the knockout cells. We saw compensatory changes in the ΔIRAK4 clones, which Ingenuity Pathway Analysis (IPA) software predicted to be functioning in aberrant cellular growth and cancer. From these results, we demonstrated that the IRAK pathway has a constitutive function in PEL. These genes that were upregulated in the WT cells compared to ΔIRAK4 cells are not canonically linked to the IRAK pathway, and it is likely that this constitutive signaling is unique to PEL.

To see if we could complement IRAK1, IRAK4, and MYD88 knockouts, we used IRAK1 expression plasmids that were either of the PEL genotype or not, as well as kinase dead mutants of each. We determined that the IRAK pathway was not affected beyond the individual knockouts. It is known that overexpression of IRAK1 results in activation of the pathway independent of external stimulation, and we saw this was the case, verifying that

downstream members of the pathway were not harmed during the making of the knockouts (19, 97, 232, 249).

Our CRISPR and shRNA results lead us to conclude that single target therapeutics developed against the IRAK pathway would not function in PEL, which is in agreement with data from other studies that show NFκB is not essential in PEL despite earlier literature using the NFκB inhibitor, BAY11-7082 , to kill PEL cells (12, 58, 61, 64, 151). We explored this phenomenon of inhibitor off-target effects and it is summarized in the next section.

IRAK Inhibitor have Off-target Effects

We discovered that using six commercially available IRAK inhibitors resulted in a wide range of EC50 values in PEL. This was interesting because, if these inhibitors successfully targeted IRAK1/4, we would expect a similar EC50 value among the inhibitors, not the broad spectrum of results that we saw observed. We performed Kinome scan analyses on each of these inhibitors and discovered that the inhibitor with the highest specificity for IRAK1/4 was our least effective inhibitor at blocking PEL growth and survival. We realized that off-target effects were resulting in the death of PEL for some of our inhibitors, since the least specific inhibitor had the lowest EC50 value.

We also wanted to look at BTK inhibitors in PEL because some groups are exploring the possibility of combining inhibition of the IRAK pathway with inhibition of the BTK pathway (119, 120, 128, 235, 236, 250). It should be noted that BTK is not expressed in PEL, and thus BTK inhibitors should not be effective in PEL. We went on to show that inhibition of IRAK4 knockout cell lines or MYD88 knockout cell lines with IRAK inhibitors or a MYD88 inhibitor, st2825, did not result in a change of EC50 values for the inhibitor when compared to the WT cell lines with the knockout. These findings stress that inhibitors can be

non-specific and have off-target effects. Although certain inhibitors can be useful as therapeutic tools, researchers must approach the use of inhibitors with caution and not draw invalid conclusions from that data.

Techniques can Yield Variable Results

We have used various techniques in this thesis research to probe the IRAK pathway, and the differences in the techniques warrant discussion. First, when using CRISPR and selecting for clones, the population is narrowed down to one cell type, where only the cells that have incorporated the guide and Cas9 survive. Any cells that do not adapt to gene knockouts die, leading to survival of the most resistant cells. Although the CRISPR results demonstrate that PEL cells can lose individual members of the IRAK pathway and survive, we have selected heavily for this survival over a period of several weeks. In a clinically relevant setting, there are usually subtypes of cancerous cells that respond differently to treatments, and we may be selecting these out during CRISPR selection.

Table 3. 1: Comparison of molecular targeting techniques.

This table displays four common techniques used to probe the importance of a target for cellular survival.

Techniq ue	Tran sient	Allows for selectio n	Off target effects	Dual target s	Resistanc e	Clonal Selection	Lentivir us infection
shRNA	No	Yes	Low	No	Yes	No	Yes
siRNA	Yes	No	Low	No	-	No	No
CRISPR	No	Yes	Low	No	No	Yes	Yes
inhibitor s	Yes	No	Variabl e-Likely	Yes	Yes	No	No

When using shRNA, we saw a greater variability than in CRISPR experiments. During shRNA experiments, we examined bulk culture that had not undergone clonal selection and thus, depending on the cell line, the phase of growth, and general health of the cells involved, the results could be variable. shRNA can also be silenced readily by cells that still retain the selection marker but no longer show knockdown of the target. This is different from the CRISPR system, which makes permanent changes to the targeted gene by cutting the DNA and inserting/deleting bases. In our studies, we saw that there could be slight growth inhibition in cells that have been shRNA-treated for the IRAK pathway, which was quickly overcome. Since this is a bulk culture, we believe it may have a more valid short-term phenotype than in the CRISPR techniques, but cells adapt even quicker to silence the shRNA and overcome the inhibition of the pathway. Off-target affects for shRNA and CRISPR techniques are comparable, but if shRNA is silenced by a compensatory mechanism, then the phenotype is lost, unlike when using CRISPR (251, 252).

The last technique we used to explore the IRAK pathway was inhibitors, which is a drastically different approach to shRNA and CRISPR. Inhibitors are convenient as they do

not require lentivirus production or selection and function quickly and uniformly. Two major drawbacks of using inhibitors, which hinder the effectiveness of the technique, are off-target effects and the dependence on the target to be either constitutively activated or conditionally inhibited for survival. In this study, we demonstrate the off-target effect of inhibitors as well as how it can be harder to make conclusions about results than when using RNAi approaches, where sequencing methods can be conducted to look for off-target effects with shRNA or CRISPR experiments. For specific inhibitors such as the IRAK inhibitor 1-4 that we used in this study, this technique can be relevant, since we demonstrated that the kinase activity was not important for PEL survival. Where this inhibitor technique would be most relevant is in situations that a protein has two functions, kinase dependent and independent. The IRAK1 protein is known to act this way in certain systems where the kinase activity is dispensable but the protein is required for survival due to kinase independent functions (19, 103, 109, 130, 131). By combining all three approaches in this study, we have been able to comprehensively examine the IRAK pathway in PEL and account for the strength and weaknesses of each approach.

The Relevance of the IRAK Pathway in PEL with the Conserved IRAK1 SNV

Throughout this study, we are examining the effect of the IRAK pathway in PEL cell lines that are tissue culture adapted and long removed from the clinical setting. This is important to note since the IRAK pathway could play a more significant role PEL development in the clinical setting. We see that 95% of PEL patient samples have the SNV in IRAK1 that results in increased basal levels of NFκB signaling and a pro-inflammatory environment (135, 136, 244, 253). This is interesting as KSHV establishes a pro-inflammatory environment upon development of PEL (35, 54, 56, 57, 60, 254, 255). If individuals already have a favorable

environment for KSHV infection, then the effect of the IRAK1 SNV could act in synergy with the virus to establish a more aggressive infection that ultimately results in PEL.

As only a minority of individuals infected with KSHV develop PEL, there are factors independent of viral infection that are required to develop PEL, and it is likely that IRAK1 is one of these factors. Moving forward, the IRAK1 SNV could be studied in longitudinal studies to determine if individuals with the IRAK1 SVN have higher rates of KSHV infection and PEL than those who have WT IRAK1. Based on the current knowledge about the IRAK pathway in KSHV and PEL, we hypothesize that the IRAK SNV rs1059702 (F196S) predisposes individuals to develop PEL following infection with KSHV. Since a higher basal signaling level of NFκB would occur in individuals with the variant, these levels could enhance the establishment of KSHV infection, latency, and disease progression in B-cells thus resulting in a higher chance of developing PEL. Additionally, targeting this pathway may not matter in a cell line environment, but in the human environment with many more variables, pursuing inhibition of the IRAK pathway could result in a benefit to the patient.

Future Directions

There are numerous additional experiments that can be done to better understand the role of the IRAK pathway in PEL and how it functions in disease progression. A large number of studies could be conducted to explore the role of the IRAK1 rs1059702 (F196S) in infection. To do this, one would need to use a standard KSHV infection model and have one set of cells with the PEL IRAK1 variant and one without the variant. Infection rates could be measured by genome copy numbers and we could measure the viral reactivation ability following infection. This could allow researchers to identify if the IRAK1 SNV plays

a role in early infection and could even be expanded to a mouse model since mice have IRAK1 homologs.

CRISPR technology is advancing at a rapid rate and providing new tools for researching genomic questions such as the importance of the SNV in PEL. Using template gene editing methods, we could attempt to swap the SNV variants in PEL cells line and observe the effects through NFκB activation, virus reactivation from latency, and genome copy number. This technique is still being developed and requires a template plasmid as well as the CRISPR plasmid, however, with optimization we most likely could generate these variants in PEL cell lines.

Another future area of interest would be looking at double knockouts of the IRAK pathway, such as knockout of both MYD88 and IRAK1 or a different combination of knockouts. It is likely that double knockouts might have greater effects on the survival of PEL. However, preliminary work done with siRNA and individual knockouts did not lead to cell death. To conduct the double knockout experiments, it would be best to use a CRISPR plasmid that has multiple guides so that the cells only undergo one round of clonal selection.

We saw in the RNA-seq data that the IRAK pathway has a set of functions where genes are constitutively active when IRAK4 is present but are turned off when it is absent, and this would be an exciting lead to follow in future research. Many of these genes were involved in cellular movement and adhesion, and they mapped in IPA to “cancer” pathways. We also saw that in each IRAK4 knockout there was a compensatory set of genes that were up-regulated, and we believe that this was to account for the loss of the IRAK4 dependent genes. Following up on this RNA-seq data in future research, one could tease out how the

IRAK pathway functions in a resting state in PEL and whether the IRAK pathway has functions that have yet to be discovered and that could be applicable to other systems.

We could also perform IP-mass spectrometry in wild type PEL cells for IRAK1, MYD88, and IRAK4, both stimulated and unstimulated, to see what the binding partners are. Additionally, we could perform the respective IP in each of the knockouts to see how these partners change. We hypothesize that there are canonical and non-canonical functions of all three proteins, and by taking away the canonical pathway through knockouts, we could observe binding partners in a knockout setting as well as the potential downstream results of those partnerships.

Another interesting follow-up study could examine the IRAK inhibitor 4 more closely. Out of all the inhibitors, IRAK inhibitor 4 killed PEL but did not have any hits on the Kinome scan. Conducting experiments to see what this inhibitor targets could lead to identification of unknown pathways in PEL. We could also utilize RNA-seq to determine what happens to gene expression at sub IC50 levels. This would allow us to determine what the effects of the inhibitors are and potentially trace it back to inhibitor targets.

Conclusion

In conclusion, from this thesis work we have demonstrated that the IRAK pathway is dispensable in PEL in a tissue culture environment. As such, we do not believe that the IRAK pathway would function as a single-target therapeutic in PEL. There is potential in further studies that inhibiting the IRAK pathway in combination therapy could have a positive outcome, because we hypothesize that members of the IRAK pathway have functions outside of the canonical pathway in PEL. IRAK1 is known to function in regulating IRF7, STAT3, and IL-10, which are critical proteins in PEL. STAT3 and IL-10 are known to be important

for KSHV to establish infection (19, 100, 184, 255-257). MYD88 has functions outside of the IRAK pathway and is critical to almost all TLRs and several ILRs (216, 258-262). Since vFLIP already controls NFκB activation downstream of the IRAK proteins, it is highly likely that the IRAK pathway is important in PEL to a degree but that KSHV has the ability to circumvent the canonical activation in PEL (54, 55, 60). These interactions are only hypothesized to take place in PEL and require further exploration.

This thesis advances the scientific communities' knowledge of the IRAK pathway in PEL and will help to ensure that incorrect treatment regiments based on IRAK pathway targets are not administered to patients with PEL. We hypothesize that the IRAK pathway still serves a function in PEL, potentially early in the development of the disease, and as we understand the relevance of the pathway over time, we may be able to use this knowledge to recognize early warning signs of KSHV-infected individuals that are at risk of developing PEL.

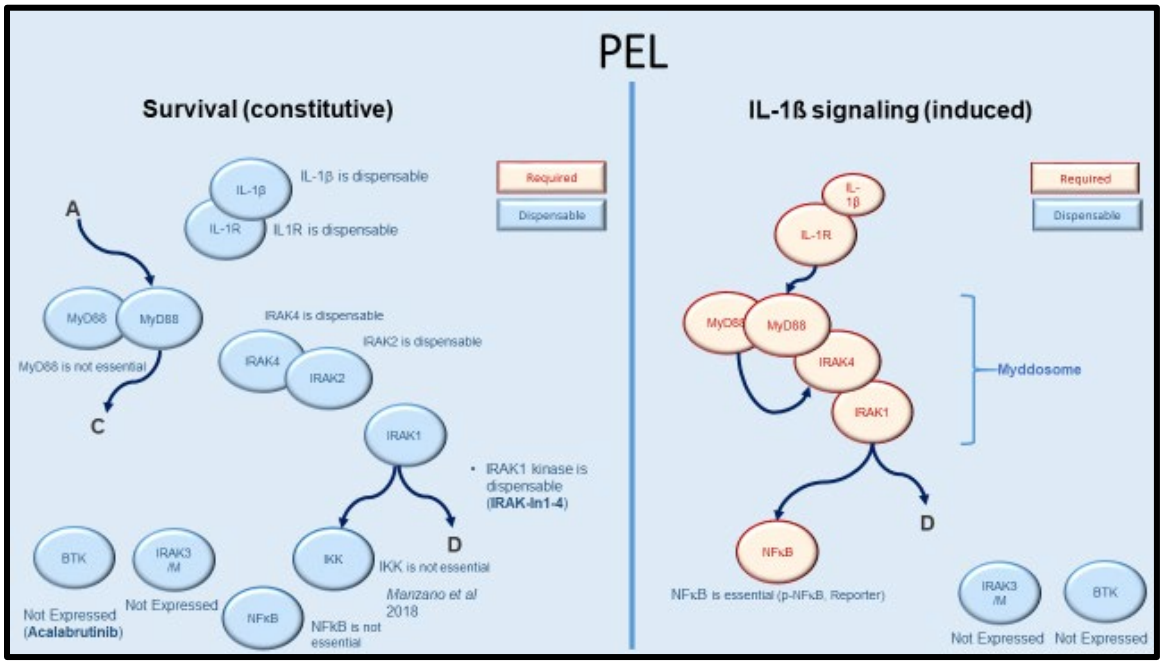

Figure III. 1 Summary of the IRAK pathway in PEL

APPENDIX A: SUPPORTING INFORMATION

Overview

Examination of the IRAK pathway in the context of PEL required many experiments, of which only a subset was published in the 2020 paper. In Appendix A, additional experimental results that were performed to gain insight into the IRAK pathway in PEL are included. Some of the experiments are proof of concept, reagent testing, or use of a different technique, such as shRNA versus CRISPR. Additionally, multiple cell lines are represented in this appendix, as well as tables with information on inhibitors, plasmids used in this study, and more.

Results

In addition to the IRAK pathway, we examined another gene that had a conserved variation in PEL known as the ABCD1 gene. ABCD1 is a fatty lipid transport gene, and we can see through Figure AA. 1 that knockdown (KD) of this gene has no effect on BCBL-1 growth in culture. We also determined that IRAK1 has three classical splice variants as well as a fourth, previously unidentified, splice variant. We see that F196S and S532L variants in IRAK1, which are known to increase NFκB levels in other systems, are present in PEL (140, 253, 263, 264) (Figure AA. 2**)**. We validated that the IRAK pathway is expressed in PEL (Figure AA. 3) through western blot analysis. Due to other studies focusing on the combination of BTK and IRAK4 inhibitors, we wanted to explore the BTK pathway in the context of PEL (119, 236, 250, 265). We verified that BTK is not expressed in PEL, and that BTK inhibitors are more effective in the non-PEL BJAB cell line that does express BTK. We also see that inhibitors of BTK kill cells proportionately to the specificity of each inhibitor (Figure AA. 4**)**.

Since much of this study relied on using TNF-α and IL-1β, we tested these reagents in U2OS cells, which are known to respond to both stimulants, by IFA, western blot, and luciferase assay (Figure AA. 5**)**. We also tested these western blot and luciferase assays in BCBL-1 cells, and confirmed that TNF-α and IL-1β activate NFκB (Figure AA. 6**).** We titrated the optimal IL-1β concentration to stimulate cells with, as well as the best amount of CTG reagent (Figure AA. 7). We also validated the IRAK1 expression plasmids through restriction digest, western blot and sequencing, as seen in Figure AA. 8.

In addition to the CRISPR results described in chapter two, we have conducted extensive shRNA experiments as well. For these experiments, we looked at the short-term effects of KD of different IRAK pathway members. We saw that IL1R was dispensable for BCBL-1 survival, with the growth curve representing one shRNA spinfection experiment and colony formation assays performed after the spin (Figure AA. 9**)**. We confirmed the results from the shRNA experiment by using CRIPSR (Figure AA. 10). This experiment differed from the CRISPR experiments in chapter two because those experiments were after two rounds of single clone selection whereas this IL1R test was conducted on a bulk culture that did not undergo clonal selection. We still see a reduction in IL1R protein and no inhibition of BCBL-1 survival (Figure AA. 10**)**.

We performed shRNA KD on MYD88 (Figure AA. 11**)**. We did this in both PEL BCBL-1 cells and BJAB control cells. We determined that, in BCBL-1 cells, some experiments resulted in a lower survival rate when infected with shRNA targeting MYD88 as compared to the BJAB cells; however, long-term survival of MYD88 KD BCBL1 still occurred. In Figure AA. 12, we obtained IRAK1 KD in both BCBL-1 and BJAB cells and once again see the same trend as in the MYD88 KD experiments. Figure AA. 13-14

demonstrate that knockdown of IRAK4 does not have any short-term effects on PEL lines, BCBL-1 and BC-1, nor on the non-PEL BJAB cell line. CRISPR KO of IRAK4 in BJAB also did not result in any growth defects (Figure AA. 15**)**.

Looking at resting state NFκB levels, we saw that NFκB was constitutively activated in BC-1 but not BCBL-1 cells (Figure AA. 16). We performed RNA-seq and Exome-seq analysis on all of our clones shown in chapter two. For the RNA-seq data, we concluded a list of host pathways that are changed in our IRAK4 cells compared to WT BCBL-1 cells. The top pathways on this list are involved with cellular adhesion and migration (Figure AA. 17). Exome sequencing data for the IRAK pathway knockouts show that we have cuts at the CRISPR guide sites and that there are shared SNVs across the different pathway knockouts, as expected for both BC1 and BCBL1 (Figure AA. 18-21). Some of the CRISPR guides resulted in deletions, seen via PCR, and others resulted in insertions and deletions.

In addition to the results in chapter two, we further explored each of the inhibitors used in this study. We determined the EC50 values, the Kinome profiles, and the effects of each inhibitor on the reduction of luciferase activity **(**Figure AA. 22**)**. The MYD88 inhibitor, ST2825, had no change in EC50 values in any of the IRAK pathway knockout cell lines compared to WT values (Figure AA. 23). In mice, we observed that IRAK inhibitor 1 and 4 could clear infected cells from the mice; however, inhibitor 1-4 failed to do this (Figure AA. 24). Furthermore, we saw that IRAK inhibitor 1 resulted in higher mouse mortality. We used each of these inhibitors in colony formation assays, and there was no reduction in colony numbers, as can be see visually in Figure AA. 25. Reactivation of BCBL-1 IRAK pathway knockouts displayed very slight differences in virus reactivation, with MYD88 knockout lines producing slightly more virus (Figure AA. 26). RNA-seq results for KSHV genes in

ΔIRAK4 BCBL-1 cells showed that virus reactivation corresponds with time point taken more so than with knocking out IRAK4 (Figure AA. 27). The final figures of this appendix show the complete western blots for the various figures in chapter two and this appendix (Figure AA. 28-34).

Discussion

The research represented in this thesis provides supporting data for the 2020 IRAK paper published in JVI chapter two. As explained in chapter two, we found similar results using shRNA as we did using CRISPR techniques despite the differences in experimental set-up. A slight variation with the toxicity of the shRNA assays was observed. As seen in Figure AA. 11-12, shRNA resulted in lower cell survival and decrease in colony formation assays compared to CRISPR. One explanation for this could be that there is a short-term growth disadvantage when IRAK1 or MYD88 is knocked down in cells that can be quickly overcome with CRISPR and stable clonal selection. Another potential reason could be differences in viral titers used in the spinfection experiments. However, each experiment was conducted in non-PEL BJAB cells to control viral titer, and the drop in short-term viability was not seen in BJAB cells.

For inhibitor experiments (Table 3), we determined the inhibitors that target IRAK1 or IRAK4, yet these inhibitors are also non-specific and appear to inhibit cell growth through off-target effects. Additionally, other inhibitors such as MYD88 inhibitor ST2825 had no difference in EC50 values in MYD88 KO cells versus WT cells (Figure AA. 20). We also saw that with BTK inhibitors, despite BTK not being expressed in PEL, some of these inhibitors do kill PEL cells. This would be due to off-target effects of the inhibitor, which

drives home the point that small molecules can have many off-target effects. In conclusion, the results shown in this appendix are supplemental to chapter two and strengthen the findings of this thesis work presented in chapter two as well as published in the 2020 IRAK paper in the Journal of Virology.

Materials and Methods

Methods are described in chapter two with the following exceptions, which were only conducted in experiments described in the appendix.

Lentivirus production: Lentivirus particles were produced in 293T cells using ViraPower (Thermo-Fisher) or were purchased from Sigma Aldrich Sanger clone library. CRISPR plasmids were obtained from Genscript, Sigma, or Addgene as specified in supplemental table 1. Plasmids expressing shRNA were obtained from the UNC lentiviral core. Table 1 contains a detailed list of plasmids used in this study. Packaging mix and transfer plasmid were co-transfected using ViraPower according to the manufactures protocol, into 293T cells. Virus particles where harvested 48-72 hours post transfection, filtered, aliquoted and stored at -80 C until use.

Spinfection procedure: 500,000 cells were placed in 15 mL conical tubes with 1 mL of serum free media, 2 mL of lenti particles, and 10 µg/mL of polybrene for in house lentivirus prep. For purchased particles, 50,000 cells were plated in 24 well plates with 100 µL of serum free media and 200 µL of particles, MOI of 5, were added and 10 µg/mL polybrene. The plates/tubes were spun for 90 minutes at 2500 RPM. Media was changed 18 hours following spin. Selection media was added 24 hours post spin, with 2.5 µg/ml of puromycin for selection. Half of the cells were plated into colony formation assays for single cell clone

selection, see colony formation assay methods. Trypan Blue (Sigma) cell counting was used for all growth proliferation assays and live dead cell counting.

NFκB translocation IFA: U2OS cells were seeded at 250,000 cells/ml and grown on a glass cover slip. The following day, cells were treated with TNF, IL-1β or PBS for one hour. 4% paraformaldehyde was used as a fixation agent. 10% BSA was used to block cells for 1 hour with 0.2% triton X serving as the permeabilization agent. Primary antibody was used at a concentration of 1:500 and incubated for two hours at RT. Vector Labs Texas Red or Fluorescein secondary was used 1:500 and cells imaged using a Leica DM500 B scope and Image Q software. Cells were examined for NFκB translocation to the nucleus**.**

Mouse inhibitor studies: Mice were inoculated intraperitoneal with 1 million BCBL-1-TREX-LUC cells, which express luciferase protein and can be measured via imaging. Three days after injection, IRAK inhibitors were given to the mice at a dose of 78 mg/kg on Mondays, Wednesdays and Fridays for three weeks. Mice were imaged and luciferase values representing the PEL effusions growth were measured at the three-week termination point.

Restriction digest: All CRISPR plasmids in this study underwent restriction digest using Thermo Scientific fast digest enzymes according to manufactures protocol. Digestion products were run on a 1.5% agarose gel and imaged on a Biorad Gel Doc XR.

Tables

Table AA. 1: Table of plasmids used in this study.

All plasmids used in this study were giving a unique pDD number. Resistant markers for growth in both bacteria and mammalian cells, DNA sequences if the plasmid contains CRISPR guides or shRNA, and the company and catalog numbers.

pDD	Backbone	Plasmid description	Bacterial resistance marker	Cell resistant marker	shRNA target sequence	Company	Catalog number
2079	pLKO.1	shRNA targeting ABCD1	amp	puromycin	GCACGAGATGTTCCAGGTATT	TRC with the Broad institute	TRCN0000059434
2080	pLKO.1	shRNA targeting ABCD1	amp	puromycin	CGCACAGAAGCCTTCACTATT	TRC with the Broad institute	TRCN0000059435
2081	pLKO.1	shRNA targeting ABCD1	amp	puromycin	GTATGTTATGCTGGAGCAGTT	TRC with the Broad institute	TRCN0000059437
2082	pLKO.1	shRNA targeting ABCD1	amp	puromycin	CCTAATTTATTGGATTCCCTA	TRC with the Broad institute	TRCN0000059433
2083	pLKO.1	shRNA targeting ABCD1	amp	puromycin	CGCACCTTCCTGTCGGTGTAT	TRC with the	TRCN0000059436

						Broad institute	
2084	pLKO.1	shRNA targeting ATP7A	amp	puromycin	CCTCTTGGTATGGATTGTAAT	TRC with the Broad institute	TRCN0000043177
2085	pLKO.1	shRNA targeting ATP7A	amp	puromycin	GCTCCCTAAACAGTGTTGTTA	TRC with the Broad institute	TRCN0000043176
2086	pLKO.1	shRNA targeting ATP7A	amp	puromycin	GCTGTATTAGTAGCAGTTGAT	TRC with the Broad institute	TRCN0000043174
2087	pLKO.1	shRNA targeting ATP7A	amp	puromycin	CCATTCATGTACTAGCACTAT	TRC with the Broad institute	TRCN0000043173
2088	pLKO.1	shRNA targeting ATP7A	amp	puromycin	GCCGCTTCTGACTTCAACTAA	TRC with the Broad institute	TRCN0000043175
2089	pLKO.1	shRNA targeting GFP	amp	puromycin	Unknown	TRC with the Broad	

						institute	
2090	pMAX3	CRISPR for EBV	amp	NA produces GFP	GCCCTGGACCAACCCGGCCC	Wang J1, 2014 PNAS	
2091	pMAX3	CRISPR for EBV	amp	NA produces GFP	GGCCGCTGCCCCGCTCCGGG	Wang J1, 2014 PNAS	
2092	pMAX3	CRISPR for EBV	amp	NA produces GFP	GGAAGACAATGTGCCGCCA	Wang J1, 2014 PNAS	
2093	pMAX3	CRISPR for EBV	amp	NA produces GFP	TCTGGACCAGAAGGCTCCGG	Wang J1, 2014 PNAS	
2094	pMAX3	CRISPR for EBV	amp	NA produces GFP	GCTGCCGCGGAGGGTGATGA	Wang J1, 2014 PNAS	
2095	pMAX3	CRISPR for EBV	amp	NA produces GFP	GGTGGCCCACCGGGTCCGCT	Wang J1, 2014 PNAS	
2096	pMAX3	CRISPR for EBV	amp	NA produces GFP	GTCCTCGAGGGGGCCGTCGC	Wang J1, 2014	

						PNAS	
2104	pLKO.1	shRNA targeting STAT3	amp	puromycin	CGGATCATAAGGTCAGGAGAT	TRC with the Broad institute	TRCN0000020839
2105	pLKO.1	shRNA targeting STAT3	amp	puromycin	GCTGACCAACAATCCCAAGAA	TRC with the Broad institute	TRCN0000020840
2106	pLKO.1	shRNA targeting STAT3	amp	puromycin	GCTGAAATCATCATGGGCTAT	TRC with the Broad institute	TRCN0000020841
2107	pLKO.1	shRNA targeting STAT3	amp	puromycin	GCACAATCTACGAAGAATCAA	TRC with the Broad institute	TRCN0000020842
2108	pLKO.1	shRNA targeting STAT3	amp	puromycin	GCAAAGAATCACATGCCACTT	TRC with the Broad institute	TRCN0000020843
2109	pLP/VSVG	VSVG for producing lenti	amp	NA	NA	Thermo-fisher	

2110	pLP2	produces packaging for lenti production	amp	NA	NA	Thermo-fisher	
2111	pLP1	produces packaging for lenti production	amp	NA	NA	Thermo-fisher	
2112	pLenti6	produces luciferase + control	amp	NA	NA	Thermo-fisher	
2113	pLKO.1	shRNA targeting IRAK4	amp	puromycin	CAGTTTCACATAAGGAGATTT	TRC with the Broad institute	TRCN0000002063
2114	pLKO.1	shRNA targeting IRAK4	amp	puromycin	CCTCTGCTTAGTATATGTTTA	TRC with the Broad institute	TRCN0000002064
2115	pLKO.1	shRNA targeting IRAK4	amp	puromycin	CCCAGACATTAAGAAGGTTCA	TRC with the Broad institute	TRCN0000002065
2116	pLKO.1	shRNA targeting IRAK4	amp	puromycin	GCCTGACCTAATCCAAGTGAA	TRC with the Broad institute	TRCN0000002066
2117	pLKO.1	shRNA targeting IRAK4	amp	puromycin	GCTAATACACTA	TRC with	TRCN0001067 9

					CCTTCTAAA	the Broad institute	
2118	pLKO.1	shRNA targeting IL-1R	amp	puromycin	CCCGTGAACTTCCTTTGACTT	TRC with the Broad institute	TRCN0000059258
2119	pLKO.1	shRNA targeting IL-1R	amp	puromycin	GCCATATTTAAGCAGAAACTA	TRC with the Broad institute	TRCN0000059259
2120	pLKO.1	shRNA targeting IL-1R	amp	puromycin	GCCAAGAATACACATGGTATA	TRC with the Broad institute	TRCN0000059260
2121	pLKO.1	shRNA targeting IL-1R	amp	puromycin	GCTCTTGTTCAGGATGGAATT	TRC with the Broad institute	TRCN0000059261
2122	pLKO.1	shRNA targeting IL-1R	amp	puromycin	CCCGGGTAATAGAATTTATTA	TRC with the Broad institute	TRCN0000059262
2123	pDeNy	MYD88 dominant negative	zeocin	zeocin	NA	InvivoGene	pDeNy MYD88

2124	pDeNy	IRAK1 dominant negative	zeocin	zeocin	NA	InvivoGene	pDeNy IRAK1
2125	pFUGW	CAS9 expression plasmid	amp	Blasticidin	NA	Addgene	52962
2126	lenti-guide	empty vector control	amp	puromycin	NA	Addgene	52963
2127	lenti-guide	CRISPR for IRAK4	amp	puromycin	CCTGGGAGCAAAAGACTCGC	Addgene	75664
2128	lenti-guide	CRISPR for IRAK4	amp	puromycin	TGTAAACATATACTAAGCAG	Addgene	75665
2129	lenti-guide	CRISPR for IRAK4	amp	puromycin	CTCATGTGCCAAGAAAGTGG	Addgene	75666
2130	pLentiCRISPR v2	CRISPR for ABCD1	amp	puromycin	CCTGTCGTTCCGCAGCCGTC	Genscript	crRNA 1
2131	pLentiCRISPR v2	CRISPR for ABCD1	amp	puromycin	CGACGACATGATCCGCTCAA	Genscript	crRNA 2
2132	pLentiCRISPR v2	Empt vector CRISPR	amp	puromycin		Addgene	Damania Lab UNC
2133	pLentiCRISPR v2	Scramble control CRISPR	amp	puromycin		Addgene	Damania Lab UNC
2134	pLentiCRISPR v2	CRISPR for IRAK4	amp	puromycin	CCTGGGAGCAAAAGACTCGC	Genscript	crRNA1
2135	pLentiCRISPR v2	CRISPR for IRAK4	amp	puromycin	ATGGCACCAGAAGCTTTGCG	Genscript	crRNA2

2136	pLentiCRISPR v2	CRISPR for IRAK4	amp	puromycin	ACACCGTGAACCTCAGTTAT	Genscript	crRNA3
2137	P-select-ZEo	Empty vector for DD	zeocin	zeocin	NA	InvivoGene	
2138	pMXs-IRES-Puro	WT mouse IRAK4	amp	puromycin	NA	PI Xiaoxia Li, CMSI# CW2485347	
2139	pMXs-IRES-Puro	EV	amp	puromycin	NA	PI Xiaoxia Li, CMSI# CW2485347	
2140	pMXs-IRES-Puro	K231M mouse IRAK4	amp	puromycin	NA	PI Xiaoxia Li, CMSI# CW2485347	
2141	pMXs-IRES-Puro	L360A mouse IRAK4	amp	puromycin	NA	PI Xiaoxia Li, CMSI# CW2485347	
2142	pMXs-IRES-Puro	R361E mouse IRAK4	amp	puromycin	NA	PI Xiaoxia	

						Li, CM SI# CW 248 534 7	
2143	pLKO.1	shRNA targeting IRAK1	amp	puromycin	GCTGAA GTAGGA GGATCA TTT	TR C with the Bro ad insti tute	TRCN00 0012113 7
2144	pLKO.1	shRNA targeting IRAK1	amp	puromycin	GCCACC GCAGAT TATCAT CAA	TR C with the Bro ad insti tute	TRCN00 0012113 8
2145	pLKO.1	shRNA targeting MYD88	amp	puromycin	ACAGAC AAACTA TCGACT GAA	TR C with the Bro ad insti tute	TRCN00 0000802 6
2146	pLKO.1	shRNA targeting MYD88	amp	puromycin	CCTGTC TCTGTT CTTGAA CGT	TR C with the Bro ad insti tute	TRCN00 0001122 3
2147	pCMV6-Entry	expression vector for IRAK1	kan	G418	D340N	Orig ene/ Blu eher on	
2148	pCMV6-Entry	expression vector for IRAK1	kan	G418	196f	Orig ene/ Blu eher on	

2149	pCMV6-Entry	expression vector for IRAK1	kan	G418	196f/D340N	Origene/Blueheron	
2150	pLentiCRISPR v2	CRISPR for IRAK1	amp	puromycin	CAACCGGGCCCTCTTACCTG	Genscript	
2151	pLentiCRISPR v2	CRISPR for IRAK1	amp	puromycin	ACCGAACTGGCACCAGTCGG	Genscript	
2152	pLentiCRISPR v2	CRISPR for IRAK1	amp	puromycin	CCCACCGAACTGGCACCAGT	Genscript	
2153	pLentiCRISPR v2	CRISPR for IL-1R1	amp	puromycin	AAGCAGAAACTACCCGTTGC	Genscript	
2154	pLentiCRISPR v2	CRISPR for IL-1R1	amp	puromycin	AAGTCCTCCGTCTCCTGCAA	Genscript	
2155	pLentiCRISPR v2	CRISPR for IL-1R1	amp	puromycin	GCAAGCAATATCCTATTACC	Genscript	
2156	U6-gRNA:PGK-puro-2A-tagBFP	CRISPR IRAK2	amp	puromycin	AAGCTGCCAAAGGCTTTTCTGG	Sigma	HS5000033157
2157	U6-gRNA:PGK-puro-2A-tagBFP	CRISPR IRAK2	amp	puromycin	GCAGGGTGTGAGCATCACGCGG	Sigma	HS5000033158
2158	U6-gRNA:PGK-puro-2A-tagBFP	CRISPR IL-1R1	amp	puromycin	GTATATTGTCAAGAAGTAGAGG	Sigma	HS5000025663
2159	U6-gRNA:PGK-puro-2A-tagBFP	CRISPR IL-1R1	amp	puromycin	AGGCTCATCGTGATGAATGTGG	Sigma	HS5000025664
2160	U6-gRNA:PGK-puro-2A-tagBFP	CRIPSR IRAK1	amp	puromycin	CTTCACTGCAGTCCACTCCAGG	Sigma	HS5000019451

2161	U6-gRNA:PGK-puro-2A-tagBFP	CRISPR IRAK1	amp	puromycin	CAGCTGCTCCACCTCGGTCAGG	Sigma	HS5000019452
2162	U6-gRNA:PGK-puro-2A-tagBFP	CRISPR MYD88	amp	puromycin	GACAACCACCACCATCCGGCGG	Sigma	HS5000001249
2163	U6-gRNA:PGK-puro-2A-tagBFP	CRISPR MYD88	amp	puromycin	GTCACATTCCTTGCTCTGCAGG	Sigma	HS5000001250

Table AA. 2: Antibodies used in this study:

Catalog numbers, the protein that the antibody targets, size in kilo Daltons that is predicted for the gel to run and what is the species the antibody was raised in are displayed in this table.

Catalog Number	Protein	Size KD	Species	Company
#4970	Actin	42	Rabbit	Cell Signaling
#3700S	Actin	42	Mouse	Cell Signaling
#2272	MYC-TAG	NA	Rabbit	Cell Signaling
#05-724	MYC-TAG	NA	Mouse	Millipore
MABE1668	Cas9	160	Mouse	Millipore
#9662S	Casp3	17, 19, 35	Rabbit	Cell Signaling
#9579S	Cleav-Casp3	17, 19	Rabbit	Cell Signaling
#5625S	Cleav-PARP	89	Rabbit	Cell Signaling
#3865	IL-1RA	18	Rabbit	Cell Signaling
ab180894	IL1-RL2	55	Rabbit	Abcam
#4504	IRAK1	75-105	Rabbit	Cell Signaling
GTX50994	IRAK1 209P	75	Rabbit	Genetex
A1074	IRAK1 209P	75	Rabbit	Assay Biotech
custom	IRAK1 209P	75	Rabbit	Genscript
ab218130	IRAK1 P209	75	Rabbit	Abcam
PA5-38633	IRAK1 P209	75-105	Rabbit	Thermo-Fisher
ab139739	IRAK1 P387	75-105	Rabbit	Abcam
MAB6690	IRAK2	75	Mouse	R&D systems
ab62419	IRAK2	75	Rabbit	Abcam
#4363	IRAK4	55	Rabbit	Cell Signaling
AF3919	IRAK4	55	Goat	RD
ab5985	IRAK4	55	Rabbit	Abcam
#11927	IRAK4 P	55	Rabbit	Cell Signaling
ab113656	IRAK4 P	55	Mouse	Abcam

ab8116	IRAKM	70	Rabbit	Abcam
#4283	MYD88	33	Rabbit	Cell Signaling
ab2064	MYD88	33	Rabbit	Abcam
PA5-15149	TAK1	75ish	Rabbit	Thermo-Fisher
MA515073	TAK1 P	75ish	Rabbit	Sigma
#8028	TRAF6	60ish	Rabbit	Cell Signaling
ab94393	IL-1R	73	Rabbit	Abcam
PA5-29227	IL-1R	75	Rabbit	Thermo-Fisher
sc-393998	IL-1R	80	Mouse	Santa Cruz
MAB2162	ABCD1	65	Mouse	Millipore
#4904	STAT3	75	Rabbit	Cell Signaling
#9145	P-STAT3	75	Rabbit	Cell Signaling
#9131	P-STAT3	75	Rabbit	Cell Signaling
#8242	NFκB p65	80	Rabbit	Cell Signaling
#3033	pp65	80	Rabbit	Cell Signaling
Hydridoma	vIL-6	25	Mouse	NA
#MA5-14769	ORF45	65	Mouse	Invitrogen

Table AA. 3: Small Molecule inhibitors used in this study:

This table displays the various inhibitors used in this study, their chemical formulas, CAS numbers, EC50 values in PEL BCBL-1 cells, and the ability to inhibit colony formation at two concentrations.

Name	Formula	CAS No.	EC50 BCBL-1	Colony Inhibition at 1 µM	Colony Inhibition at 10 µM
IRAK inh1	C17H19N5	1042224-63-4	15.9 ± 11	yes	yes
IRAK inh2	C17H14N4O2	928333-30-6	10.9 ± 9.6	no	yes
IRAK inh3	C21H21N5O4S	1012343-93-9	53 ± 8	no	no
IRAK inh4	C33H35F3N6O3	1012104-68-5	5.5 ± 0.5	no	yes
IRAK inh1/4	C20H21N5O4	1042224-63-4	274 ± 52	no	no
IRAK inh6	C20H20N4O3S	1042672-97-8	16.6 ± 17	no	no
BAY11-7082	C10H9NO2S	19542-67-7	0.6 ± 0.2	yes	yes
ST2825	C27H28Cl2N4O5S	894787-30-5	8.4 ± 3.4	no	yes
Acalabrutinib	C26H23N7O2	1420477-60-6	98 ± 6.5	no	no
AVL-292	C22H22FN5O3	1202757-89-8	3.45 ± 1.1	yes	yes
PCI-32765 (Ibrutinab)	C25H24N6O2	936563-96-1	19.6 ± 20	no	yes

Table AA. 1: Pathways that are always on in WT BCBL-1 cells according to IPA analysis. These pathways have members that are active in resting state WT BCBL-1. This activation is lost in IRAK4 knockout cells.

Diseases or Functions Annotation	p-Value	Molecules	# Molecules
Abdominal cancer	0.00185	ARHGAP30,B2M,BCL7A,ENG,EPB41L3,FTL,HSP90AA1,RPS12,SELPLG,SLC16A3,SULT1A1,YWHAQ	12
Cancer of secretory structure	0.00268	ARHGAP30,B2M,BCL7A,ENG,EPB41L3,HSP90AA1,RPS12,SELPLG,SLC16A3,SULT1A1,YWHAQ	11
Genital tract cancer	0.000322	ARHGAP30,B2M,ENG,EPB41L3,HSP90AA1,RPS12,SELPLG,SLC16A3,SULT1A1,YWHAQ	10
Genital tumor	0.000408	ARHGAP30,B2M,ENG,EPB41L3,HSP90AA1,RPS12,SELPLG,SLC16A3,SULT1A1,YWHAQ	10
Pelvic cancer	0.000629	ARHGAP30,B2M,ENG,EPB41L3,HSP90AA1,RPS12,SELPLG,SLC16A3,SULT1A1,YWHAQ	10
Malignant genitourinary solid tumor	0.00222	ARHGAP30,B2M,ENG,EPB41L3,HSP90AA1,RPS12,SELPLG,SLC16A3,SULT1A1,YWHAQ	10
Breast or gynecological cancer	0.000903	ARHGAP30,B2M,ENG,EPB41L3,HSP90AA1,RPS12,SLC16A3,SULT1A1,YWHAQ	9
Uterine cancer	0.000111	ARHGAP30,B2M,ENG,EPB41L3,HSP90AA1,RPS12,SLC16A3,SULT1A1	8

Endometrial cancer	0.000539	ARHGAP30,B2M,ENG,EPB41L3,HSP90AA1,SLC16A3,SULT1A1	7
Upper gastrointestinal tract cancer	0.000632	B2M,BCL7A,ENG,EPB41L3,HSP90AA1,RPS12,SULT1A1	7
Respiratory system tumor	0.00115	ARHGAP30,B2M,EPB41L3,FTL,HSP90AA1,RPS12,SULT1A1	7
Prostatic tumor	0.00208	B2M,ENG,EPB41L3,HSP90AA1,SELPLG,SLC16A3,YWHAQ	7
Advanced extracranial solid tumor	1.42E-05	B2M,ENG,EPB41L3,FTL,HSP90AA1,SLC16A3	6
Secondary tumor	0.000163	B2M,ENG,EPB41L3,FTL,HSP90AA1,SLC16A3	6
Non-small cell lung carcinoma	0.000736	ARHGAP30,B2M,EPB41L3,FTL,HSP90AA1,SULT1A1	6
Cell proliferation of tumor cell lines	0.00208	ENG,EPB41L3,FTL,HSP90AA1,SLC16A3,YWHAQ	6
Upper gastrointestinal carcinoma	0.00288	B2M,ENG,EPB41L3,HSP90AA1,RPS12,SULT1A1	6
Liver carcinoma	0.0242	B2M,ENG,EPB41L3,FTL,HSP90AA1,SULT1A1	6

Figures

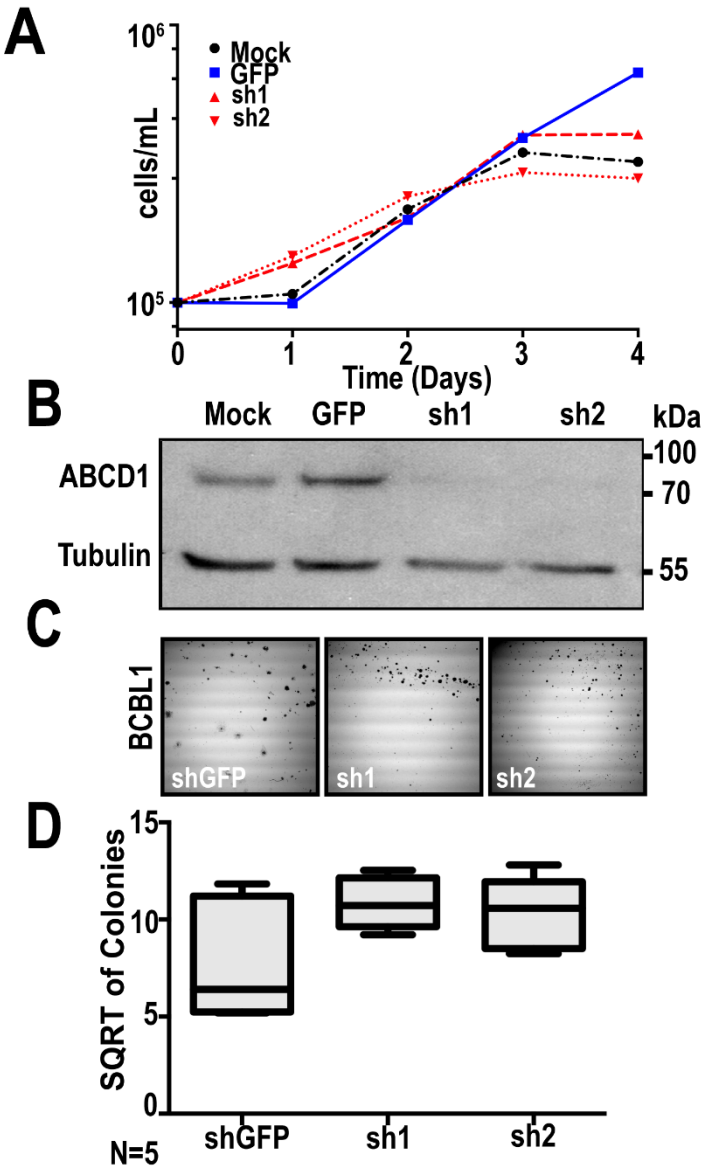

Figure AA. 1: Knockdown of ABCD1 has no effect on PEL growth.

A) ABCD1 western blot verifying knockdown, loading control is β-actin. **B)** Growth curves for ABCD1 KD stable BCBL-1 cells via though Trypan blue cell counting. Two different ABCD1 shRNA and a GFP targeting non-control were used in this experiment. **C)** Representative images from colony formation assays of ABCD1 KD stable BCBL-1 cells plated at a low cell density in 1% methylcellulose medium and grown for three weeks. Colony formation was imaged at 40X magnification. **D)** Quantification of colony formation in BCBL-1 ABCD1 KD stable cell lines using ImageJ.

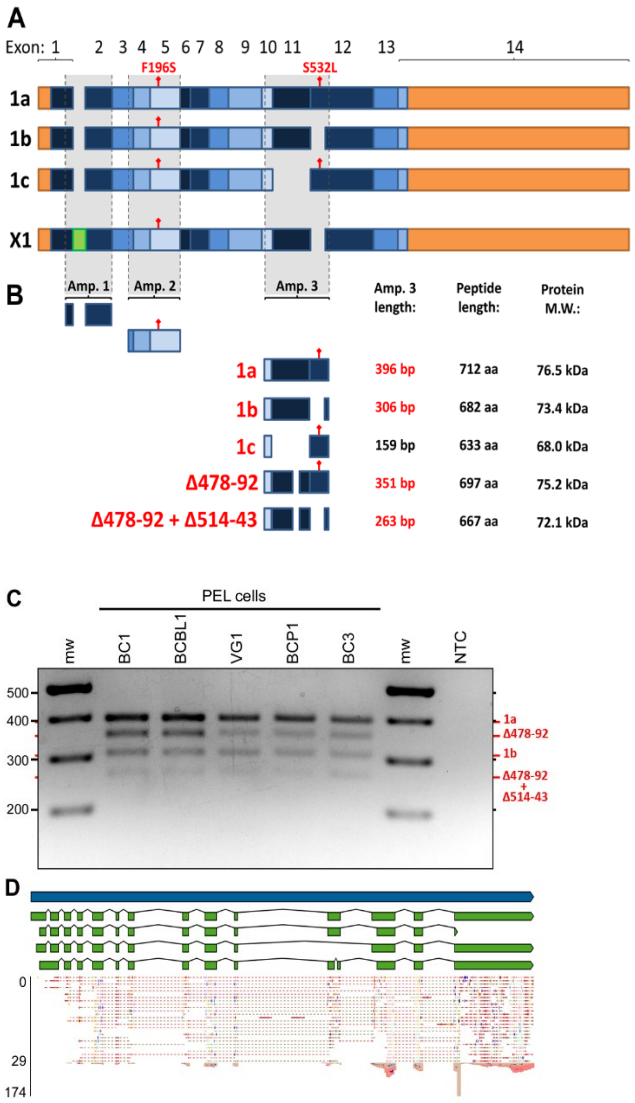

Figure AA. 2: **PEL cells contain F196S and S532L Variants in IRAK1.**

cDNA from several PEL cell lines was PCR-amplified and subjected to Sanger sequencing. All of the cells examined contain F196S and S532L Variants. **A)** Scale schematic of the four IRAK1 transcript isoforms listed on NCBI, including the three major transcripts from the literature – 1a, 1b, and 1c. 5' and 3' UTRs are in orange, coding portions of exons are in shades of blue, inclusion of a potential intron in transcript X1 is in green, gaps indicate regions not present in specific isoforms, and regions amplified by PCR are shaded gray. **B)** Scale schematic showing all variations of IRAK1 amplicons detected in PEL cells. The

potential intron from transcript X1 in amplicon 1 was not detected. Amplicon 3 spans the only known region of variation in IRAK1 isoforms across exons 10 to 12. The three major transcripts plus two potential new transcript isoforms (in red text) were sequenced in BC-1 cells. Δ# denotes which codons are deleted relative to the 1a transcript. Length of amplicon 3 (in red text) corresponds to bands in panel C. **C)** Agarose gel electrophoresis of amplicon 3. NTC, non-template control; mw, molecular weight marker.

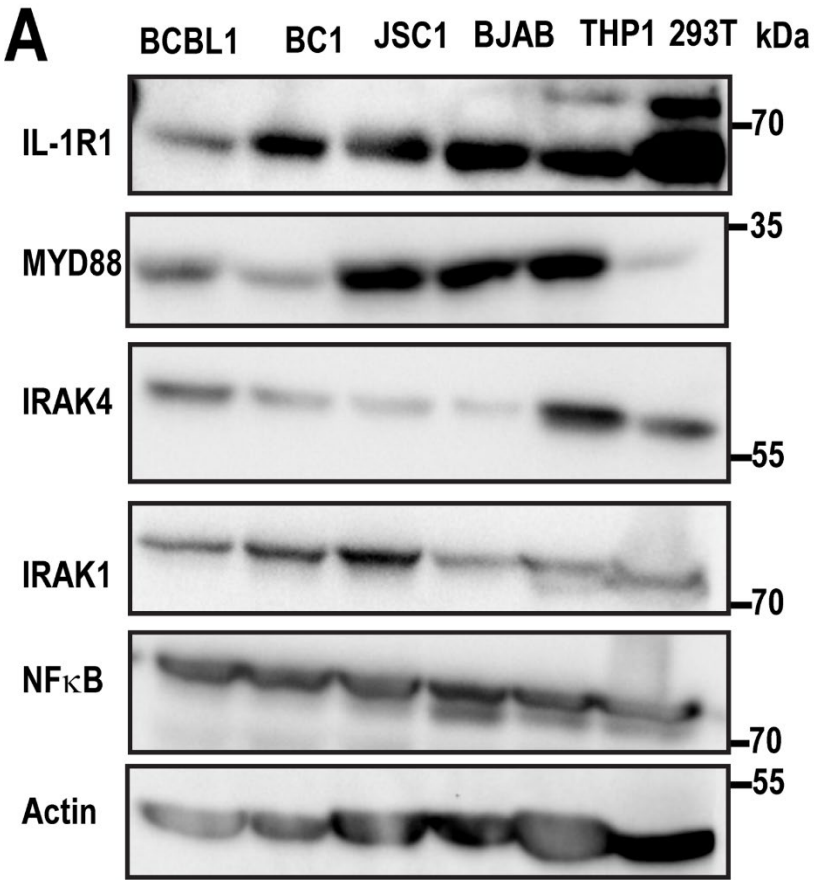

Figure AA. 3: Western blot of the IRAK pathway in PEL and other cell lines.

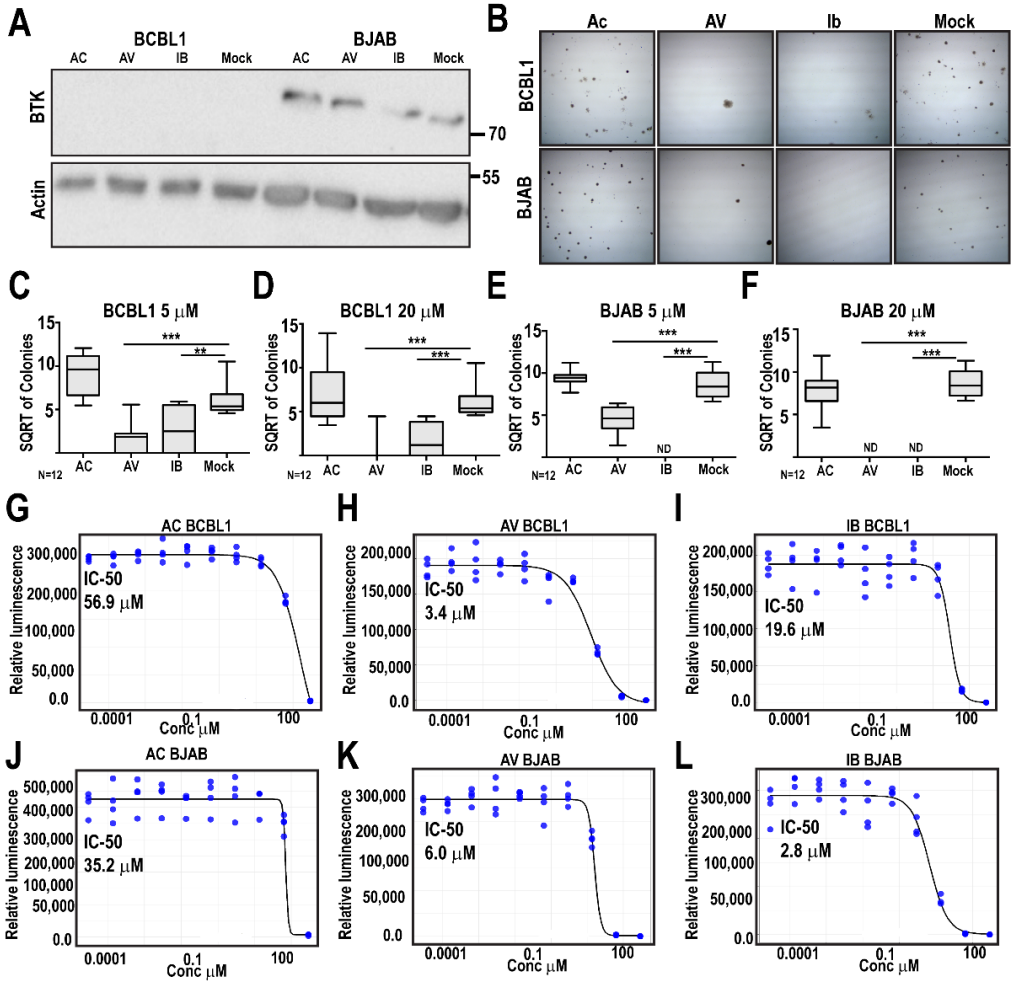

Figure AA. 4: BTK is not expressed in PEL.

BTK was examined to determine if the protein played a role in PEL. **A)** Western blot analysis of Total BTK in BCBL-1 and BJAB cells treated with three BTK inhibitors. AC = Acalabrutinib, AV = AVL-292, and IB = Ibrutinib. Actin was probed to show even loading. **B)** Representative images of colony formation assays showing the effectiveness of the three BTK inhibitors in killing cells when treated with 5 μM of each inhibitor**. C-F)** Quantification of colony formation assays at both 5 and 20 μM for BCBL-1 and BJAB via ImageJ. Tukey Test was used to determine confidence intervals**. G-L)** IC50 curves for each inhibitor in each cell line generated from CTG assays after drug treatment and generated on R using DL4RP code.

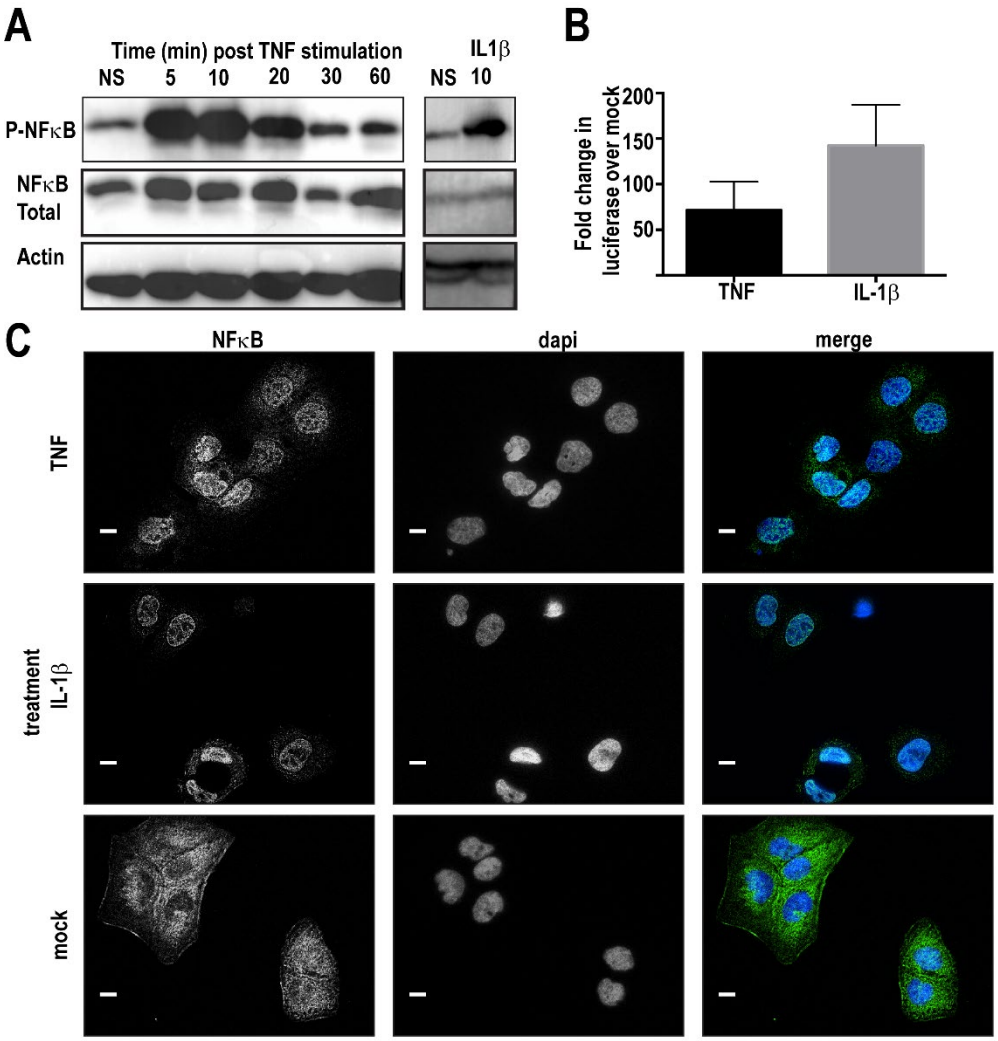

Figure AA. 5: **U2OS cells have functional IL-1β signaling.**

A) Western blot for total, P-NFκB, and actin. Cells were stimulated with TNF-α, or IL-1β for the noted amount of time. **B)** A luciferase assay testing for the activation of NFκB driven luciferase following TNF-α or IL-1β stimulation. Values are represented as a fold change over non-stimulated PBS control. **C)** NFκB translocation observed via Immunofluorescence. Cells were treated with TNF-α, or IL-1β for one hour and nuclear translocation of NFκB was examined by probing for P65. Single channels are in gray scale. Scale bars are 20 μM.

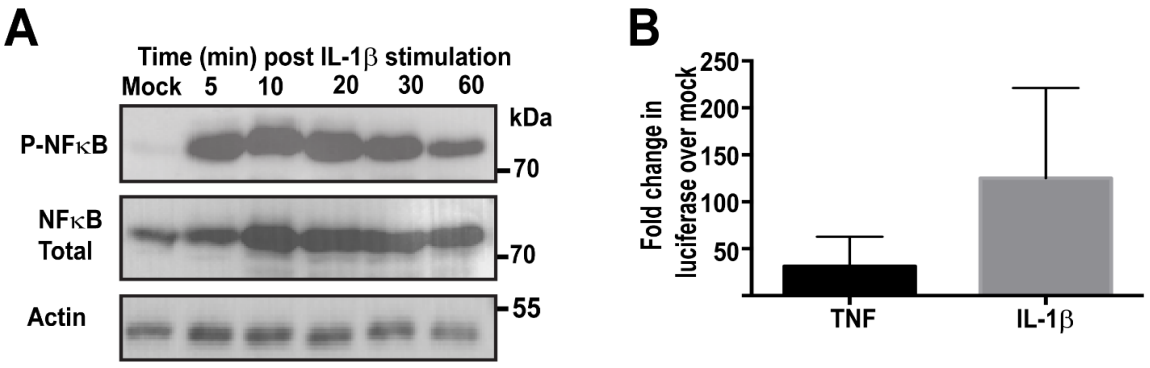

Figure AA. 6: TNF and IL-1β activate NFκB in PEL.

A) Time course western blot of p-NFκB in BCBL-1 cells following stimulation with IL-1β.

B) Luciferase assay measuring luminescence following stimulation of cells with TNF or IL-1B when luciferase is on a plasmid with an NFκB driven promoter.

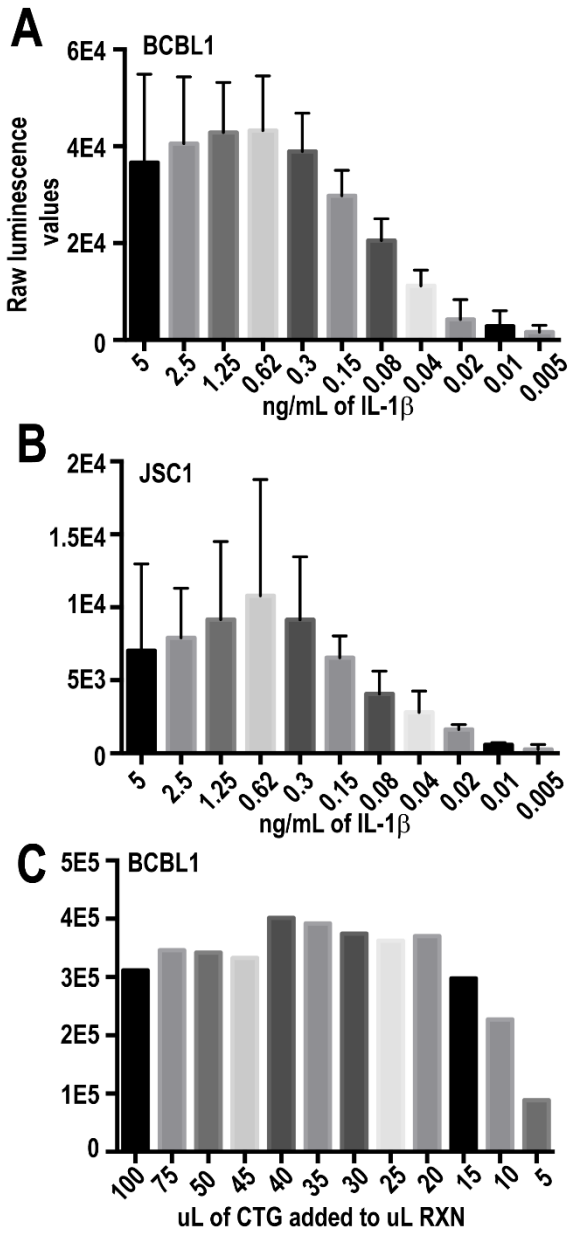

Figure AA. 7: IL-1β and CTG titration in BCBL-1 cells.

A) Titration of IL-1β in PEL cell line BCBL-1 to determine proper dosing for use in various studies using IL-1β. **B)** Titration of IL-1β in PEL cell line JSC1 cells to determine proper dosing. **C)** CTG reagent titration in BCBL-1 cells.

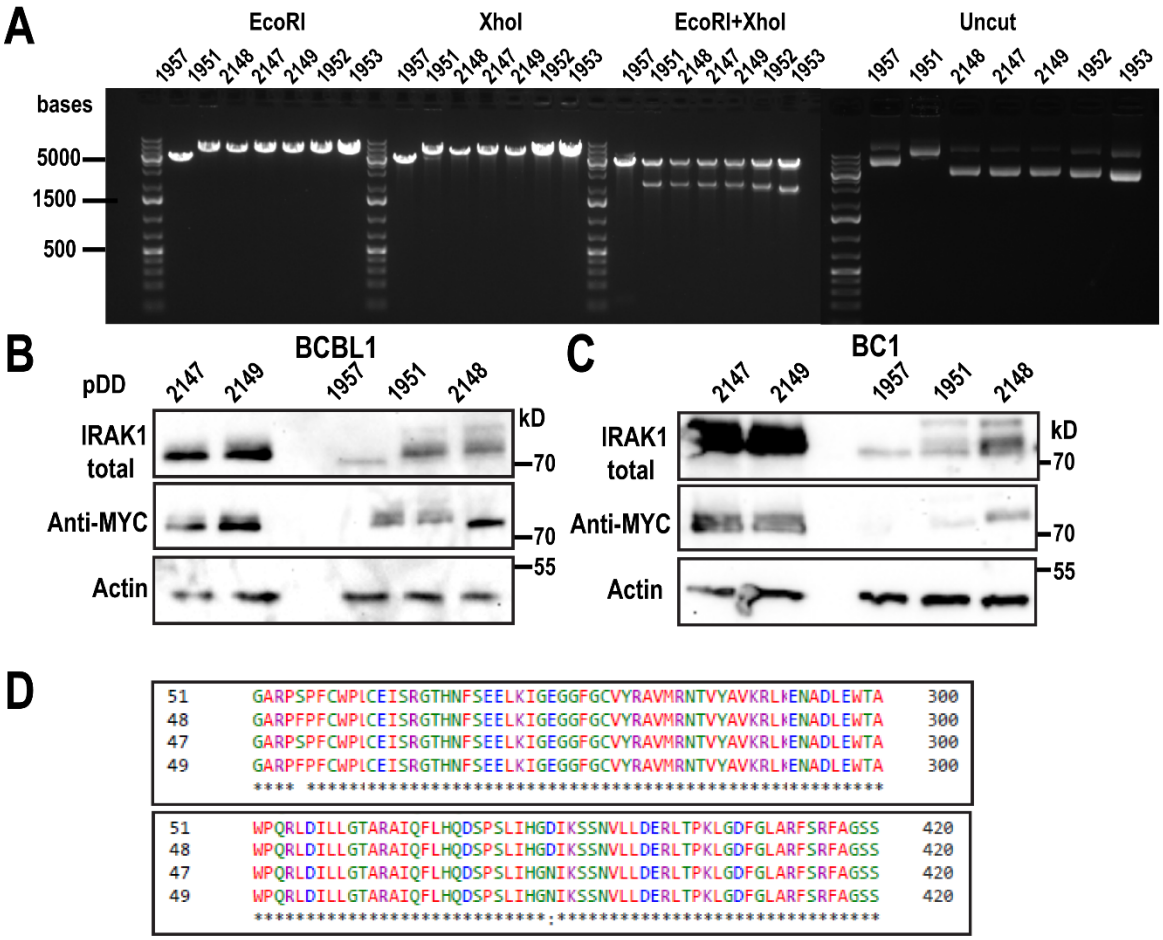

Figure AA. 8 Validation of IRAK expression plasmids.

A) Restriction digest of IRAK1 expression plasmids. **B)** Western blot of IRAK expression plasmids in BCBL-1 cells. **C)** Western blot of IRAK expression plasmids in BC-1 cells. **D)** Sequences alignment of IRAK expression plasmids showing the mutated residues at position 196 and 340.

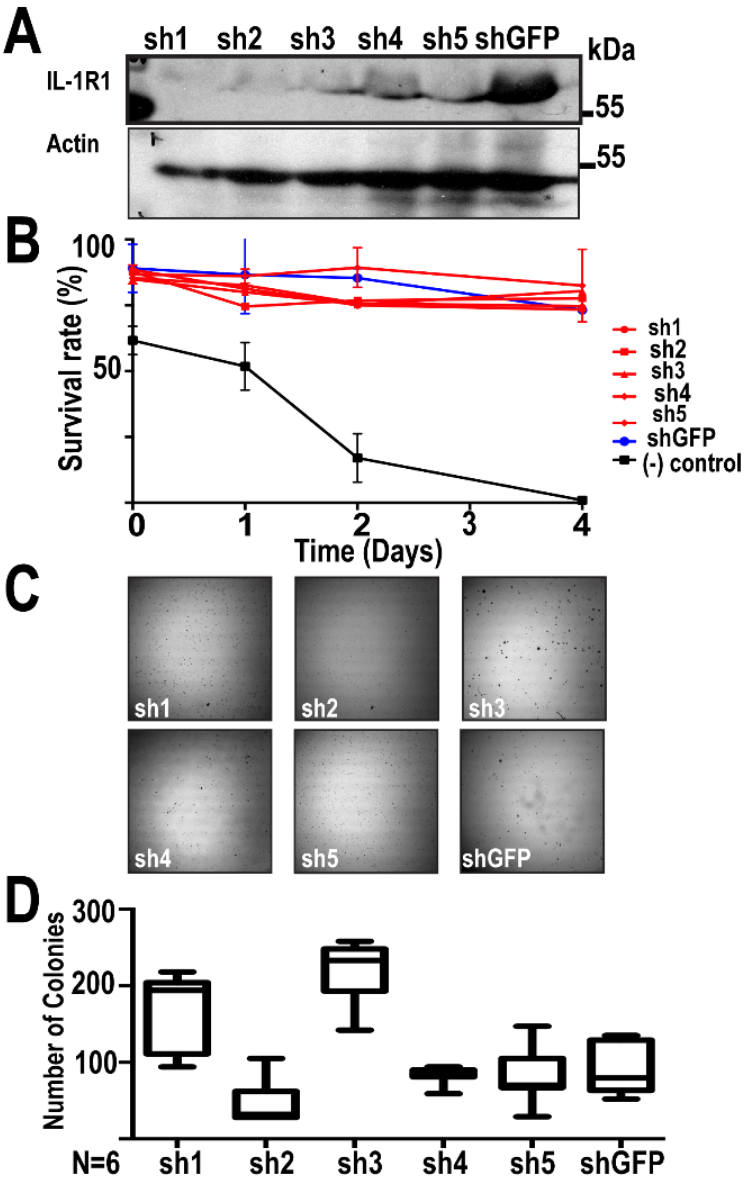

Figure AA. 9: **IL1R shRNA figure BCBL-1.**

A) IL-1R1 western blot of BCBL-1 cells, loading control is β-actin. **B)** Survival curves following shRNA knockdown for IL-1R1 KD BCBL-1 cells via Trypan blue cell counting. Five different IL-1R1 and a no-targeting GFP control guides were used in this experiment. Negative control is WT BCBL-1 with no resistance inferred to puromycin. **C)** Representative images from colony formation assays of IL-1R1 KD BCBL-1 cells plated at a low cell density in 1% methylcellulose medium and grown for three weeks. Images are at 40X magnification. **D)** Quantification of colony formation in BCBL-1 IL-1R1 KD via ImageJ.

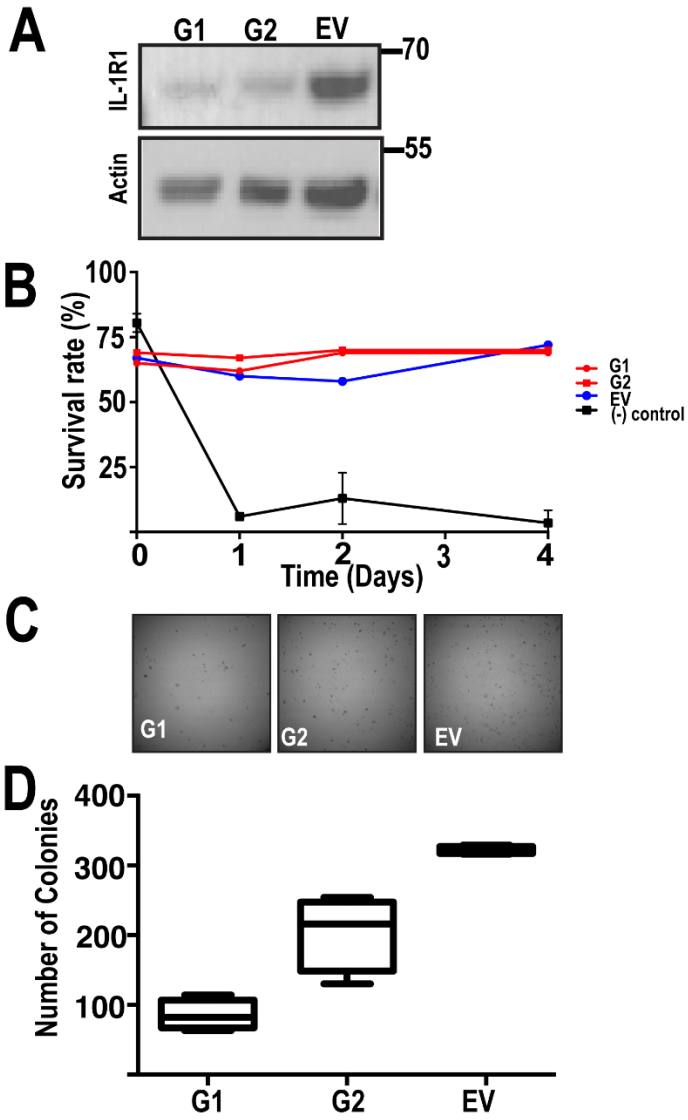

Figure AA. 10: **IL1R CRSIPR BCBL-1.**

A) IL-1R1 CRIPSR western blot of BCBL-1 cells, loading control is β-actin **B)**. Survival curves following CRISPR knockout for IL-1R1 KD BCBL-1 cells via Trypan blue cell counting. Two different IL-1R1 and an empty vector control were used in this experiment. **C)** Representative images from colony formation assays of IL-1R1 KO BCBL-1 cells plated at a low cell density in 1% methylcellulose medium and grown for three weeks. Images are at 40X magnification. **D)** Quantification of colony formation in BCBL-1 IL-1R1 KO as quantified by ImageJ.

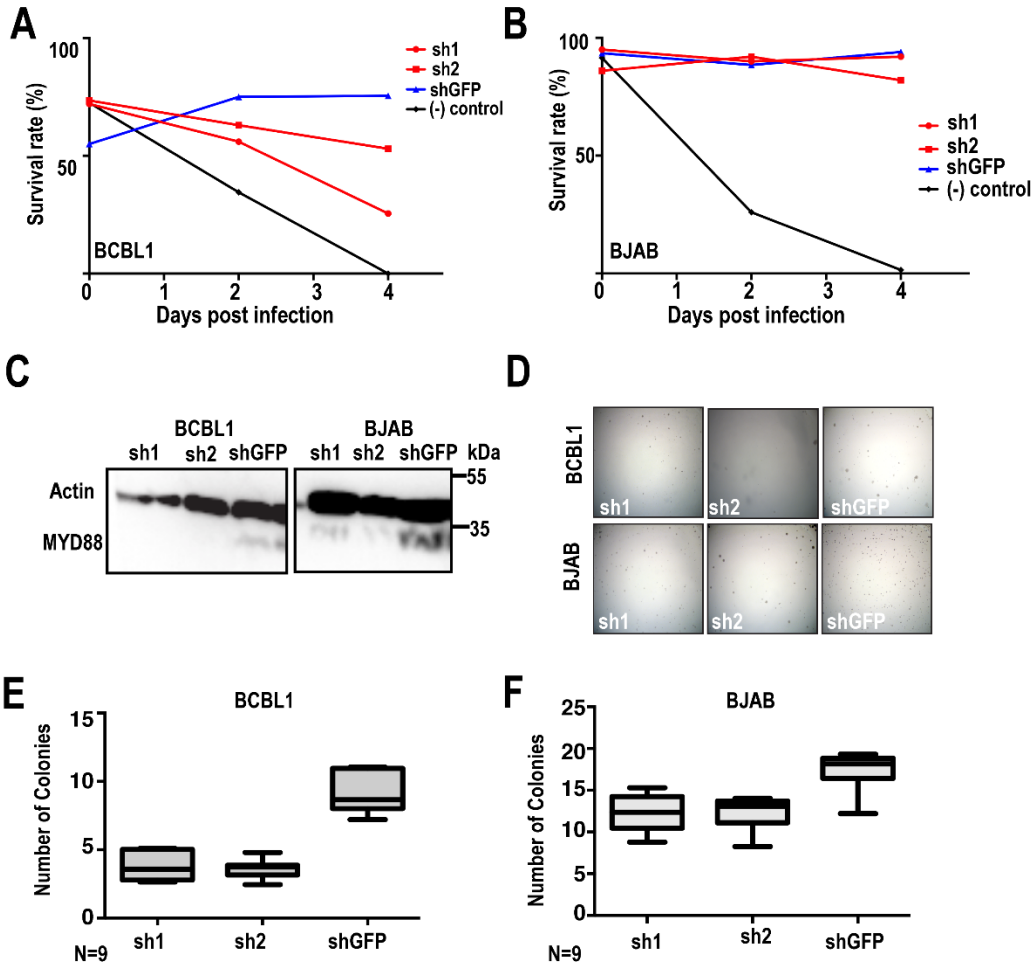

Figure AA. 11: MYD88 shRNA data.

A) Survival curves for BC-1 treated with shRNA targeting MYD88. Live/dead cell counts are obtained using Trypan blue. Two shRNA targeting MYD88 were used as was a non-targeting GFP control. (-) control is WT cell lines **B)** Survival curves for BJAB treated with shRNA targeting MYD88. **C)** Western blot for MYD88 showing knock down in, BC-1 and BJAB cells. **D)** Colony formation assay images for MYD88 shRNA treated cells BC-1 and BJAB. Images are 40X **E)** Quantification of colony formation assays for MYD88 shRNA treated BC-1 cells. Quantified in ImageJ **F)** Quantification of colony formation assays for MYD88 shRNA treated BJAB cells.

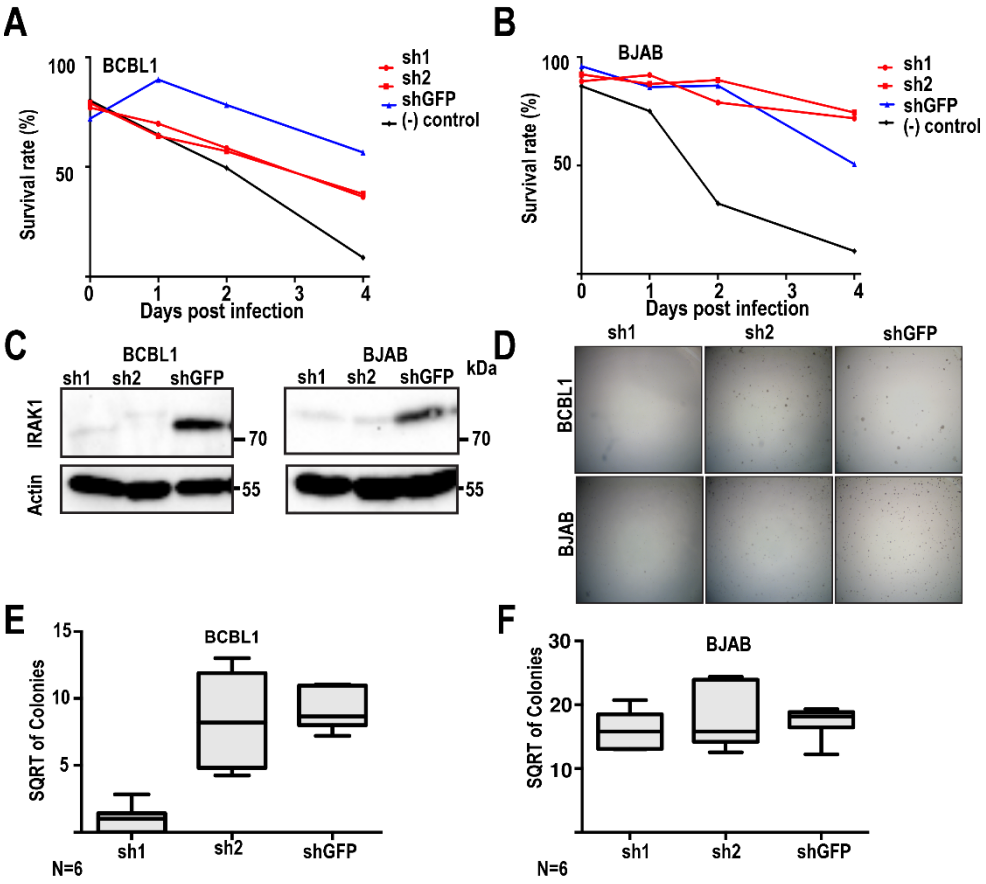

Figure AA. 12: **IRAK1 shRNA results.**

A) Survival curves for BCBL-1 treated with shRNA targeting IRAK1. Live/dead cell counts are obtained using Trypan blue. Two shRNA targeting IRAK1 were used as was a non-targeting GFP control. (-) control is WT cell lines. **B)** Survival curves for BJAB treated with shRNA targeting IRAK1. **C)** Western blot for IRAK1 showing knock down in, BCBL-1 and BJAB cells. **D)** Colony formation assay images for IRAK1 shRNA treated cells BCBL-1 and BJAB. Images are 40X **E)** Quantification of colony formation assays for IRAK1 shRNA

treated BCBL-1 cells. Quantified in ImageJ **F)** Quantification of colony formation assays for IRAK1 shRNA treated BJAB cells.

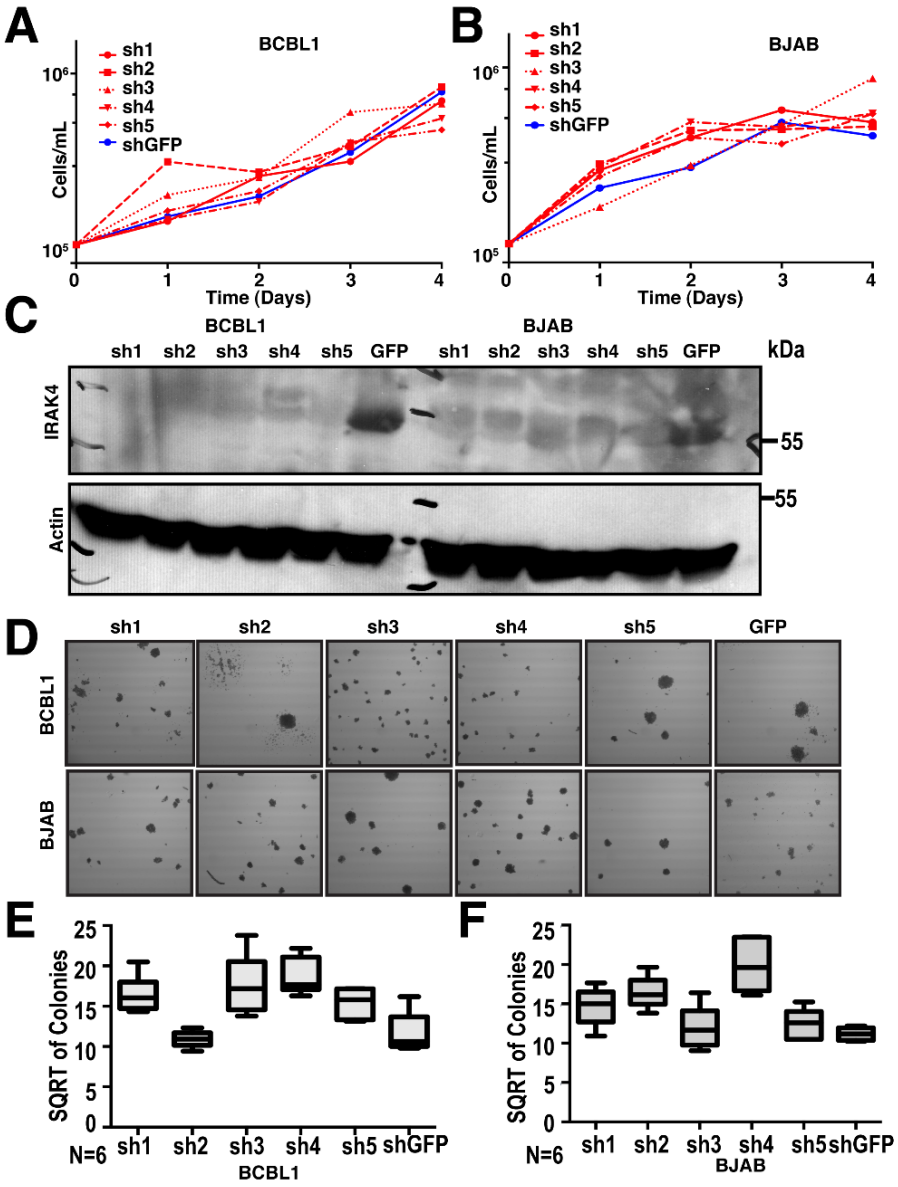

Figure AA. 13: **IRAK4 shRNA data.**

A) Growth curves for IRAK4 KD stable BCBL-1 cells via Trypan blue cell counting. Five different IRAK4 and a no-targeting GFP control guides were used in this experiment. **B)** IRAK4 western blot of BCBL-1 cells, loading control is β-actin**. C)** Representative images from colony formation assays of IRAK4 KD BCBL-1 cells plated at a low cell density in 1% methylcellulose medium and grown for three weeks. Images are at 40X magnification. **D)** Quantification of colony formation in BCBL-1 IRAK4 KD obtained via ImageJ.

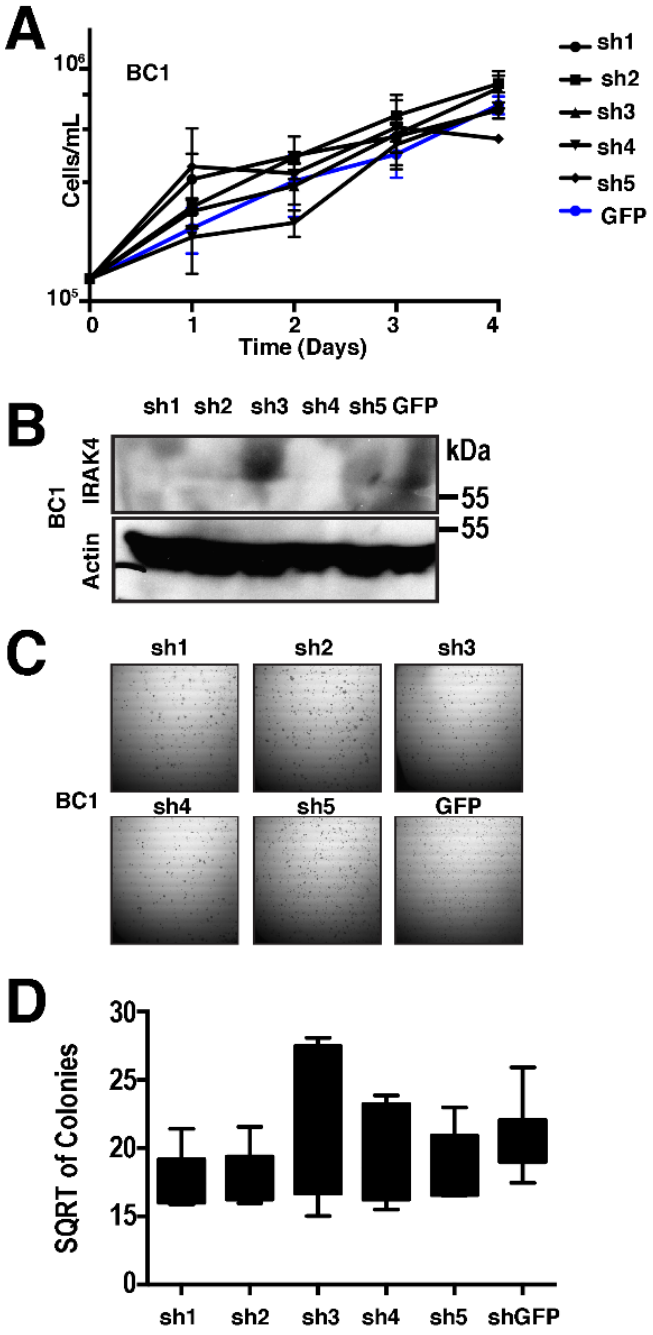

Figure AA. 14: IRAK4 shRNA has no effect in BC-1.

A) Growth curves for IRAK4 KD stable BC-1 cells via Trypan blue cell counting. Five different IRAK4 and a no-targeting GFP control guides were used in this experiment. **B)** IRAK4 western blot of BC-1 cells, loading control is β-actin. **C)** Representative images from colony formation assays of IRAK4 KD BC-1 cells plated at a low cell density in 1% methylcellulose medium and grown for three weeks. Images are at 40X magnification. **D)** Quantification of colony formation in BC-1 IRAK4 KD obtained via ImageJ.

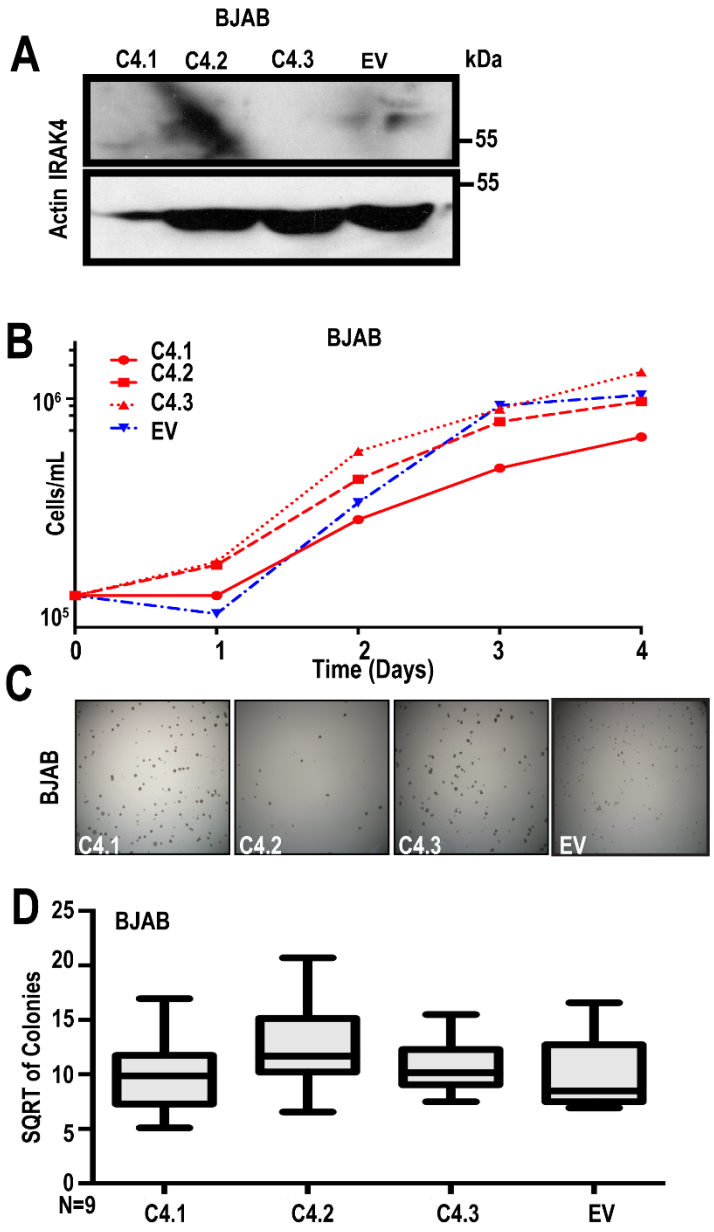

Figure AA. 15: CRISPR knockout of IRAK4 has no effect on BJAB cells.

A) IRAK4 western blot of BJAB cell lines showing complete KO, loading control is β-actin. **B)** Growth curves for BJAB IRAK4 KO clones obtained via Trypan blue cell counting. Two different IRAK4 KO clones and an empty vector control were used in this experiment. **C)** Representative images from colony formation assays of IRAK4 KO BJAB and BJAB cells imaged at 10X magnification. Cells are plated at a low cell density in 1% methylcellulose medium and grown for three weeks. **D)** Quantification of colony formation in BJAB IRAK4 KO stable cell lines. Colony counts were obtained using ImageJ.

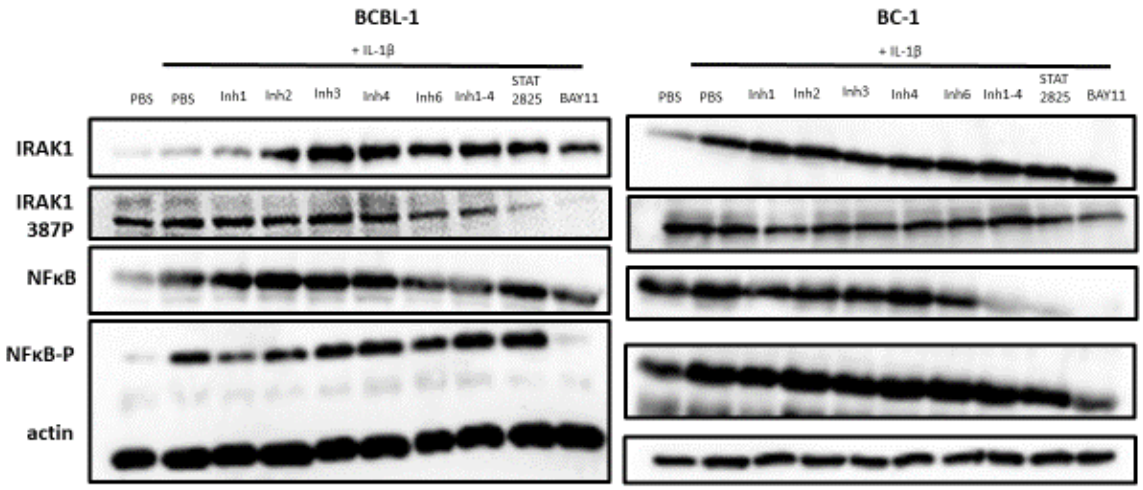

Figure AA. 16: NFκB is constitutively activated in BC-1 but not BCBL-1 cells.

Cells were treated with IL-1β in the presences or absence of the 6 IRAK inhibitors, MYD88 inhibitor and the NFκB inhibitor BAY11-7082 . Lysates were collected 15 minutes post IL-1β stimulation.

Figure AA. 17. IPA pathway analysis on IRAK4 knockout RNA-seq.

IPA pathway analysis on RNA-seq data for the top changes in pathways when comparing WT to ΔIRAK4 cells. Orange means the pathway is up in the Knockout and blue means it is down. The X axis is by the –log(P-value).

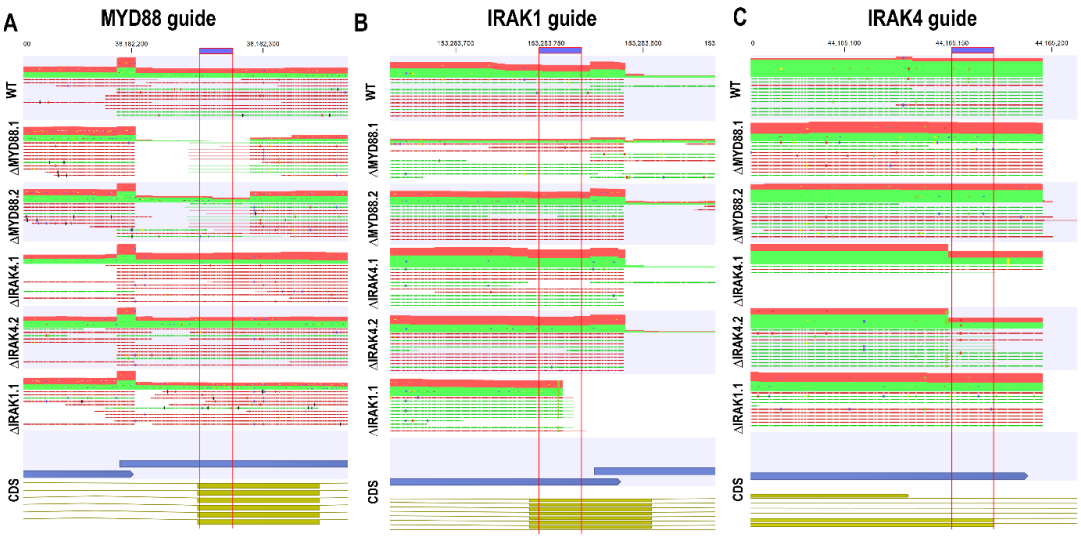

Figure AA. 18: **Exome sequencing data for the IRAK pathway knockouts in BCBL1**:

A) Highlights that there is a deletion seen in the MYD88 knockout lines but not the other three cell lines. **B)** Demonstrates knockout of IRAK1. **C)** Demonstrates knockout of IRAK4 as seen by the reduction in coverage.

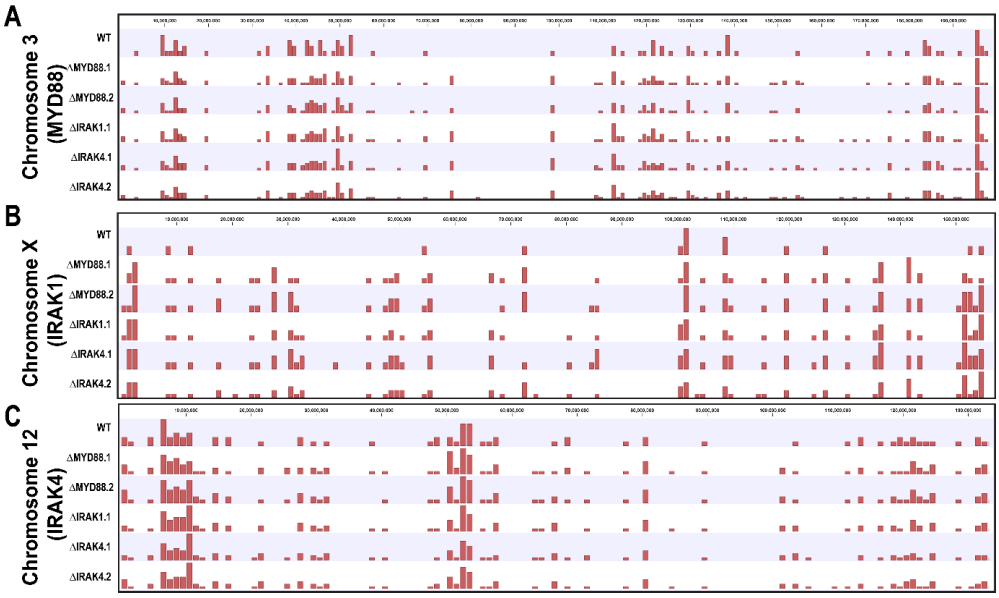

Figure AA. 19 Exome sequencing variant calling in BCBL1

A) Chromosome 3 which contains MYD88 **B)** X chromosome which contains IRAK1. **C)** Chromosome 12 which contains IRAK4.

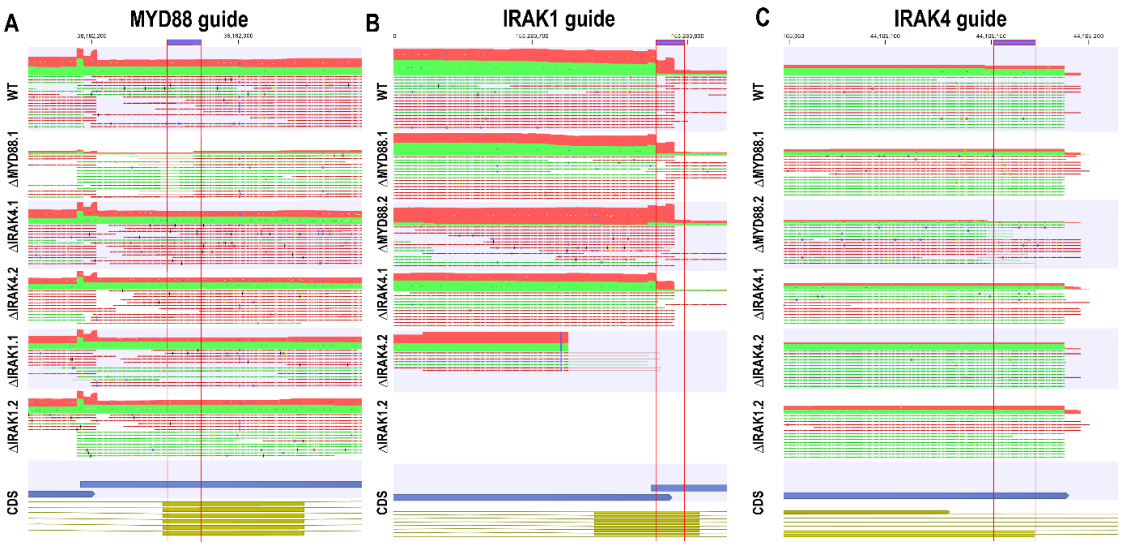

Figure AA. 20 Exome sequencing data for the IRAK pathway knockouts in BC1.

A) Highlights that there is a deletion seen in the MYD88 knockout lines but not the other three cell lines. **B)** Demonstrates knockout of IRAK1. **C)** Demonstrates knockout of IRAK4 as seen by the reduction in coverage.

Figure AA. 21 Exome sequencing variant calling in BC1.

A) Chromosome 3 which contains MYD88 **B)** X chromosome which contains IRAK1. **C)** Chromosome 12 which contains IRAK4.

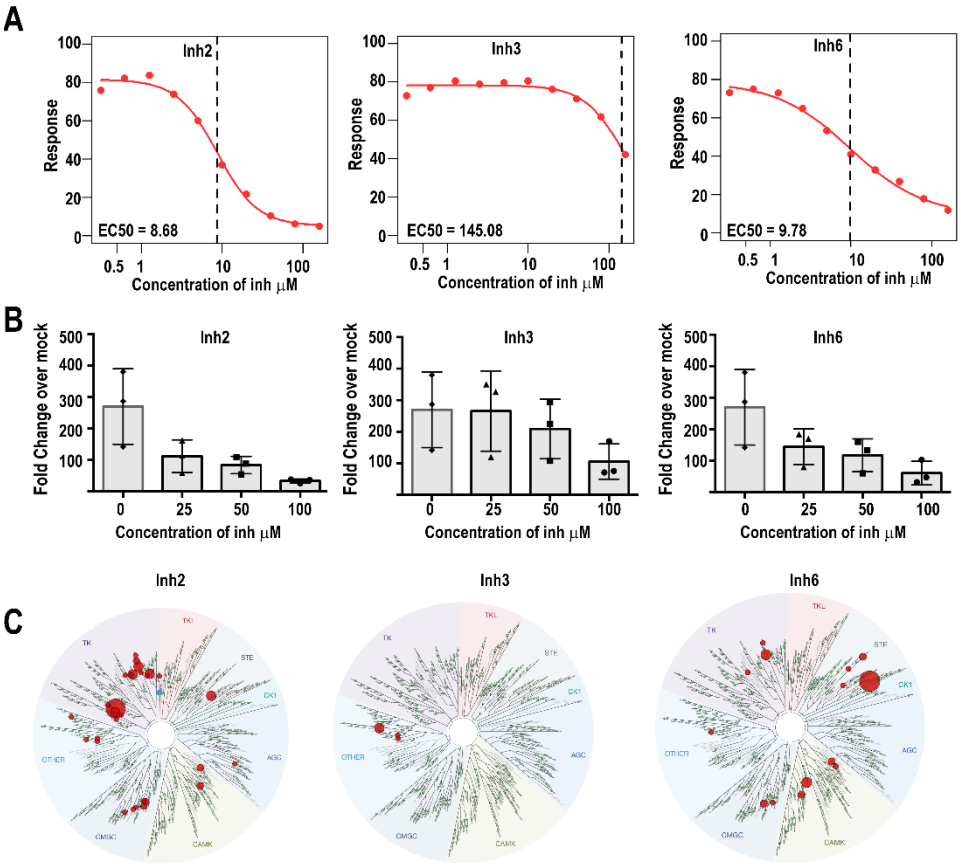

Figure AA. 22: **IRAK inhibitors are non-specific.**

A) EC50 curves for 6 commercially available IRAK inhibitor in μM. Inh1 (CAS No: 1042224-63-4), inh2 (CAS No: 928333-30-6), inh3 (CAS No: 1012343-93-9), inh4 (CAS No: 1012104-68-5), inh6 (CAS No: 1042672-97-8), and inh1-4 (CAS No: 509093-47-4). The EC50 value on each plot is the average of three experiments. **B)** Quantification of luciferase production in cells transfected with an NFκB driven luciferase plasmid, incubated with inhibitor, stimulated with 1 ng/μL IL-1β. Luciferase values were measured 6 hours post stimulation. All values are fold change over mock PBS stimulation. **C)** A DiscoverX Kinome scan analysis for each IRAK inhibitor at 250 nM. Arrows point to either Purple and Blue dots represent IRAK4 and IRAK1 kinase respectively. Size of the circle is proportional to percent activity inhibited by the inhibitors.

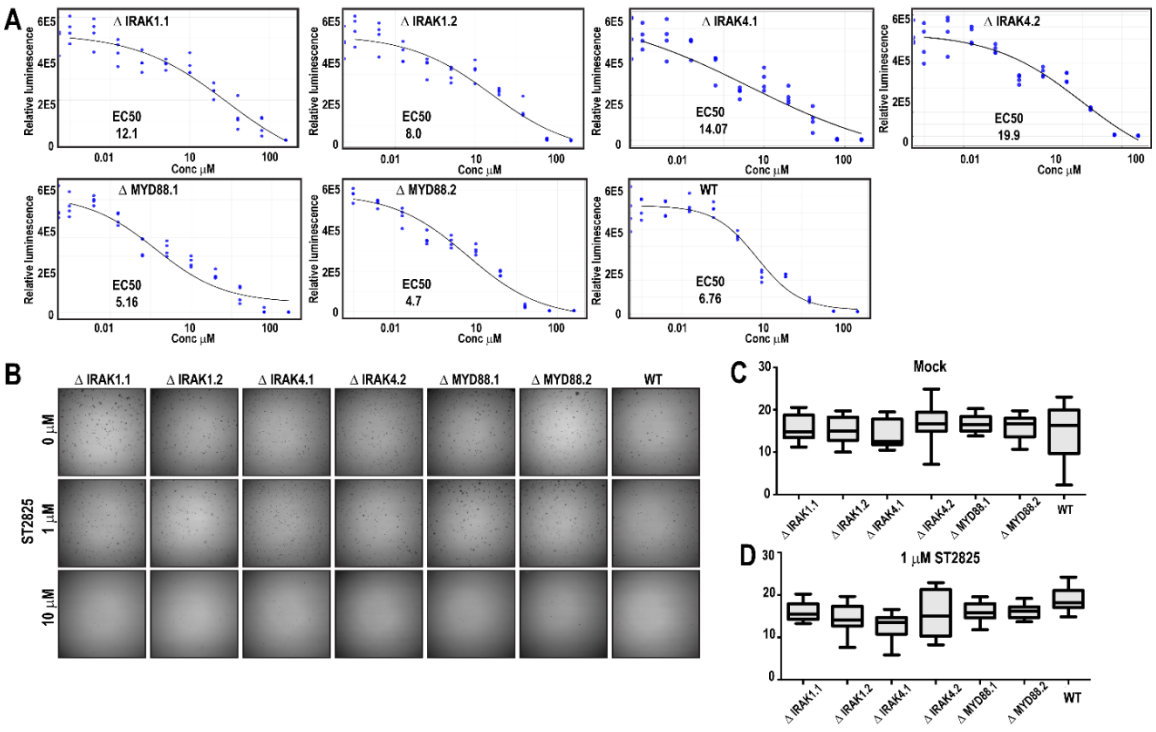

Figure AA. 23 MYD88 inhibitor ST2825 EC50 in IRAK knockouts

A) Panel A has represented EC50 curves for the MYD88 dimerization inhibitor ST2825 for each of the IRAK knockout cells. **B)** Colony formation assay for each pathway knockout following treatment with ST2825. **C)** Quantification of the colony formation information from panel C when cells had no inhibitor treatment. **D)** Quantification of colony formation when cells were treated with 1 μM of inhibitor.

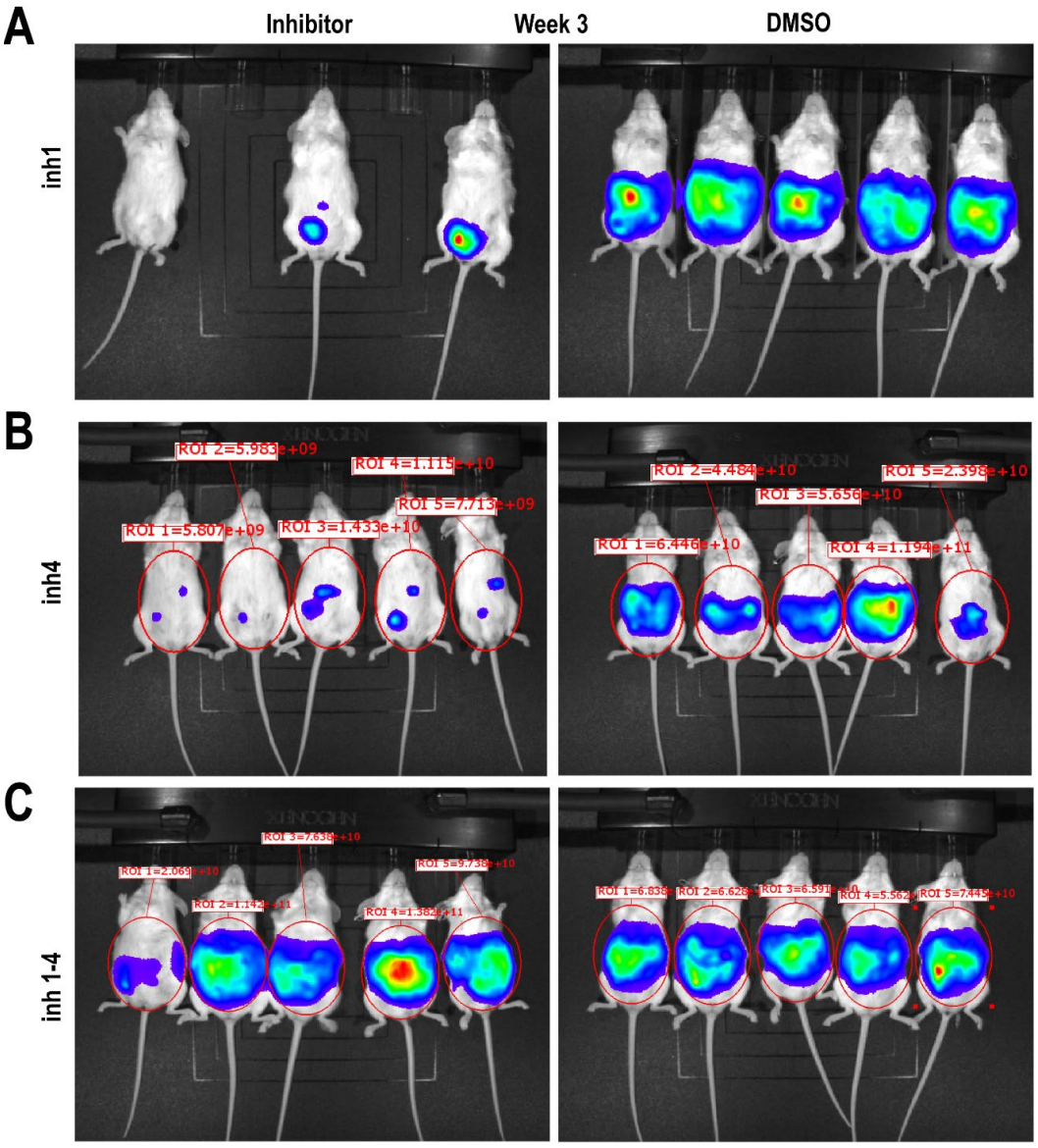

Figure AA. 24: **IRAK mouse inhibitor data.**

Mice were inoculated with 1 million BC-1 -TREX-LUC cells, three days after injection IRAK inhibitors were given to the mice, Mondays, Wednesdays and Fridays for three weeks. Mice were imaged and luciferase values representing the PEL effusions were measured at the three week termination point. **A)** IRAK inhibitor 1 **B)** IRAK inhibitor 4 **C)** IRAK inhibitor 1-4.

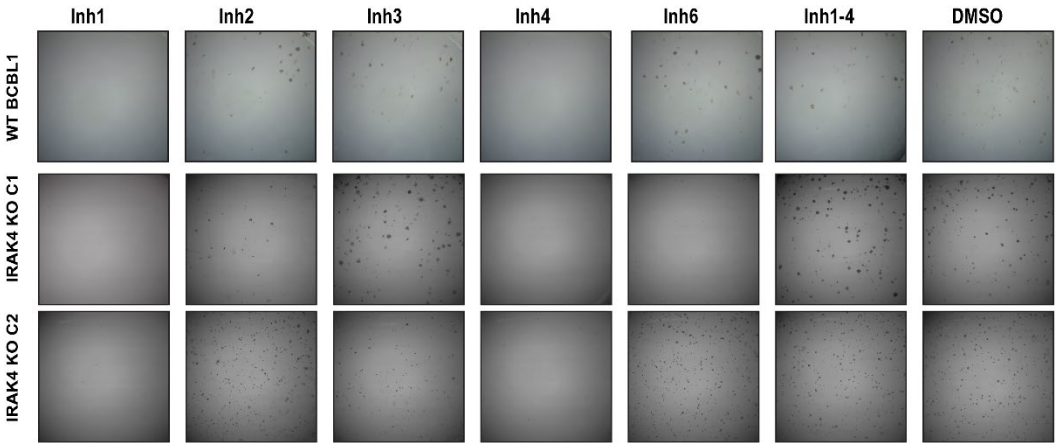

Figure AA. 25: CFA supplemental data

IRAK4 knockout cells were treated with inhibitors during colony formation assays with at 10 μM.

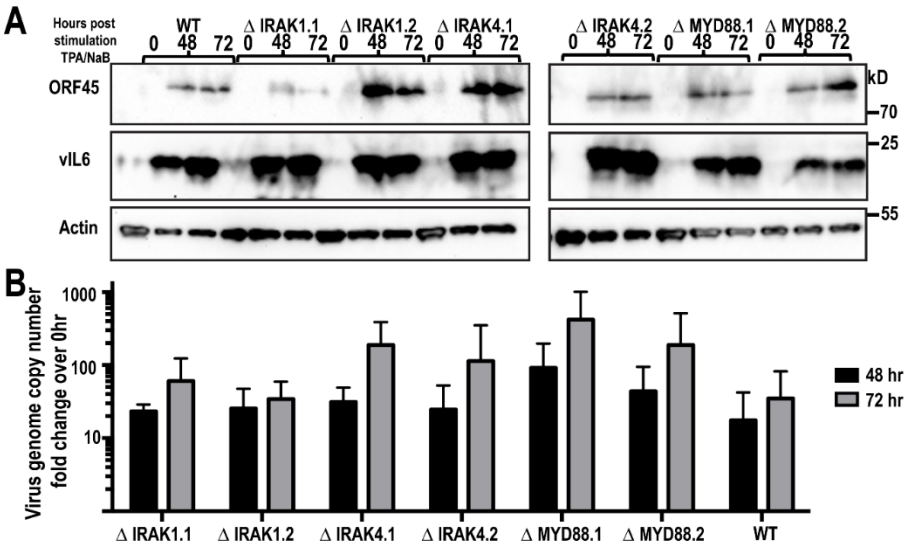

Figure AA. 26: Reactivation of BCBL-1 IRAK pathway knockouts.

A) Western blots for lytic KSHV markers ORF45 and vIL-6 on IRAK pathway, ΔMYD88, ΔIRAK1 and ΔIRAK4 BCBL-1 cells following reactivation with 1 mM sodium butyrate and 25 ng/mL PMA. **B)** Lysates were harvested at 0, 48, and 72 hours, and genome copy numbers/mL were calculated using qPCR.

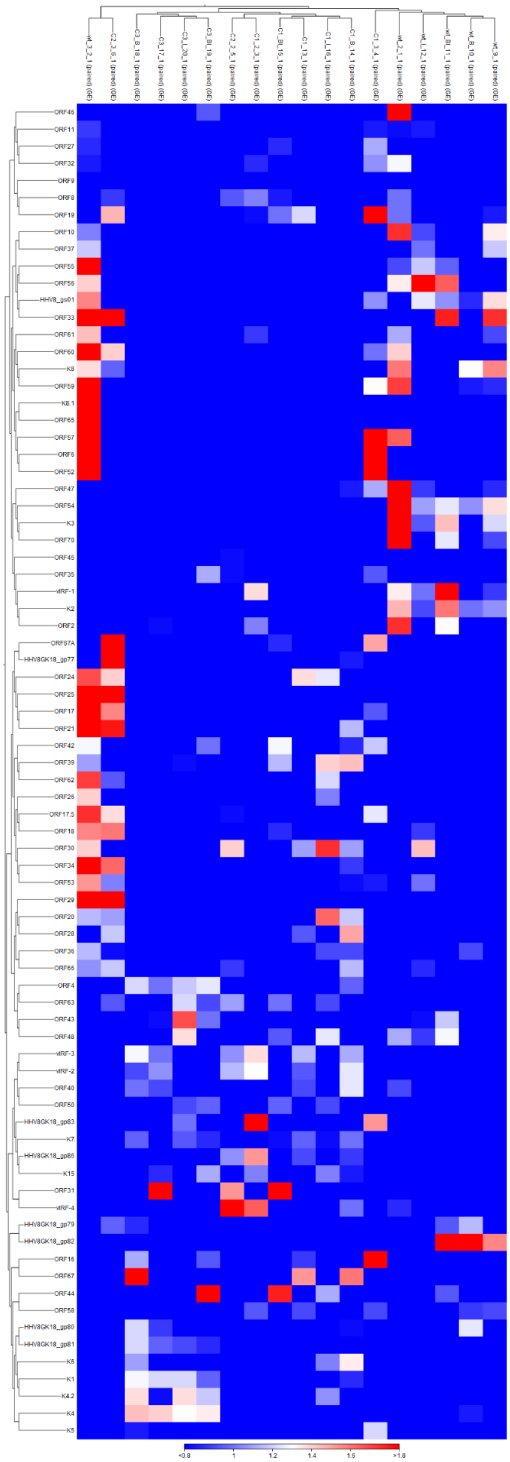

Figure AA. 27: RNA-seq results for virus genes in ΔIRAK4 BCBL-1.

A heat map of KSHV expression patterns with blue being low expression and red high. Scale is on the bottom.

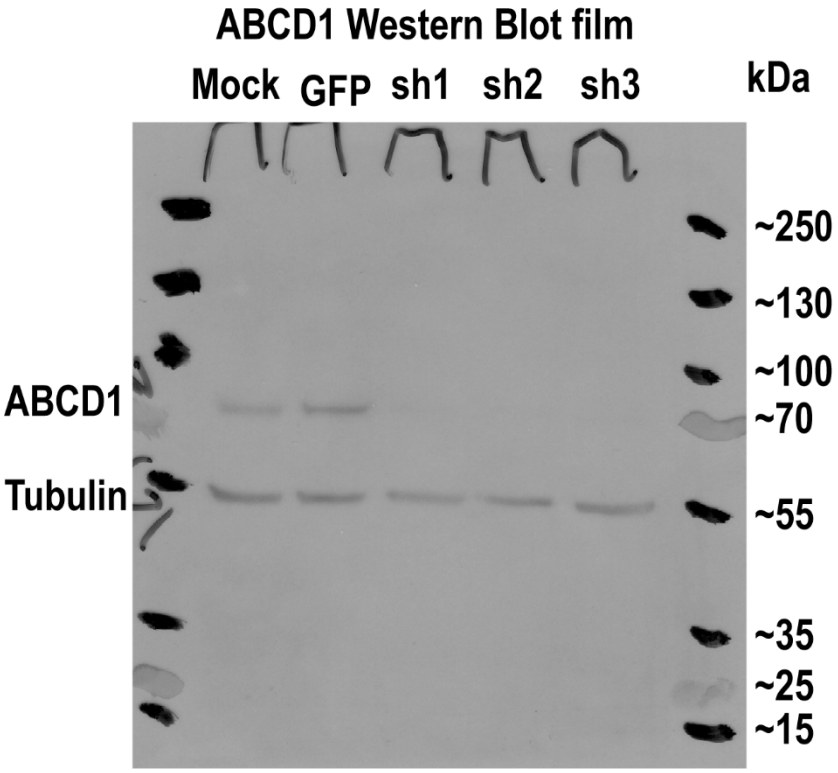

Figure AA. 28: ABCD1 complete western blot.

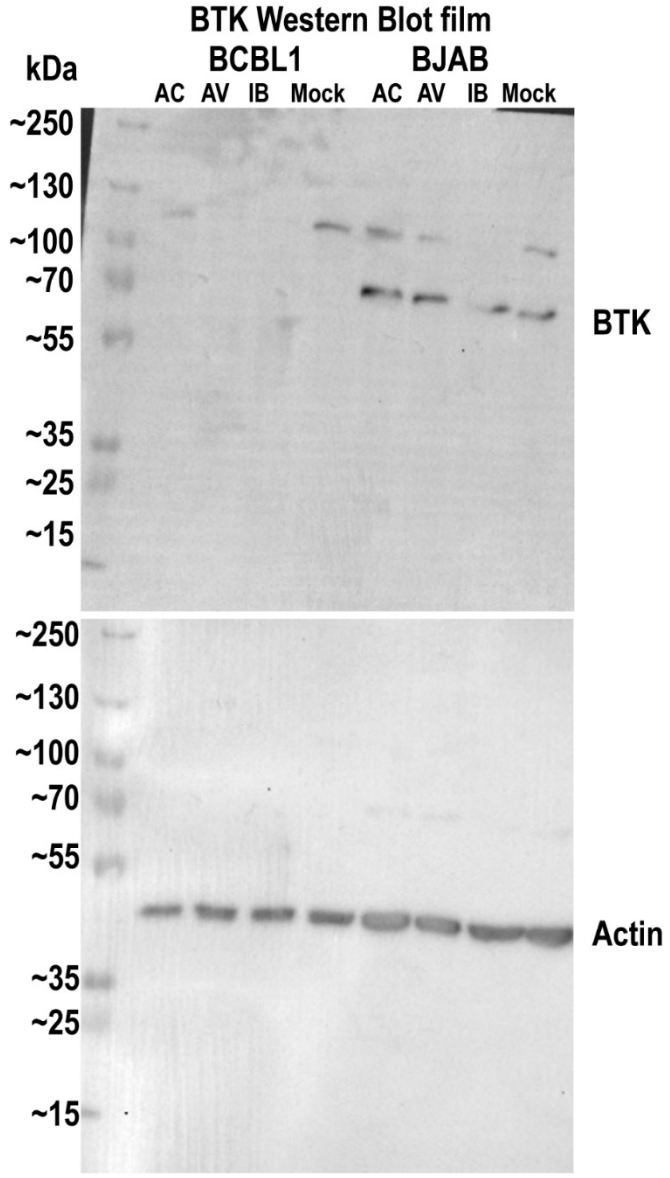

Figure AA. 29: BTK complete western blot.

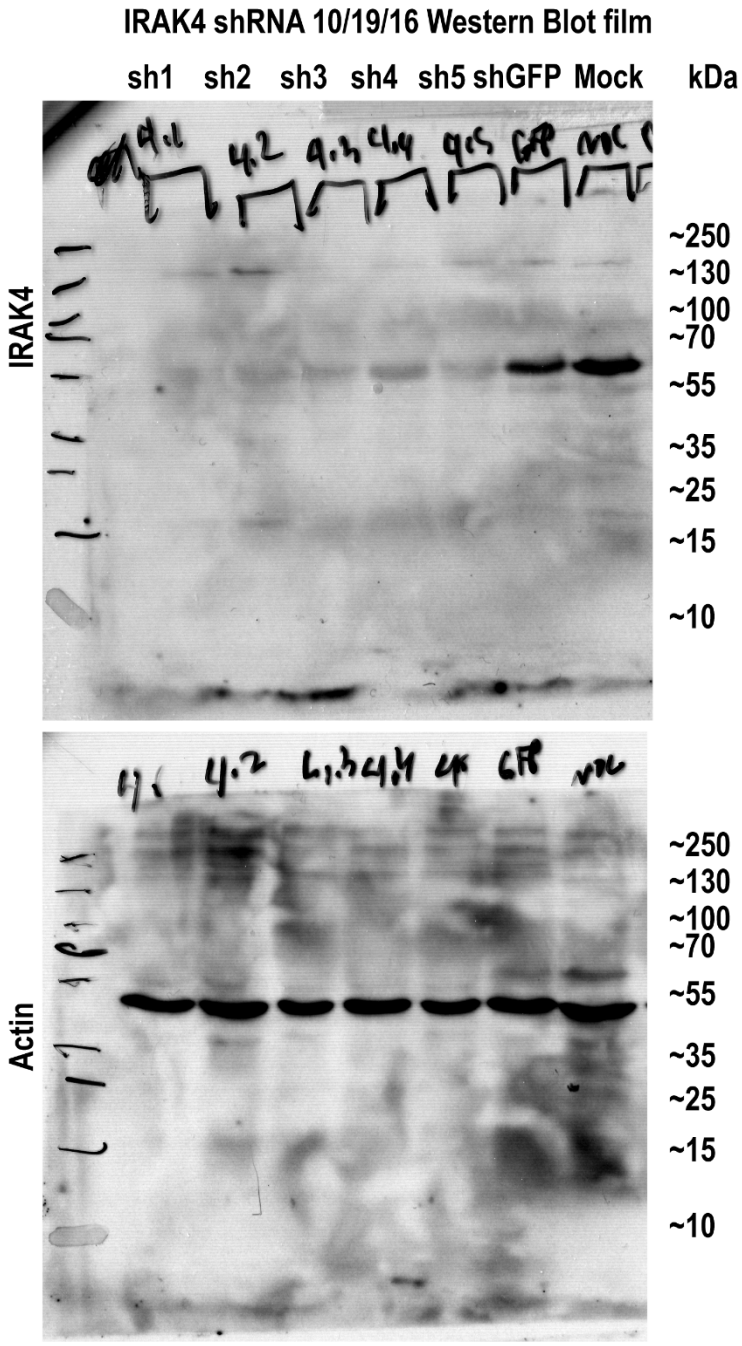

Figure AA. 30: IRAK4 shRNA BCBL-1 complete western blot.

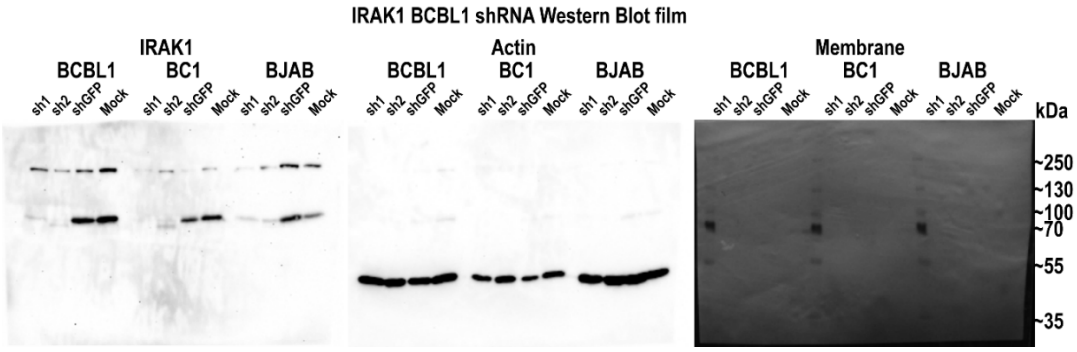

Figure AA. 31: IRAK1 shRNA complete blots.

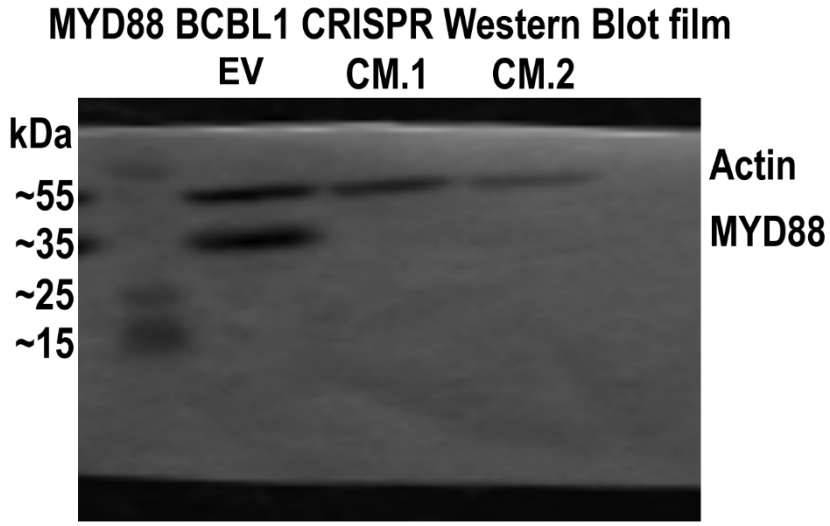

Figure AA. 32 BCBL-1 MYD88 CRISPR complete western blot

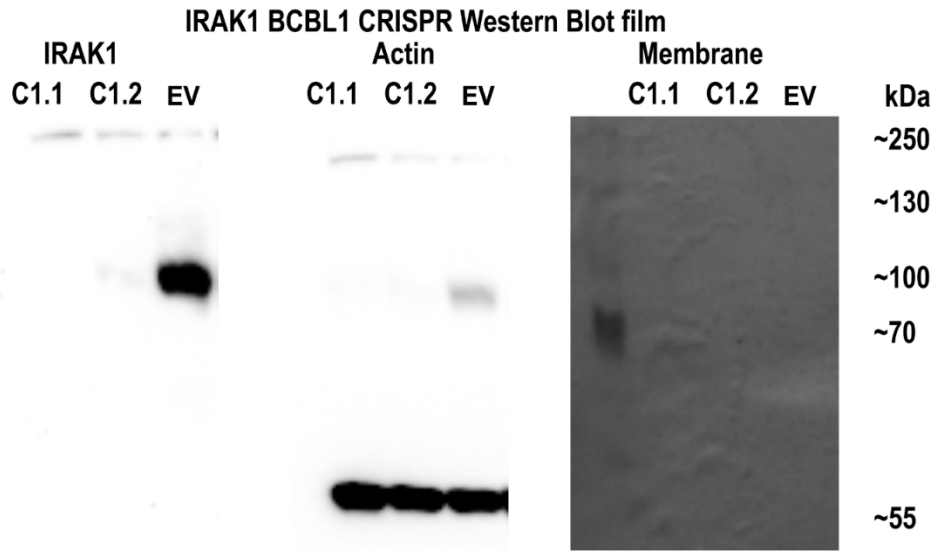

Figure AA. 33 IRAK1 CRISPR complete western blot BCBL-1.

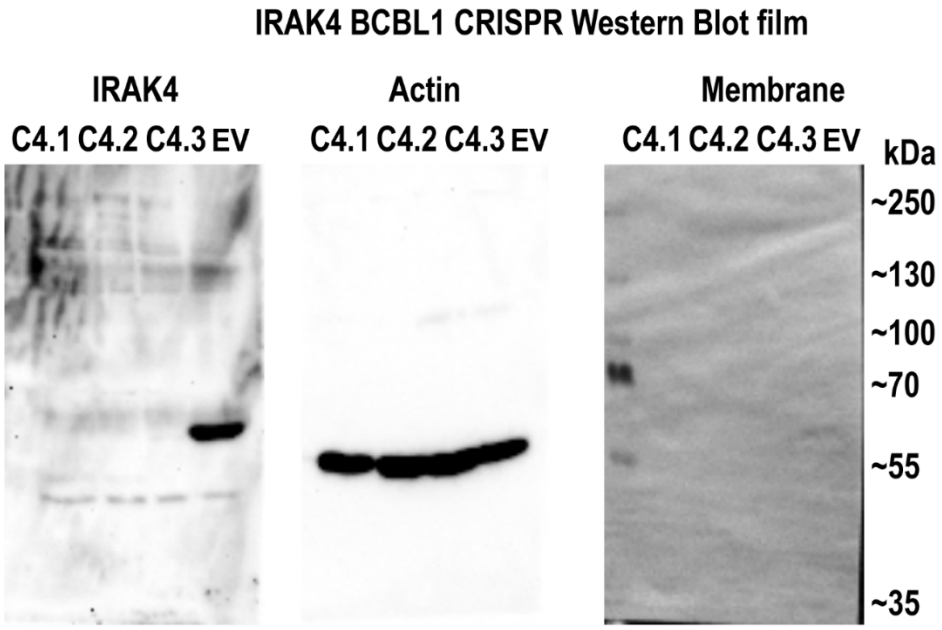

Figure AA. 34: IRAK4 CRISPR complete western blot.

REFERENCES

1. Metzger MJ, Villalba A, Carballal MJ, Iglesias D, Sherry J, Reinisch C, Muttray AF, Baldwin SA, Goff SP. 2016. Widespread transmission of independent cancer lineages within multiple bivalve species. Nature 534:705-9.

2. Wong K, van der Weyden L, Schott CR, Foote A, Constantino-Casas F, Smith S, Dobson JM, Murchison EP, Wu H, Yeh I, Fullen DR, Joseph N, Bastian BC, Patel RM, Martincorena I, Robles-Espinoza CD, Iyer V, Kuijjer ML, Arends MJ, Brenn T, Harms PW, Wood GA, Adams DJ. 2019. Cross-species genomic landscape comparison of human mucosal melanoma with canine oral and equine melanoma. Nat Commun 10:353.

3. Rothschild BM, Tanke DH, Helbling M, 2nd, Martin LD. 2003. Epidemiologic study of tumors in dinosaurs. Naturwissenschaften 90:495-500.

4. Society AC. 2019. Cancer Facts & Figures 2019, *on* American Cancer society. https://www.cancer.org/research/cancer-facts-statistics/all-cancer-facts-figures/cancer-facts-figures-2019.html. Accessed

5. NCI. 2020. Types of Cancer. https://www.cancer.gov/types. Accessed
6. Hopcraft SE, Damania B. 2017. Tumour viruses and innate immunity. Philos Trans R Soc Lond B Biol Sci 372.

7. Gao P, Zheng J. 2011. Oncogenic virus-mediated cell fusion: new insights into initiation and progression of oncogenic viruses--related cancers. Cancer Lett 303:1-8.

8. Kgatle MM, Spearman CW, Kalla AA, Hairwadzi HN. 2017. DNA Oncogenic Virus-Induced Oxidative Stress, Genomic Damage, and Aberrant Epigenetic Alterations. Oxid Med Cell Longev 2017:3179421.

9. Sun F, Xiao Y, Qu Z. 2015. Oncovirus Kaposi sarcoma herpesvirus (KSHV) represses tumor suppressor PDLIM2 to persistently activate nuclear factor kappaB (NF-kappaB) and STAT3 transcription factors for tumorigenesis and tumor maintenance. J Biol Chem 290:7362-8.

10. Panea RI, Love CL, Shingleton JR, Reddy A, Bailey JA, Moormann AM, Otieno JA, Ong'echa JM, Oduor CI, Schroeder KMS, Masalu N, Chao NJ, Agajanian M, Major MB, Fedoriw Y, Richards KL, Rymkiewicz G, Miles RR, Alobeid B, Bhagat G, Flowers CR, Ondrejka SL, Hsi ED, Choi WWL, Au-Yeung RKH, Hartmann W, Lenz G, Meyerson H, Lin YY, Zhuang Y, Luftig MA, Waldrop A, Dave T, Thakkar D, Sahay H, Li G, Palus BC, Seshadri V, Kim SY, Gascoyne RD, Levy S, Mukhopadyay M, Dunson DB, Dave SS. 2019. The whole-genome landscape of Burkitt lymphoma subtypes. Blood 134:1598-1607.

11. Sin SH, Kim Y, Eason A, Dittmer DP. 2015. KSHV Latency Locus Cooperates with Myc to Drive Lymphoma in Mice. PLoS Pathog 11:e1005135.

12. Manzano M, Patil A, Waldrop A, Dave SS, Behdad A, Gottwein E. 2018. Gene essentiality landscape and druggable oncogenic dependencies in herpesviral primary effusion lymphoma. Nat Commun 9:3263.

13. Dai L, Cao Y, Jiang W, Zabaleta J, Liu Z, Qiao J, Qin Z. 2017. KSHV co-infection down-regulates HPV16 E6 and E7 from cervical cancer cells. Oncotarget.

14. Hanahan D, Weinberg RA. 2011. Hallmarks of cancer: the next generation. Cell 144:646-74.
15. Faure A, Hayes M, Sugden B. 2019. How Kaposi's sarcoma-associated herpesvirus stably transforms peripheral B cells towards lymphomagenesis. Proc Natl Acad Sci U S A 116:16519-16528.

16. Klebe S, Leigh J, Henderson DW, Nurminen M. 2019. Asbestos, Smoking and Lung Cancer: An Update. Int J Environ Res Public Health 17.

17. Carbone A, Vaccher E, Gloghini A, Pantanowitz L, Abayomi A, de Paoli P, Franceschi S. 2014. Diagnosis and management of lymphomas and other cancers in HIV-infected patients. Nat Rev Clin Oncol 11:223-38.

18. Boumahdi S, de Sauvage FJ. 2020. The great escape: tumour cell plasticity in resistance to targeted therapy. Nat Rev Drug Discov 19:39-56.

19. Gottipati S, Rao NL, Fung-Leung WP. 2008. IRAK1: a critical signaling mediator of innate immunity. Cell Signal 20:269-76.

20. Ringwood L, Li L. 2008. The involvement of the interleukin-1 receptor-associated kinases (IRAKs) in cellular signaling networks controlling inflammation. Cytokine 42:1-7.

21. Bahia MS, Kaur M, Silakari P, Silakari O. 2015. Interleukin-1 receptor associated kinase inhibitors: potential therapeutic agents for inflammatory- and immune-related disorders. Cell Signal 27:1039-55.

22. Rhyasen GW, Starczynowski DT. 2015. IRAK signalling in cancer. Br J Cancer 112:232-7.
23. Singh A, Singh V, Tiwari RL, Chandra T, Kumar A, Dikshit M, Barthwal MK. 2015. The IRAK-ERK-p67phox-Nox-2 axis mediates TLR4, 2-induced ROS production for IL-1beta transcription and processing in monocytes. Cell Mol Immunol.

24. Cheng BY, Lau EY, Leung HW, Leung CO, Ho NP, Gurung S, Cheng LK, Lin CH, Lo RC, Ma S, Ng IO, Lee TK. 2018. IRAK1 augments cancer stemness and drug resistance via the AP-1/AKR1B10 signaling cascade in hepatocellular carcinoma. Cancer Res.

25. da Silva-Diz V, Lorenzo-Sanz L, Bernat-Peguera A, Lopez-Cerda M, Munoz P. 2018. Cancer cell plasticity: Impact on tumor progression and therapy response. Semin Cancer Biol 53:48-58.

26. Bedard PL, Hansen AR, Ratain MJ, Siu LL. 2013. Tumour heterogeneity in the clinic. Nature 501:355-64.

27. Visvader JE. 2011. Cells of origin in cancer. Nature 469:314-22.

28. Blanpain C. 2013. Tracing the cellular origin of cancer. Nat Cell Biol 15:126-34.

29. Kokubu Y, Tabu K, Muramatsu N, Wang W, Murota Y, Nobuhisa I, Jinushi M, Taga T. 2016. Induction of protumoral CD11c(high) macrophages by glioma cancer stem cells through GM-CSF. Genes Cells 21:241-51.

30. Yano S, Nakataki E, Ohtsuka S, Inayama M, Tomimoto H, Edakuni N, Kakiuchi S, Nishikubo N, Muguruma H, Sone S. 2005. Retreatment of lung adenocarcinoma patients with gefitinib who had experienced favorable results from their initial treatment with this selective epidermal growth factor receptor inhibitor: a report of three cases. Oncol Res 15:107-11.

31. Shibue T, Weinberg RA. 2017. EMT, CSCs, and drug resistance: the mechanistic link and clinical implications. Nat Rev Clin Oncol 14:611-629.

32. Menon DR, Das S, Krepler C, Vultur A, Rinner B, Schauer S, Kashofer K, Wagner K, Zhang G, Rad EB, Haass NK, Soyer HP, Gabrielli B, Somasundaram R, Hoefler G, Herlyn M, Schaider H. 2015. A stress-induced early innate response causes multidrug tolerance in melanoma, p 4545, Oncogene, vol 34, England.

33. McHugh D, Caduff N, Barros MHM, Ramer PC, Raykova A, Murer A, Landtwing V, Quast I, Styles CT, Spohn M, Fowotade A, Delecluse HJ, Papoudou-Bai A, Lee YM, Kim JM, Middeldorp J, Schulz TF, Cesarman E, Zbinden A, Capaul R, White RE, Allday MJ, Niedobitek G, Blackbourn DJ, Grundhoff A, Munz C. 2017. Persistent KSHV Infection Increases EBV-Associated Tumor Formation In Vivo via Enhanced EBV Lytic Gene Expression. Cell Host Microbe 22:61-73.e7.

34. Bigi R, Landis JT, An H, Caro-Vegas C, Raab-Traub N, Dittmer DP. 2018. Epstein-Barr virus enhances genome maintenance of Kaposi sarcoma-associated herpesvirus. Proc Natl Acad Sci U S A 115:E11379-e11387.

35. Giffin L, Damania B. 2014. KSHV: pathways to tumorigenesis and persistent infection. Adv Virus Res 88:111-59.

36. Dittmer DP, Damania B. 2016. Kaposi sarcoma-associated herpesvirus: immunobiology, oncogenesis, and therapy. J Clin Invest 126:3165-75.

37. Mularoni A, Gallo A, Riva G, Barozzi P, Miele M, Cardinale G, Vizzini G, Volpes R, Grossi P, Di Carlo D, Luca A, Trenti T, Luppi M, Conaldi PG. 2017. Successful Treatment of KSHV Inflammatory Cytokine Syndrome (KICS) after Kidney-Liver Transplant: Correlations with HHV8 miRNome and Specific T-Cell Response. Am J Transplant.

38. Caro-Vegas C, Sellers S, Host KM, Seltzer J, Landis J, Fischer WA, 2nd, Damania B, Dittmer DP. 2020. Runaway Kaposi Sarcoma-associated herpesvirus replication correlates with systemic IL-10 levels. Virology 539:18-25.

39. Wen KW, Damania B. 2010. Kaposi Sarcoma-associated Herpesvirus (KSHV): Molecular Biology and Oncogenesis. Cancer Lett 289:140-50.

40. Ganem D. 2007. KSHV-induced oncogenesis. *In* Arvin A, Campadelli-Fiume G, Mocarski E, Moore PS, Roizman B, Whitley R, Yamanishi K (ed), Human Herpesviruses: Biology, Therapy, and Immunoprophylaxis. Cambridge University PressCopyright (c) Cambridge University Press 2007., Cambridge.

41. Ueda K. 2018. KSHV Genome Replication and Maintenance in Latency. Adv Exp Med Biol 1045:299-320.

42. Dittmer DP, Damania B. 2013. Kaposi sarcoma associated herpesvirus pathogenesis (KSHV) – an update. Curr Opin Virol 3:238-44.

43. Wang Y, Lin Y, Guo Y, Pu X, Li M. 2017. Functional dissection of human targets for KSHV-encoded miRNAs using network analysis. Sci Rep 7:3159.

44. Abere B, Mamo TM, Hartmann S, Samarina N, Hage E, Ruckert J, Hotop SK, Busche G, Schulz TF. 2017. The Kaposi's sarcoma-associated herpesvirus (KSHV) non-structural membrane protein K15 is required for viral lytic replication and may represent a therapeutic target. PLoS Pathog 13:e1006639.

45. Chang J, Renne R, Dittmer D, Ganem D. 2000. Inflammatory cytokines and the reactivation of Kaposi's sarcoma-associated herpesvirus lytic replication. Virology 266:17-25.

46. Grundhoff A, Ganem D. 2001. Mechanisms governing expression of the v-FLIP gene of Kaposi's sarcoma-associated herpesvirus. J Virol 75:1857-63.

47. Ambinder RF, Cesarman E. 2007. Clinical and pathological aspects of EBV and KSHV infection. *In* Arvin A, Campadelli-Fiume G, Mocarski E, Moore PS, Roizman B, Whitley R, Yamanishi K (ed), Human Herpesviruses: Biology, Therapy, and Immunoprophylaxis. Cambridge University PressCopyright (c) Cambridge University Press 2007., Cambridge.

48. Zuo J, Hislop AD, Leung CS, Sabbah S, Rowe M. 2013. Kaposi's sarcoma-associated herpesvirus-encoded viral IRF3 modulates major histocompatibility complex class II (MHC-II) antigen presentation through MHC-II transactivator-dependent and -independent mechanisms: implications for oncogenesis. J Virol 87:5340-50.

49. Hwang SW, Kim D, Jung JU, Lee HR. 2017. KSHV-encoded viral interferon regulatory factor 4 (vIRF4) interacts with IRF7 and inhibits interferon alpha production. Biochem Biophys Res Commun.

50. Watanabe T, Sugimoto A, Hosokawa K, Fujimuro M. 2018. Signal Transduction Pathways Associated with KSHV-Related Tumors. Adv Exp Med Biol 1045:321-355.

51. Fakhari FD, Jeong JH, Kanan Y, Dittmer DP. 2006. The latency-associated nuclear antigen of Kaposi sarcoma-associated herpesvirus induces B cell hyperplasia and lymphoma. J Clin Invest 116:735-42.

52. Garrigues HJ, Howard K, Barcy S, Ikoma M, Moses AV, Deutsch GH, Wu D, Ueda K, Rose TM. 2017. Full-length isoforms of KSHV LANA accumulate in the cytoplasm of cells undergoing the lytic cycle of replication. J Virol.

53. Thakker S, Strahan RC, Scurry AN, Uppal T, Verma SC. 2018. KSHV LANA upregulates the expression of epidermal growth factor like domain 7 to promote angiogenesis. Oncotarget 9:1210-1228.

54. Guasparri I, Keller SA, Cesarman E. 2004. KSHV vFLIP is essential for the survival of infected lymphoma cells. J Exp Med 199:993-1003.

55. Matta H, Chaudhary PM. 2004. Activation of alternative NF-kappa B pathway by human herpes virus 8-encoded Fas-associated death domain-like IL-1 beta-converting enzyme inhibitory protein (vFLIP). Proc Natl Acad Sci U S A 101:9399-404.

56. Ballon G, Chen K, Perez R, Tam W, Cesarman E. 2011. Kaposi sarcoma herpesvirus (KSHV) vFLIP oncoprotein induces B cell transdifferentiation and tumorigenesis in mice. J Clin Invest 121:1141-53.

57. Ehrlich ES, Chmura JC, Smith JC, Kalu NN, Hayward GS. 2014. KSHV RTA abolishes NFkappaB responsive gene expression during lytic reactivation by targeting vFLIP for degradation via the proteasome. PLoS One 9:e91359.

58. Keller SA, Schattner EJ, Cesarman E. 2000. Inhibition of NF-kappaB induces apoptosis of KSHV-infected primary effusion lymphoma cells. Blood 96:2537-42.

59. Bharti AC, Aggarwal BB. 2002. Nuclear factor-kappa B and cancer: its role in prevention and therapy. Biochem Pharmacol 64:883-8.

60. Grossmann C, Podgrabinska S, Skobe M, Ganem D. 2006. Activation of NF-kappaB by the latent vFLIP gene of Kaposi's sarcoma-associated herpesvirus is required for the spindle shape of virus-infected endothelial cells and contributes to their proinflammatory phenotype. J Virol 80:7179-85.

61. Keller SA, Hernandez-Hopkins D, Vider J, Ponomarev V, Hyjek E, Schattner EJ, Cesarman E. 2006. NF-kappaB is essential for the progression of KSHV- and EBV-infected lymphomas in vivo. Blood 107:3295-302.

62. Sun SC, Cesarman E. 2011. NF-kappaB as a target for oncogenic viruses. Curr Top Microbiol Immunol 349:197-244.

63. Djerbi M, Screpanti V, Catrina AI, Bogen B, Biberfeld P, Grandien A. 1999. The inhibitor of death receptor signaling, FLICE-inhibitory protein defines a new class of tumor progression factors. J Exp Med 190:1025-32.

64. Sadagopan S, Sharma-Walia N, Veettil MV, Raghu H, Sivakumar R, Bottero V, Chandran B. 2007. Kaposi's sarcoma-associated herpesvirus induces sustained NF-kappaB activation

during de novo infection of primary human dermal microvascular endothelial cells that is essential for viral gene expression. J Virol 81:3949-68.

65. Blattman NN, Lagunoff M, Blattman JN, Corey L. 2014. Nuclear factor kappa B is required for the production of infectious human herpesvirus 8 virions. Front Microbiol 5:129.

66. Ntoufa S, Vilia MG, Stamatopoulos K, Ghia P, Muzio M. 2016. Toll-like receptors signaling: A complex network for NF-kappaB activation in B-cell lymphoid malignancies. Semin Cancer Biol 39:15-25.

67. Bowie AG. 2008. Insights from vaccinia virus into Toll-like receptor signalling proteins and their regulation by ubiquitin: role of IRAK-2. Biochem Soc Trans 36:449-52.

68. Keating SE, Bowie AG. 2009. Role of non-degradative ubiquitination in interleukin-1 and toll-like receptor signaling. J Biol Chem 284:8211-5.

69. Zhu J, Mohan C. 2010. Toll-like receptor signaling pathways--therapeutic opportunities. Mediators Inflamm 2010:781235.

70. Narayanan KB, Park HH. 2015. Toll/interleukin-1 receptor (TIR) domain-mediated cellular signaling pathways. Apoptosis 20:196-209.

71. Janssens S, Beyaert R. 2002. A universal role for MyD88 in TLR/IL-1R-mediated signaling. Trends Biochem Sci 27:474-82.

72. Ren Y, Ding D, Pan B, Bu W. 2017. The TLR13-MyD88-NF-kappaB signalling pathway of Cyclina sinensis plays vital roles in innate immune responses. Fish Shellfish Immunol.

73. Uppal T, Sarkar R, Dhelaria R, Verma SC. 2018. Role of Pattern Recognition Receptors in KSHV Infection. Cancers (Basel) 10.

74. Gregory SM, West JA, Dillon PJ, Hilscher C, Dittmer DP, Damania B. 2009. Toll-like receptor signaling controls reactivation of KSHV from latency. Proc Natl Acad Sci U S A 106:11725-30.

75. Abend JR, Ramalingam D, Kieffer-Kwon P, Uldrick TS, Yarchoan R, Ziegelbauer JM. 2012. Kaposi's sarcoma-associated herpesvirus microRNAs target IRAK1 and MYD88, two components of the toll-like receptor/interleukin-1R signaling cascade, to reduce inflammatory-cytokine expression. J Virol 86:11663-74.

76. Gruffaz M, Vasan K, Tan B, Ramos da Silva S, Gao SJ. 2017. TLR4-mediated inflammation promotes KSHV-induced cellular transformation and tumorigenesis by activating the STAT3 pathway. Cancer Res.

77. Klepfish A, Sarid R, Shtalrid M, Shvidel L, Berrebi A, Schattner A. 2001. Primary effusion lymphoma (PEL) in HIV-negative patients--a distinct clinical entity. Leuk Lymphoma 41:439-43.

78. Chen YB, Rahemtullah A, Hochberg E. 2007. Primary effusion lymphoma. Oncologist 12:569-76.

79. Said JW, Tasaka T, Takeuchi S, Asou H, de Vos S, Cesarman E, Knowles DM, Koeffler HP. 1996. Primary effusion lymphoma in women: report of two cases of Kaposi's sarcoma herpes virus-associated effusion-based lymphoma in human immunodeficiency virus-negative women. Blood 88:3124-8.

80. Okada S, Goto H, Yotsumoto M. 2014. Current status of treatment for primary effusion lymphoma. Intractable Rare Dis Res 3:65-74.

81. Klein U, Gloghini A, Gaidano G, Chadburn A, Cesarman E, Dalla-Favera R, Carbone A. 2003. Gene expression profile analysis of AIDS-related primary effusion lymphoma (PEL) suggests a plasmablastic derivation and identifies PEL-specific transcripts. Blood 101:4115-21.

82. Kim Y, Park CJ, Roh J, Huh J. 2014. Current concepts in primary effusion lymphoma and other effusion-based lymphomas. Korean J Pathol 48:81-90.

83. Kati S, Tsao EH, Gunther T, Weidner-Glunde M, Rothamel T, Grundhoff A, Kellam P, Schulz TF. 2013. Activation of the B cell antigen receptor triggers reactivation of latent Kaposi's sarcoma-associated herpesvirus in B cells. J Virol 87:8004-16.

84. Drexler HG, Meyer C, Gaidano G, Carbone A. 1999. Constitutive cytokine production by primary effusion (body cavity-based) lymphoma-derived cell lines. Leukemia 13:634-40.

85. Drexler HG, Uphoff CC, Gaidano G, Carbone A. 1998. Lymphoma cell lines: in vitro models for the study of HHV-8+ primary effusion lymphomas (body cavity-based lymphomas). Leukemia 12:1507-17.

86. Ramos JC, Sin SH, Staudt MR, Roy D, Vahrson W, Dezube BJ, Harrington W, Jr., Dittmer DP. 2012. Nuclear factor kappa B pathway associated biomarkers in AIDS defining malignancies. Int J Cancer 130:2728-33.

87. Bhatt AP, Bhende PM, Sin SH, Roy D, Dittmer DP, Damania B. 2010. Dual inhibition of PI3K and mTOR inhibits autocrine and paracrine proliferative loops in PI3K/Akt/mTOR-addicted lymphomas. Blood 115:4455-63.

88. Sychev ZE, Hu A, DiMaio TA, Gitter A, Camp ND, Noble WS, Wolf-Yadlin A, Lagunoff M. 2017. Integrated systems biology analysis of KSHV latent infection reveals viral induction and reliance on peroxisome mediated lipid metabolism. PLoS Pathog 13:e1006256.

89. Cha S, Kang MS, Seo T. 2018. KSHV vPK inhibits Wnt signaling via preventing interactions between beta-catenin and TCF4. Biochem Biophys Res Commun.

90. Sin SH, Roy D, Wang L, Staudt MR, Fakhari FD, Patel DD, Henry D, Harrington WJ, Jr., Damania BA, Dittmer DP. 2007. Rapamycin is efficacious against primary effusion lymphoma (PEL) cell lines in vivo by inhibiting autocrine signaling. Blood 109:2165-73.

91. Granato M, Gilardini Montani MS, Romeo MA, Santarelli R, Gonnella R, D'Orazi G, Faggioni A, Cirone M. 2017. Metformin triggers apoptosis in PEL cells and alters bortezomib-induced Unfolded Protein Response increasing its cytotoxicity and inhibiting KSHV lytic cycle activation. Cell Signal 40:239-247.

92. Caro-Vegas C, Bailey A, Bigi R, Damania B, Dittmer DP. 2019. Targeting mTOR with MLN0128 Overcomes Rapamycin and Chemoresistant Primary Effusion Lymphoma. MBio 10.

93. Chen W, Hilton IB, Staudt MR, Burd CE, Dittmer DP. 2010. Distinct p53, p53:LANA, and LANA Complexes in Kaposi's Sarcoma-Associated Herpesvirus Lymphomas ▿ , p 3898-908, J Virol, vol 84.

94. de Oliveira DE, Ballon G, Cesarman E. 2010. NF-kappaB signaling modulation by EBV and KSHV. Trends Microbiol 18:248-57.

95. Gopalakrishnan R, Matta H, Chaudhary PM. 2013. A purine scaffold HSP90 inhibitor BIIB021 has selective activity against KSHV-associated primary effusion lymphoma and blocks vFLIP K13-induced NF-kappaB. Clin Cancer Res 19:5016-26.

96. Briggs LC, Chan AWE, Davis CA, Whitelock N, Hotiana HA, Baratchian M, Bagneris C, Selwood DL, Collins MK, Barrett TE. 2017. IKKgamma mimetic peptides block the resistance to apoptosis associated with KSHV infection. J Virol.

97. Su LC, Xu WD, Huang AF. 2020. IRAK family in inflammatory autoimmune diseases. Autoimmun Rev:102461.

98. Song YJ, Jen KY, Soni V, Kieff E, Cahir-McFarland E. 2006. IL-1 receptor-associated kinase 1 is critical for latent membrane protein 1-induced p65/RelA serine 536 phosphorylation and NF-kappaB activation. Proc Natl Acad Sci U S A 103:2689-94.

99. Walsh MC, Lee J, Choi Y. 2015. Tumor necrosis factor receptor- associated factor 6 (TRAF6) regulation of development, function, and homeostasis of the immune system. Immunol Rev 266:72-92.

100. Jain A, Kaczanowska S, Davila E. 2014. IL-1 Receptor-Associated Kinase Signaling and Its Role in Inflammation, Cancer Progression, and Therapy Resistance. Front Immunol 5:553.

101. Thomas R. 2005. The TRAF6-NF kappa B signaling pathway in autoimmunity: not just inflammation. Arthritis Res Ther 7:170-3.

102. Heiseke AF, Jeuk BH, Markota A, Straub T, Lehr HA, Reindl W, Krug AB. 2015. IRAK1 Drives Intestinal Inflammation by Promoting the Generation of Effector Th Cells with Optimal Gut-Homing Capacity. J Immunol 195:5787-94.

103. Singer JW, Fleischman A, Al-Fayoumi S, Mascarenhas JO, Yu Q, Agarwal A. 2018. Inhibition of interleukin-1 receptor-associated kinase 1 (IRAK1) as a therapeutic strategy. Oncotarget 9:33416-33439.

104. Takeuchi O, Akira S. 2002. MyD88 as a bottle neck in Toll/IL-1 signaling. Curr Top Microbiol Immunol 270:155-67.

105. Su J, Richter K, Zhang C, Gu Q, Li L. 2007. Differential regulation of interleukin-1 receptor associated kinase 1 (IRAK1) splice variants. Mol Immunol 44:900-5.

106. Nguyen T, De Nardo D, Masendycz P, Hamilton JA, Scholz GM. 2009. Regulation of IRAK-1 activation by its C-terminal domain. Cell Signal 21:719-26.

107. Ferrao R, Zhou H, Shan Y, Liu Q, Li Q, Shaw DE, Li X, Wu H. 2014. IRAK4 dimerization and trans-autophosphorylation are induced by Myddosome assembly. Mol Cell 55:891-903.

108. Landstrom M. 2010. The TAK1-TRAF6 signalling pathway. Int J Biochem Cell Biol 42:585-9.

109. Bruni D, Sebastia J, Dunne S, Schroder M, Butler MP. 2013. A novel IRAK1-IKKepsilon signaling axis limits the activation of TAK1-IKKbeta downstream of TLR3. J Immunol 190:2844-56.

110. Zhang J, Macartney T, Peggie M, Cohen P. 2017. Interleukin-1 and TRAF6-dependent activation of TAK1 in the absence of TAB2 and TAB3. Biochem J.

111. Strickson S, Emmerich CH, Goh ET, Zhang J, Kelsall IR, Macartney T, Hastie CJ, Knebel A, Peggie M, Marchesi F, Arthur JS, Cohen P. 2017. Roles of the TRAF6 and Pellino E3 ligases in MyD88 and RANKL signaling. Proc Natl Acad Sci U S A.

112. Yamin TT, Miller DK. 1997. The interleukin-1 receptor-associated kinase is degraded by proteasomes following its phosphorylation. J Biol Chem 272:21540-7.

113. Huang Y, Li T, Sane DC, Li L. 2004. IRAK1 serves as a novel regulator essential for lipopolysaccharide-induced interleukin-10 gene expression. J Biol Chem 279:51697-703.

114. Wesche H, Gao X, Li X, Kirschning CJ, Stark GR, Cao Z. 1999. IRAK-M is a novel member of the Pelle/interleukin-1 receptor-associated kinase (IRAK) family. J Biol Chem 274:19403-10.

115. Huang YS, Misior A, Li LW. 2005. Novel role and regulation of the interleukin-1 receptor associated kinase (IRAK) family proteins. Cell Mol Immunol 2:36-9.

116. Akdis M, Aab A, Altunbulakli C, Azkur K, Costa RA, Crameri R, Duan S, Eiwegger T, Eljaszewicz A, Ferstl R, Frei R, Garbani M, Globinska A, Hess L, Huitema C, Kubo T, Komlosi Z, Konieczna P, Kovacs N, Kucuksezer UC, Meyer N, Morita H, Olzhausen J, O'Mahony L, Pezer M, Prati M, Rebane A, Rhyner C, Rinaldi A, Sokolowska M, Stanic B, Sugita K, Treis A, van de Veen W, Wanke K, Wawrzyniak M, Wawrzyniak P, Wirz OF, Zakzuk JS, Akdis CA. 2016. Interleukins (from IL-1 to IL-38), interferons, transforming growth factor beta, and TNF-alpha: Receptors, functions, and roles in diseases. J Allergy Clin Immunol 138:984-1010.

117. Kawagoe T, Sato S, Matsushita K, Kato H, Matsui K, Kumagai Y, Saitoh T, Kawai T, Takeuchi O, Akira S. 2008. Sequential control of Toll-like receptor-dependent responses by IRAK1 and IRAK2. Nat Immunol 9:684-91.

118. Uematsu S, Sato S, Yamamoto M, Hirotani T, Kato H, Takeshita F, Matsuda M, Coban C, Ishii KJ, Kawai T, Takeuchi O, Akira S. 2005. Interleukin-1 receptor-associated kinase-1 plays an essential role for Toll-like receptor (TLR)7- and TLR9-mediated interferon-{alpha} induction. J Exp Med 201:915-23.

119. Yang G, Zhou Y, Liu X, Xu L, Cao Y, Manning RJ, Patterson CJ, Buhrlage SJ, Gray N, Tai YT, Anderson KC, Hunter ZR, Treon SP. 2013. A mutation in MYD88 (L265P) supports the survival of lymphoplasmacytic cells by activation of Bruton tyrosine kinase in Waldenstrom macroglobulinemia. Blood 122:1222-32.

120. Dubois S, Viailly PJ, Bohers E, Bertrand P, Ruminy P, Marchand V, Maingonnat C, Mareschal S, Picquenot JM, Penther D, Jais JP, Tesson B, Peyrouze P, Figeac M, Desmots F, Fest T, Haioun C, Lamy T, Copie-Bergman C, Fabiani B, Delarue R, Peyrade F, Andre M, Ketterer N, Leroy K, Salles G, Molina TJ, Tilly H, Jardin F. 2016. Biological and clinical relevance of associated genomic alterations in MYD88 L265P and non-L265P mutated diffuse large B-cell lymphoma: analysis of 361 cases. Clin Cancer Res.

121. Alegria V, Prieto-Torres L, Santonja C, Cordoba R, Manso R, Requena L, Rodriguez-Pinilla SM. 2017. MYD88 L265P mutation in cutaneous involvement by Waldenstrom macroglobulinemia. J Cutan Pathol.

122. Qiu H, Gong S, Xu L, Cheng H, Gao L, Chen J, Hu X, Yang J. 2018. MYD88 L265P mutation promoted malignant B cell resistance against T cell-mediated cytotoxicity via upregulating the IL-10/STAT3 cascade. Int Immunopharmacol 64:394-400.

123. Ngo VN, Young RM, Schmitz R, Jhavar S, Xiao W, Lim KH, Kohlhammer H, Xu W, Yang Y, Zhao H, Shaffer AL, Romesser P, Wright G, Powell J, Rosenwald A, Muller-Hermelink HK, Ott G, Gascoyne RD, Connors JM, Rimsza LM, Campo E, Jaffe ES, Delabie J, Smeland EB, Fisher RI, Braziel RM, Tubbs RR, Cook JR, Weisenburger DD, Chan WC, Staudt LM. 2011. Oncogenically active MYD88 mutations in human lymphoma. Nature 470:115-9.

124. Wang JQ, Jeelall YS, Ferguson LL, Horikawa K. 2014. Toll-Like Receptors and Cancer: MYD88 Mutation and Inflammation. Front Immunol 5:367.

125. Lee JH, Jeong H, Choi JW, Oh H, Kim YS. 2017. Clinicopathologic significance of MYD88 L265P mutation in diffuse large B-cell lymphoma: a meta-analysis. Sci Rep 7:1785.

126. Weber ANR, Cardona Gloria Y, Cinar O, Reinhardt HC, Pezzutto A, Wolz OO. 2018. Oncogenic MYD88 mutations in lymphoma: novel insights and therapeutic possibilities. Cancer Immunol Immunother.

127. Castillo JJ, Gustine JN, Meid K, Xu L, Hunter ZR, Treon SP. 2017. Comparing Apples to Oranges: A commentary on the Mayo study of MYD88 significance in Waldenstrom's Macroglobulinemia. Am J Hematol.

128. Kelly PN, Romero DL, Yang Y, Shaffer AL, 3rd, Chaudhary D, Robinson S, Miao W, Rui L, Westlin WF, Kapeller R, Staudt LM. 2015. Selective interleukin-1 receptor-associated kinase

4 inhibitors for the treatment of autoimmune disorders and lymphoid malignancy. J Exp Med 212:2189-201.

129. Landgren O, Tageja N. 2014. MYD88 and beyond: novel opportunities for diagnosis, prognosis and treatment in Waldenstrom's Macroglobulinemia. Leukemia 28:1799-803.

130. Rhyasen GW, Bolanos L, Fang J, Jerez A, Wunderlich M, Rigolino C, Mathews L, Ferrer M, Southall N, Guha R, Keller J, Thomas C, Beverly LJ, Cortelezzi A, Oliva EN, Cuzzola M, Maciejewski JP, Mulloy JC, Starczynowski DT. 2013. Targeting IRAK1 as a therapeutic approach for myelodysplastic syndrome. Cancer Cell 24:90-104.

131. Adams AK, Bolanos LC, Dexheimer PJ, Karns RA, Aronow BJ, Komurov K, Jegga AG, Casper KA, Patil YJ, Wilson KM, Starczynowski DT, Wells SI. 2015. IRAK1 is a novel DEK transcriptional target and is essential for head and neck cancer cell survival. Oncotarget 6:43395-407.

132. Ye ZH, Gao L, Wen DY, He Y, Pang YY, Chen G. 2017. Diagnostic and prognostic roles of IRAK1 in hepatocellular carcinoma tissues: an analysis of immunohistochemistry and RNA-sequencing data from the cancer genome atlas. Onco Targets Ther 10:1711-1723.

133. Sun M, Yang P, Yang Y, Ye J. 2017. Upregulated IRAK1 and IRAK4 promoting the production of IFN-gamma and IL-17 in Behcet's disease. Int Ophthalmol.

134. Carbone A, Gloghini A. 2008. KSHV/HHV8-associated lymphomas. Br J Haematol 140:13-24.

135. Yang D, Chen W, Xiong J, Sherrod CJ, Henry DH, Dittmer DP. 2014. Interleukin 1 receptor-associated kinase 1 (IRAK1) mutation is a common, essential driver for Kaposi sarcoma herpesvirus lymphoma. Proc Natl Acad Sci U S A 111:E4762-8.

136. Han TU, Cho SK, Kim T, Joo YB, Bae SC, Kang C. 2013. Association of an activity-enhancing variant of IRAK1 and an MECP2-IRAK1 haplotype with increased susceptibility to rheumatoid arthritis. Arthritis Rheum 65:590-8.

137. Carrasco-Colom J, Jordan I, Alsina L, Garcia-Garcia JJ, Cambra-Lasaosa FJ, Martin-Mateos MA, Juan M, Munoz-Almagro C. 2015. Association of Polymorphisms in IRAK1, IRAK4 and MyD88, and Severe Invasive Pneumococcal Disease. Pediatr Infect Dis J 34:1008-13.

138. Li C, Huang S, Mo S, Zhang N, Zhou L, Mao Z, Lv W, Li J, Zhou Y. 2015. Susceptibility of autoimmune diseases in three polymorphisms of infection-associated gene IRAK1. 9.

139. Khalifa O, Balandraud N, Lambert N, Auger I, Roudier J, Senechal A, Genevieve D, Picard C, Lefranc G, Touitou I, Mrenda BM, Benedito C, Pardoux E, Gagez AL, Pers YM, Jorgensen C, Mahjoub T, Apparailly F. 2017. TMEM187-IRAK1 Polymorphisms Associated with Rheumatoid Arthritis Susceptibility in Tunisian and French Female Populations: Influence of Geographic Origin. J Immunol Res 2017:4915950.

140. Kaufman KM, Zhao J, Kelly JA, Hughes T, Adler A, Sanchez E, Ojwang JO, Langefeld CD, Ziegler JT, Williams AH, Comeau ME, Marion MC, Glenn SB, Cantor RM, Grossman JM, Hahn

BH, Song YW, Yu CY, James JA, Guthridge JM, Brown EE, Alarcon GS, Kimberly RP, Edberg JC, Ramsey-Goldman R, Petri MA, Reveille JD, Vila LM, Anaya JM, Boackle SA, Stevens AM, Freedman BI, Criswell LA, Pons Estel BA, Lee JH, Lee JS, Chang DM, Scofield RH, Gilkeson GS, Merrill JT, Niewold TB, Vyse TJ, Bae SC, Alarcon-Riquelme ME, Jacob CO, Moser Sivils K, Gaffney PM, Harley JB, Sawalha AH, Tsao BP. 2013. Fine mapping of Xq28: both MECP2 and IRAK1 contribute to risk for systemic lupus erythematosus in multiple ancestral groups. Ann Rheum Dis 72:437-44.

141. Polizzotto MN, Uldrick TS, Wang V, Aleman K, Wyvill KM, Marshall V, Pittaluga S, O'Mahony D, Whitby D, Tosato G, Steinberg SM, Little RF, Yarchoan R. 2013. Human and viral interleukin-6 and other cytokines in Kaposi sarcoma herpesvirus-associated multicentric Castleman disease. Blood 122:4189-98.

142. Ahmad H, Gubbels R, Ehlers E, Meyer F, Waterbury T, Lin R, Zhang L. 2011. Kaposi sarcoma-associated herpesvirus degrades cellular Toll-interleukin-1 receptor domain-containing adaptor-inducing beta-interferon (TRIF). J Biol Chem 286:7865-72.

143. Guo Y, Li W, Qin J, Lu C, Fan W. 2017. Kaposi's sarcoma-associated herpesvirus (KSHV)-encoded MicroRNAs promote matrix metalloproteinases (MMPs) expression and pro-angiogenic cytokine secretion in endothelial cells. J Med Virol.

144. Qin J, Li W, Gao SJ, Lu C. 2017. KSHV microRNAs: Tricks of the Devil. Trends Microbiol.
145. Simonart T, Van Vooren JP. 2002. Interleukin-1 beta increases the BCL-2/BAX ratio in Kaposi's sarcoma cells. Cytokine 19:259-66.

146. Lang ME, Lottersberger C, Roth B, Bock G, Recheis H, Sgonc R, Sturzl M, Albini A, Tschachler E, Zangerle R, Donini S, Feichtinger H, Schwarz S. 1997. Induction of apoptosis in Kaposi's sarcoma spindle cell cultures by the subunits of human chorionic gonadotropin. Aids 11:1333-40.

147. Corley PA. 1997. Induction of interleukin-1 and glucocorticoid hormones by HIV promotes viral replication and links human chromosome 2 to AIDS pathogenesis: genetic mechanisms and therapeutic implications. Med Hypotheses 48:415-21.

148. Samaniego F, Markham PD, Gendelman R, Gallo RC, Ensoli B. 1997. Inflammatory cytokines induce endothelial cells to produce and release basic fibroblast growth factor and to promote Kaposi's sarcoma-like lesions in nude mice. J Immunol 158:1887-94.

149. Maier J, Mariotti M, Comoglio PM, Soria MR. 1996. Interleukin 1 induces an autocrine loop hepatocyte growth factor/c-Met in murine Kaposi-like spindle cells. Oncogene 13:1009-15.

150. Lee J, Rhee MH, Kim E, Cho JY. 2012. BAY 11-7082 is a broad-spectrum inhibitor with anti-inflammatory activity against multiple targets. Mediators Inflamm 2012:416036.

151. Rauert-Wunderlich H, Siegmund D, Maier E, Giner T, Bargou RC, Wajant H, Stuhmer T. 2013. The IKK inhibitor Bay 11-7082 induces cell death independent from inhibition of activation of NFkappaB transcription factors. PLoS One 8:e59292.

152. Verma R, Balakrishnan L, Sharma K, Khan AA, Advani J, Gowda H, Tripathy SP, Suar M, Pandey A, Gandotra S, Prasad TS, Shankar S. 2016. A network map of Interleukin-10 signaling pathway. J Cell Commun Signal 10:61-7.

153. Mittal SK, Roche PA. 2015. Suppression of antigen presentation by IL-10. Curr Opin Immunol 34:22-7.

154. Chonov DC, Ignatova MMK, Ananiev JR, Gulubova MV. 2019. IL-6 Activities in the Tumour Microenvironment. Part 1. Open Access Maced J Med Sci 7:2391-2398.

155. Foussat A, Wijdenes J, Bouchet L, Gaidano G, Neipel F, Balabanian K, Galanaud P, Couderc J, Emilie D. 1999. Human interleukin-6 is in vivo an autocrine growth factor for human herpesvirus-8-infected malignant B lymphocytes. Eur Cytokine Netw 10:501-8.

156. Oksenhendler E, Carcelain G, Aoki Y, Boulanger E, Maillard A, Clauvel JP, Agbalika F. 2000. High levels of human herpesvirus 8 viral load, human interleukin-6, interleukin-10, and C reactive protein correlate with exacerbation of multicentric castleman disease in HIV-infected patients. Blood 96:2069-73.

157. Jones KD, Aoki Y, Chang Y, Moore PS, Yarchoan R, Tosato G. 1999. Involvement of interleukin-10 (IL-10) and viral IL-6 in the spontaneous growth of Kaposi's sarcoma herpesvirus-associated infected primary effusion lymphoma cells. Blood 94:2871-9.

158. Lurain K, Polizzotto MN, Aleman K, Bhutani M, Wyvill KM, Goncalves PH, Ramaswami R, Marshall VA, Miley W, Steinberg SM, Little RF, Wilson W, Filie AC, Pittaluga S, Jaffe ES, Whitby D, Yarchoan R, Uldrick TS. 2019. Viral, immunologic, and clinical features of primary effusion lymphoma. Blood 133:1753-1761.

159. Machado PR, Farias KJ, Genre J, Oliveira CJ, Guedes PM, da Fonseca BA. 2014. Disseminated Kaposi's sarcoma in patients with HIV infection correlates to high serum levels of IL-10. Viral Immunol 27:356-60.

160. Gruffaz M, Vasan K, Tan B, Ramos da Silva S, Gao SJ. 2017. TLR4-Mediated Inflammation Promotes KSHV-Induced Cellular Transformation and Tumorigenesis by Activating the STAT3 Pathway. Cancer Res 77:7094-7108.

161. Uldrick TS, Wang V, O'Mahony D, Aleman K, Wyvill KM, Marshall V, Steinberg SM, Pittaluga S, Maric I, Whitby D, Tosato G, Little RF, Yarchoan R. 2010. An interleukin-6-related systemic inflammatory syndrome in patients co-infected with Kaposi sarcoma-associated herpesvirus and HIV but without Multicentric Castleman disease. Clin Infect Dis 51:350-8.

162. Polizzotto MN, Uldrick TS, Wyvill KM, Aleman K, Marshall V, Wang V, Whitby D, Pittaluga S, Jaffe ES, Millo C, Tosato G, Little RF, Steinberg SM, Sereti I, Yarchoan R. 2016. Clinical Features and Outcomes of Patients With Symptomatic Kaposi Sarcoma Herpesvirus (KSHV)-associated Inflammation: Prospective Characterization of KSHV Inflammatory Cytokine Syndrome (KICS). Clin Infect Dis 62:730-738.

163. van Rhee F, Stone K, Szmania S, Barlogie B, Singh Z. 2010. Castleman disease in the 21st century: an update on diagnosis, assessment, and therapy. Clin Adv Hematol Oncol 8:486-98.

164. Fajgenbaum DC. 2018. Novel insights and therapeutic approaches in idiopathic multicentric Castleman disease. Hematology Am Soc Hematol Educ Program 2018:318-325.

165. Zondag TC, Rokx C, van Lom K, van den Berg AR, Sonneveld P, Dik WA, van Doornum GJ, Lam KH, van Laar JA. 2016. Cytokine and viral load kinetics in human herpesvirus 8-associated multicentric Castleman's disease complicated by hemophagocytic lymphohistiocytosis. Int J Hematol 103:469-72.

166. Zhang L, Li J. 2016. Pathogenesis of Castleman's Disease. Zhongguo Yi Xue Ke Xue Yuan Xue Bao 38:118-21.

167. Sasaki H, Maeda T, Hara Y, Osa M, Imai K, Moriguchi K, Mikita K, Fujikura Y, Kaida K, Kawana A. 2015. Human herpes virus-8-associated multicentric Castleman's disease in an HIV-positive patient presenting with relapsing and remitting hyponatraemia. Int J STD AIDS 26:909-11.

168. Schulz TF. 2001. KSHV/HHV8-associated lymphoproliferations in the AIDS setting. Eur J Cancer 37:1217-26.

169. Parravicini C, Chandran B, Corbellino M, Berti E, Paulli M, Moore PS, Chang Y. 2000. Differential viral protein expression in Kaposi's sarcoma-associated herpesvirus-infected diseases: Kaposi's sarcoma, primary effusion lymphoma, and multicentric Castleman's disease. Am J Pathol 156:743-9.

170. Adam N, Rabe B, Suthaus J, Grotzinger J, Rose-John S, Scheller J. 2009. Unraveling viral interleukin-6 binding to gp130 and activation of STAT-signaling pathways independently of the interleukin-6 receptor. J Virol 83:5117-26.

171. Breen EC, Gage JR, Guo B, Magpantay L, Narazaki M, Kishimoto T, Miles S, Martinez-Maza O. 2001. Viral interleukin 6 stimulates human peripheral blood B cells that are unresponsive to human interleukin 6. Cell Immunol 212:118-25.

172. Dela Cruz CS, Viswanathan SR, El-Guindy AS, Shedd D, Miller G. 2009. Complex N-linked glycans on Asn-89 of Kaposi sarcoma herpes virus-encoded interleukin-6 mediate optimal function by affecting cytokine protein conformation. J Biol Chem 284:29269-82.

173. Zhao J, Punj V, Matta H, Mazzacurati L, Schamus S, Yang Y, Yang T, Hong Y, Chaudhary PM. 2007. K13 blocks KSHV lytic replication and deregulates vIL6 and hIL6 expression: a model of lytic replication induced clonal selection in viral oncogenesis. PLoS One 2:e1067.

174. Vart RJ, Nikitenko LL, Lagos D, Trotter MW, Cannon M, Bourboulia D, Gratrix F, Takeuchi Y, Boshoff C. 2007. Kaposi's sarcoma-associated herpesvirus-encoded interleukin-6 and G-protein-coupled receptor regulate angiopoietin-2 expression in lymphatic endothelial cells. Cancer Res 67:4042-51.

175. Miyazawa M, Noguchi K, Kujirai M, Katayama K, Yamagoe S, Sugimoto Y. 2018. IL-10 promoter transactivation by the viral K-RTA protein involves the host-cell transcription factors, specificity proteins 1 and 3. J Biol Chem 293:662-676.

176. Matta H, Punj V, Schamus S, Mazzacurati L, Chen AM, Song R, Yang T, Chaudhary PM. 2008. A nuclear role for Kaposi's sarcoma-associated herpesvirus-encoded K13 protein in gene regulation. Oncogene 27:5243-53.

177. Hilton IB, Simon JM, Lieb JD, Davis IJ, Damania B, Dittmer DP. 2013. The open chromatin landscape of Kaposi's sarcoma-associated herpesvirus. J Virol 87:11831-42.

178. Darst RP, Haecker I, Pardo CE, Renne R, Kladde MP. 2013. Epigenetic diversity of Kaposi's sarcoma-associated herpesvirus. Nucleic Acids Res 41:2993-3009.

179. Muller M, Hutin S, Marigold O, Li KH, Burlingame A, Glaunsinger BA. 2015. A ribonucleoprotein complex protects the interleukin-6 mRNA from degradation by distinct herpesviral endonucleases. PLoS Pathog 11:e1004899.

180. Bhaskaran N, Ghosh SK, Yu X, Qin S, Weinberg A, Pandiyan P, Ye F. 2017. Kaposi's sarcoma-associated herpesvirus infection promotes differentiation and polarization of monocytes into tumor-associated macrophages. Cell Cycle 16:1611-1621.

181. Qin D, Zeng Y, Qian C, Huang Z, Lv Z, Cheng L, Yao S, Tang Q, Chen X, Lu C. 2008. Induction of lytic cycle replication of Kaposi's sarcoma-associated herpesvirus by herpes simplex virus type 1: involvement of IL-10 and IL-4. Cell Microbiol 10:713-28.

182. Nicholas J. 2005. Human gammaherpesvirus cytokines and chemokine receptors. J Interferon Cytokine Res 25:373-83.

183. Martinez-Maza O, Breen EC. 2002. B-cell activation and lymphoma in patients with HIV. Curr Opin Oncol 14:528-32.

184. Santarelli R, Gonnella R, Di Giovenale G, Cuomo L, Capobianchi A, Granato M, Gentile G, Faggioni A, Cirone M. 2014. STAT3 activation by KSHV correlates with IL-10, IL-6 and IL-23 release and an autophagic block in dendritic cells. Sci Rep 4:4241.

185. Quinn SR, O'Neill LA. 2014. The role of microRNAs in the control and mechanism of action of IL-10. Curr Top Microbiol Immunol 380:145-55.

186. Ramalingam D, Ziegelbauer JM. 2017. Viral microRNAs Target a Gene Network, Inhibit STAT Activation, and Suppress Interferon Responses. Sci Rep 7:40813.

187. Qin Z, Kearney P, Plaisance K, Parsons CH. 2010. Pivotal advance: Kaposi's sarcoma-associated herpesvirus (KSHV)-encoded microRNA specifically induce IL-6 and IL-10 secretion by macrophages and monocytes. J Leukoc Biol 87:25-34.

188. Chen M, Sun F, Han L, Qu Z. 2016. Kaposi's sarcoma herpesvirus (KSHV) microRNA K12-1 functions as an oncogene by activating NF-kappaB/IL-6/STAT3 signaling. Oncotarget 7:33363-73.

189. Tudor S, Giza DE, Lin HY, Fabris L, Yoshiaki K, D'Abundo L, Toale KM, Shimizu M, Ferracin M, Challagundla KB, Cortez MA, Fuentes-Mattei E, Tulbure D, Gonzalez C, Henderson J, Row M, Rice TW, Ivan C, Negrini M, Fabbri M, Morris JS, Yeung SC, Vasilescu C, Calin GA. 2014. Cellular and Kaposi's sarcoma-associated herpes virus microRNAs in sepsis and surgical trauma. Cell Death Dis 5:e1559.

190. Chugh PE, Sin SH, Ozgur S, Henry DH, Menezes P, Griffith J, Eron JJ, Damania B, Dittmer DP. 2013. Systemically circulating viral and tumor-derived microRNAs in KSHV-associated malignancies. PLoS Pathog 9:e1003484.

191. Ballon G, Akar G, Cesarman E. 2015. Systemic expression of Kaposi sarcoma herpesvirus (KSHV) Vflip in endothelial cells leads to a profound proinflammatory phenotype and myeloid lineage remodeling in vivo. PLoS Pathog 11:e1004581.

192. Rangaswamy US, Speck SH. 2014. Murine gammaherpesvirus M2 protein induction of IRF4 via the NFAT pathway leads to IL-10 expression in B cells. PLoS Pathog 10:e1003858.

193. Peacock JW, Bost KL. 2001. Murine gammaherpesvirus-68-induced interleukin-10 increases viral burden, but limits virus-induced splenomegaly and leukocytosis. Immunology 104:109-17.

194. Suthaus J, Stuhlmann-Laeisz C, Tompkins VS, Rosean TR, Klapper W, Tosato G, Janz S, Scheller J, Rose-John S. 2012. HHV-8-encoded viral IL-6 collaborates with mouse IL-6 in the development of multicentric Castleman disease in mice. Blood 119:5173-81.

195. Coghill AE, Schenk JM, Mahkoul Z, Orem J, Phipps W, Casper C. 2018. Omega-3 decreases IL-6 levels in HIV and human herpesvirus-8 coinfected patients in Uganda. Aids 32:505-512.

196. Zhou F, Shimoda M, Olney L, Lyu Y, Tran K, Jiang G, Nakano K, Davis RR, Tepper CG, Maverakis E, Campbell M, Li Y, Dandekar S, Izumiya Y. 2017. Oncolytic Reactivation of KSHV as a Therapeutic Approach for Primary Effusion Lymphoma. Mol Cancer Ther 16:2627-2638.

197. Uldrick TS, Polizzotto MN, Yarchoan R. 2012. Recent advances in Kaposi sarcoma herpesvirus-associated multicentric Castleman disease. Curr Opin Oncol 24:495-505.

198. Lurain K, Yarchoan R, Uldrick TS. 2018. Treatment of Kaposi Sarcoma Herpesvirus-Associated Multicentric Castleman Disease. Hematol Oncol Clin North Am 32:75-88.

199. Nagao A, Nakazawa S, Hanabusa H. 2014. Short-term efficacy of the IL6 receptor antibody tocilizumab in patients with HIV-associated multicentric Castleman disease: report of two cases. J Hematol Oncol 7:10.

200. Uldrick TS, Polizzotto MN, Aleman K, Wyvill KM, Marshall V, Whitby D, Wang V, Pittaluga S, O'Mahony D, Steinberg SM, Little RF, Yarchoan R. 2014. Rituximab plus liposomal

doxorubicin in HIV-infected patients with KSHV-associated multicentric Castleman disease. Blood 124:3544-52.

201. Deisseroth A, Ko CW, Nie L, Zirkelbach JF, Zhao L, Bullock J, Mehrotra N, Del Valle P, Saber H, Sheth C, Gehrke B, Justice R, Farrell A, Pazdur R. 2015. FDA approval: siltuximab for the treatment of patients with multicentric Castleman disease. Clin Cancer Res 21:950-4.

202. Cong L, Ran FA, Cox D, Lin S, Barretto R, Habib N, Hsu PD, Wu X, Jiang W, Marraffini LA, Zhang F. 2013. Multiplex genome engineering using CRISPR/Cas systems. Science 339:819-23.

203. Chandrasekharan JA, Huang XM, Hwang AC, Sharma-Walia N. 2016. Altering the Anti-inflammatory Lipoxin Microenvironment: a New Insight into Kaposi's Sarcoma-Associated Herpesvirus Pathogenesis. J Virol 90:11020-11031.

204. Patil A, Manzano M, Gottwein E. 2018. CK1alpha and IRF4 are essential and independent effectors of immunomodulatory drugs in primary effusion lymphoma. Blood 132:577-586.

205. Patil A, Manzano M, Gottwein E. 2019. Genome-wide CRISPR screens reveal genetic mediators of cereblon modulator toxicity in primary effusion lymphoma. Blood Adv 3:2105-2117.

206. BeltCappellino A, Majerciak V, Lobanov A, Lack J, Cam M, Zheng ZM. 2019. CRISPR/Cas9-Mediated Knockout and In Situ Inversion of the ORF57 Gene from All Copies of the Kaposi's Sarcoma-Associated Herpesvirus Genome in BCBL-1 Cells. J Virol 93.

207. Wang LW, Shen H, Nobre L, Ersing I, Paulo JA, Trudeau S, Wang Z, Smith NA, Ma Y, Reinstadler B, Nomburg J, Sommermann T, Cahir-McFarland E, Gygi SP, Mootha VK, Weekes MP, Gewurz BE. 2019. Epstein-Barr-Virus-Induced One-Carbon Metabolism Drives B Cell Transformation. Cell Metab 30:539-555.e11.

208. Cesarman E, Chang Y, Moore PS, Said JW, Knowles DM. 1995. Kaposi's sarcoma-associated herpesvirus-like DNA sequences in AIDS-related body-cavity-based lymphomas. N Engl J Med 332:1186-91.

209. Renne R, Zhong W, Herndier B, McGrath M, Abbey N, Kedes D, Ganem D. 1996. Lytic growth of Kaposi's sarcoma-associated herpesvirus (human herpesvirus 8) in culture. Nat Med 2:342-6.

210. Makgoeng SB, Bolanos RS, Jeon CY, Weiss RE, Arah OA, Breen EC, Martinez-Maza O, Hussain SK. 2018. Markers of Immune Activation and Inflammation, and Non-Hodgkin Lymphoma: A Meta-Analysis of Prospective Studies. JNCI Cancer Spectr 2:pky082.

211. Epeldegui M, Lee JY, Martinez AC, Widney DP, Magpantay LI, Regidor D, Mitsuyasu R, Sparano JA, Ambinder RF, Martinez-Maza O. 2016. Predictive Value of Cytokines and Immune Activation Biomarkers in AIDS-Related Non-Hodgkin Lymphoma Treated with Rituximab plus Infusional EPOCH (AMC-034 trial). Clin Cancer Res 22:328-36.

212. Brockmeyer NH, Willers CP, Anders S, Mertins L, Rockstroh JK, Sturzl M. 1999. Cytokine profile of HIV-positive Kaposi's sarcoma derived cells in vitro. Eur J Med Res 4:95-100.

213. Ensoli B, Nakamura S, Salahuddin SZ, Biberfeld P, Larsson L, Beaver B, Wong-Staal F, Gallo RC. 1989. AIDS-Kaposi's sarcoma-derived cells express cytokines with autocrine and paracrine growth effects. Science 243:223-6.

214. Janssens S, Beyaert R. 2003. Functional diversity and regulation of different interleukin-1 receptor-associated kinase (IRAK) family members. Mol Cell 11:293-302.

215. Motshwene PG, Moncrieffe MC, Grossmann JG, Kao C, Ayaluru M, Sandercock AM, Robinson CV, Latz E, Gay NJ. 2009. An oligomeric signaling platform formed by the Toll-like receptor signal transducers MyD88 and IRAK-4. J Biol Chem 284:25404-11.

216. Deguine J, Barton GM. 2014. MyD88: a central player in innate immune signaling. F1000Prime Rep 6:97.

217. Cui W, Xiao N, Xiao H, Zhou H, Yu M, Gu J, Li X. 2012. beta-TrCP-mediated IRAK1 degradation releases TAK1-TRAF6 from the membrane to the cytosol for TAK1-dependent NF-kappaB activation. Mol Cell Biol 32:3990-4000.

218. Honda K, Yanai H, Mizutani T, Negishi H, Shimada N, Suzuki N, Ohba Y, Takaoka A, Yeh WC, Taniguchi T. 2004. Role of a transductional-transcriptional processor complex involving MyD88 and IRF-7 in Toll-like receptor signaling. Proc Natl Acad Sci U S A 101:15416-21.

219. Van Tassell BW, Seropian IM, Toldo S, Salloum FN, Smithson L, Varma A, Hoke NN, Gelwix C, Chau V, Abbate A. 2010. Pharmacologic inhibition of myeloid differentiation factor 88 (MyD88) prevents left ventricular dilation and hypertrophy after experimental acute myocardial infarction in the mouse. J Cardiovasc Pharmacol 55:385-90.

220. Bruno A, Boisselier B, Labreche K, Marie Y, Polivka M, Jouvet A, Adam C, Figarella-Branger D, Miquel C, Eimer S, Houillier C, Soussain C, Mokhtari K, Daveau R, Hoang-Xuan K. 2014. Mutational analysis of primary central nervous system lymphoma. Oncotarget 5:5065-75.

221. Gonzalez-Aguilar A, Idbaih A, Boisselier B, Habbita N, Rossetto M, Laurenge A, Bruno A, Jouvet A, Polivka M, Adam C, Figarella-Branger D, Miquel C, Vital A, Ghesquieres H, Gressin R, Delwail V, Taillandier L, Chinot O, Soubeyran P, Gyan E, Choquet S, Houillier C, Soussain C, Tanguy ML, Marie Y, Mokhtari K, Hoang-Xuan K. 2012. Recurrent mutations of MYD88 and TBL1XR1 in primary central nervous system lymphomas. Clin Cancer Res 18:5203-11.

222. Treon SP, Xu L, Yang G, Zhou Y, Liu X, Cao Y, Sheehy P, Manning RJ, Patterson CJ, Tripsas C, Arcaini L, Pinkus GS, Rodig SJ, Sohani AR, Harris NL, Laramie JM, Skifter DA, Lincoln SE, Hunter ZR. 2012. MYD88 L265P somatic mutation in Waldenstrom's macroglobulinemia. N Engl J Med 367:826-33.

223. Bonzheim I, Giese S, Deuter C, Susskind D, Zierhut M, Waizel M, Szurman P, Federmann B, Schmidt J, Quintanilla-Martinez L, Coupland SE, Bartz-Schmidt KU, Fend F. 2015. High

frequency of MYD88 mutations in vitreoretinal B-cell lymphoma: a valuable tool to improve diagnostic yield of vitreous aspirates. Blood 126:76-9.

224. Dubois S, Viailly PJ, Bohers E, Bertrand P, Ruminy P, Marchand V, Maingonnat C, Mareschal S, Picquenot JM, Penther D, Jais JP, Tesson B, Peyrouze P, Figeac M, Desmots F, Fest T, Haioun C, Lamy T, Copie-Bergman C, Fabiani B, Delarue R, Peyrade F, Andre M, Ketterer N, Leroy K, Salles G, Molina TJ, Tilly H, Jardin F. 2017. Biological and Clinical Relevance of Associated Genomic Alterations in MYD88 L265P and non-L265P-Mutated Diffuse Large B-Cell Lymphoma: Analysis of 361 Cases. Clin Cancer Res 23:2232-2244.

225. Loiarro M, Capolunghi F, Fanto N, Gallo G, Campo S, Arseni B, Carsetti R, Carminati P, De Santis R, Ruggiero V, Sette C. 2007. Pivotal Advance: Inhibition of MyD88 dimerization and recruitment of IRAK1 and IRAK4 by a novel peptidomimetic compound. J Leukoc Biol 82:801-10.

226. Fanto N, Gallo G, Ciacci A, Semproni M, Vignola D, Quaglia M, Bombardi V, Mastroianni D, Zibella MP, Basile G, Sassano M, Ruggiero V, De Santis R, Carminati P. 2008. Design, synthesis, and in vitro activity of peptidomimetic inhibitors of myeloid differentiation factor 88. J Med Chem 51:1189-202.

227. Wang N, Han X, Liu H, Zhao T, Li J, Feng Y, Mi X, Zhang Y, Chen Y, Wang X. 2017. Myeloid differentiation factor 88 is up-regulated in epileptic brain and contributes to experimental seizures in rats. Exp Neurol 295:23-35.

228. Love MI, Huber W, Anders S. 2014. Moderated estimation of fold change and dispersion for RNA-seq data with DESeq2. Genome Biol 15:550.

229. Fan W, Bubman D, Chadburn A, Harrington WJ, Jr., Cesarman E, Knowles DM. 2005. Distinct subsets of primary effusion lymphoma can be identified based on their cellular gene expression profile and viral association. J Virol 79:1244-51.

230. Lu P, Yang C, Guasparri I, Harrington W, Wang YL, Cesarman E. 2009. Early events of B-cell receptor signaling are not essential for the proliferation and viability of AIDS-related lymphoma, p 807-10, Leukemia, vol 23, England.

231. Jensen LE, Whitehead AS. 2001. IRAK1b, a novel alternative splice variant of interleukin-1 receptor-associated kinase (IRAK), mediates interleukin-1 signaling and has prolonged stability. J Biol Chem 276:29037-44.

232. Knop J, Martin MU. 1999. Effects of IL-1 receptor-associated kinase (IRAK) expression on IL-1 signaling are independent of its kinase activity. FEBS Lett 448:81-5.

233. Rao N, Nguyen S, Ngo K, Fung-Leung WP. 2005. A novel splice variant of interleukin-1 receptor (IL-1R)-associated kinase 1 plays a negative regulatory role in Toll/IL-1R-induced inflammatory signaling. Mol Cell Biol 25:6521-32.

234. Maschera B, Ray K, Burns K, Volpe F. 1999. Overexpression of an enzymically inactive interleukin-1-receptor-associated kinase activates nuclear factor-kappaB. Biochem J 339 (Pt 2):227-31.

235. Shiratori E, Itoh M, Tohda S. 2017. MYD88 Inhibitor ST2825 Suppresses the Growth of Lymphoma and Leukaemia Cells. Anticancer Res 37:6203-6209.

236. Feng Y, Duan W, Cu X, Liang C, Xin M. 2019. Bruton's tyrosine kinase (BTK) inhibitors in treating cancer: a patent review (2010-2018). Expert Opin Ther Pat 29:217-241.

237. Powers JP, Li S, Jaen JC, Liu J, Walker NP, Wang Z, Wesche H. 2006. Discovery and initial SAR of inhibitors of interleukin-1 receptor-associated kinase-4. Bioorg Med Chem Lett 16:2842-5.

238. Godfrey A, Anderson J, Papanastasiou A, Takeuchi Y, Boshoff C. 2005. Inhibiting primary effusion lymphoma by lentiviral vectors encoding short hairpin RNA. Blood 105:2510-8.

239. Roy D, Sin SH, Damania B, Dittmer DP. 2011. Tumor suppressor genes FHIT and WWOX are deleted in primary effusion lymphoma (PEL) cell lines. Blood 118:e32-9.

240. Luan SL, Boulanger E, Ye H, Chanudet E, Johnson N, Hamoudi RA, Bacon CM, Liu H, Huang Y, Said J, Chu P, Clemen CS, Cesarman E, Chadburn A, Isaacson PG, Du MQ. 2010. Primary effusion lymphoma: genomic profiling revealed amplification of SELPLG and CORO1C encoding for proteins important for cell migration. J Pathol 222:166-79.

241. Abeykoon JP, Paludo J, King RL, Ansell SM, Gertz MA, LaPlant BR, Halvorson AE, Gonsalves WI, Dingli D, Fang H, Rajkumar SV, Lacy MQ, He R, Kourelis T, Reeder CB, Novak AJ, McPhail E, Viswanatha D, Witzig TE, Go RS, Habermann T, Buadi FK, Dispenzieri A, Leung N, Lin Y, Thompson C, Hayman S, Kyle RA, Kumar S, Kapoor P. 2017. Impact of MYD88 Mutation Status in Waldenstrom Macroglobulinemia. Am J Hematol.

242. Sarosiek KA, Cavallin LE, Bhatt S, Toomey NL, Natkunam Y, Blasini W, Gentles AJ, Ramos JC, Mesri EA, Lossos IS. 2010. Efficacy of bortezomib in a direct xenograft model of primary effusion lymphoma. Proc Natl Acad Sci U S A 107:13069-74.

243. Cornali E, Zietz C, Benelli R, Weninger W, Masiello L, Breier G, Tschachler E, Albini A, Stürzl M. 1996. Vascular endothelial growth factor regulates angiogenesis and vascular permeability in Kaposi's sarcoma. The American journal of pathology 149:1851-1869.

244. Liu G, Tsuruta Y, Gao Z, Park YJ, Abraham E. 2007. Variant IL-1 receptor-associated kinase-1 mediates increased NF-kappa B activity. J Immunol 179:4125-34.

245. Della Mina E, Borghesi A, Zhou H, Bougarn S, Boughorbel S, Israel L, Meloni I, Chrabieh M, Ling Y, Itan Y, Renieri A, Mazzucchelli I, Basso S, Pavone P, Falsaperla R, Ciccone R, Cerbo RM, Stronati M, Picard C, Zuffardi O, Abel L, Chaussabel D, Marr N, Li X, Casanova JL, Puel A. 2017. Inherited human IRAK-1 deficiency selectively impairs TLR signaling in fibroblasts. Proc Natl Acad Sci U S A.

246. Zheng M, Perry AM, Bierman P, Loberiza F, Jr., Nasr MR, Szwajcer D, Del Bigio MR, Smith LM, Zhang W, Greiner TC. 2017. Frequency of MYD88 and CD79B mutations, and MGMT methylation in primary central nervous system diffuse large B-cell lymphoma. Neuropathology.

247. Yu X, Li W, Deng Q, Li L, Hsi ED, Young KH, Zhang M, Li Y. 2018. MYD88 L265P Mutation in Lymphoid Malignancies. Cancer Res 78:2457-2462.

248. Sabnis AJ, Bivona TG. 2019. Principles of Resistance to Targeted Cancer Therapy: Lessons from Basic and Translational Cancer Biology. Trends Mol Med 25:185-197.

249. Wee ZN, Yatim SM, Kohlbauer VK, Feng M, Goh JY, Bao Y, Lee PL, Zhang S, Wang PP, Lim E, Tam WL, Cai Y, Ditzel HJ, Hoon DS, Tan EY, Yu Q. 2015. IRAK1 is a therapeutic target that drives breast cancer metastasis and resistance to paclitaxel. Nat Commun 6:8746.

250. Castillo JJ, Hunter ZR, Yang G, Treon SP. 2017. Novel approaches to targeting MYD88 in Waldenstrom macroglobulinemia. Expert Rev Hematol:1-6.

251. Smith I, Greenside PG, Natoli T, Lahr DL, Wadden D, Tirosh I, Narayan R, Root DE, Golub TR, Subramanian A, Doench JG. 2017. Evaluation of RNAi and CRISPR technologies by large-scale gene expression profiling in the Connectivity Map. PLoS Biol 15:e2003213.

252. Peretz L, Besser E, Hajbi R, Casden N, Ziv D, Kronenberg N, Gigi LB, Sweetat S, Khawaled S, Aqeilan R, Behar O. 2018. Combined shRNA over CRISPR/cas9 as a methodology to detect off-target effects and a potential compensatory mechanism. Sci Rep 8:93.

253. Arcaroli J, Silva E, Maloney JP, He Q, Svetkauskaite D, Murphy JR, Abraham E. 2006. Variant IRAK-1 haplotype is associated with increased nuclear factor-kappaB activation and worse outcomes in sepsis. Am J Respir Crit Care Med 173:1335-41.

254. Sharma-Walia N, Chandran K, Patel K, Veettil MV, Marginean A. 2014. The Kaposi's sarcoma-associated herpesvirus (KSHV)-induced 5-lipoxygenase-leukotriene B4 cascade plays key roles in KSHV latency, monocyte recruitment, and lipogenesis. J Virol 88:2131-56.

255. Granato M, Gilardini Montani MS, Santarelli R, D'Orazi G, Faggioni A, Cirone M. 2017. Apigenin, by activating p53 and inhibiting STAT3, modulates the balance between pro-apoptotic and pro-survival pathways to induce PEL cell death. J Exp Clin Cancer Res 36:167.

256. Heiseke AF, Jeuk BH, Markota A, Straub T, Lehr H-A, Reindl W, Krug AB. 2015. IRAK1 Drives Intestinal Inflammation by Promoting the Generation of Effector Th Cells with Optimal Gut-Homing Capacity.

257. Li X, Bhaduri-McIntosh S. 2016. A Central Role for STAT3 in Gammaherpesvirus-Life Cycle and -Diseases. Front Microbiol 7:1052.

258. Warner N, Nunez G. 2013. MyD88: a critical adaptor protein in innate immunity signal transduction. J Immunol 190:3-4.

259. Piras V, Selvarajoo K. 2014. Beyond MyD88 and TRIF Pathways in Toll-Like Receptor Signaling. Front Immunol 5:70.

260. Coste I, Le Corf K, Kfoury A, Hmitou I, Druillennec S, Hainaut P, Eychene A, Lebecque S, Renno T. 2010. Dual function of MyD88 in RAS signaling and inflammation, leading to mouse and human cell transformation. J Clin Invest 120:3663-7.

261. Kfoury A, Virard F, Renno T, Coste I. 2014. Dual function of MyD88 in inflammation and oncogenesis: implications for therapeutic intervention. Curr Opin Oncol 26:86-91.

262. Wang L, Yu K, Zhang X, Yu S. 2018. Dual functional roles of the MyD88 signaling in colorectal cancer development. Biomed Pharmacother 107:177-184.

263. Abel K, Reneland R, Kammerer S, Mah S, Hoyal C, Cantor CR, Nelson MR, Braun A. 2006. Genome-wide SNP association: identification of susceptibility alleles for osteoarthritis. Autoimmun Rev 5:258-63.

264. Atabaki M, Hashemi M, Daneshvar H, Alijani E. 2017. Association between interleukin-1 receptor associated kinase 1 rs3027898 A/C gene polymorphism and rheumatoid arthritis. Biomed Rep 6:335-338.

265. Berglöf A, Hamasy A, Meinke S, Palma M, Krstic A, Månsson R, Kimby E, Österborg A, Smith CIE. 2015. Targets for Ibrutinib Beyond B Cell Malignancies, p 208-17, Scand J Immunol, vol 82.